EVALUATION OF THE APPLICABILITY OF AN EXPLICIT NUMERICAL METHOD TO A PLANE, TURBULENT, LOW VELOCITY, PARTIALLY CONFINED JET

By

SONG-YEONG RUO

Bachelor of Science
Taiwan Provincial Cheng-Kung University
Tainan City, Taiwan
1957

Master of Science
University of Kansas
Lawrence, Kansas
1961

Submitted to the faculty of the Graduate College
of the Oklahoma State University
in partial fulfillment of the requirements
for the degree of
DOCTOR OF PHILOSOPHY
May, 1967

EVALUATION OF THE APPLICABILITY OF AN EXPLICIT NUMERICAL METHOD TO A PLANE, TURBULENT, LOW VELOCITY, PARTIALLY CONFINED JET

Thesis Approved:

Glen W. Zumwalt
Thesis Adviser

Karl N. Reid

J. A. Weibelt

Dale D. Grosvenor

D. D. Durham
Dean of the Graduate College

ACKNOWLEDGEMENTS

The author wishes to take this opportunity to express his sincere gratitude to Dr. Glen W. Zumwalt who assumed the responsibility of thesis adviser and secured funds to support this study.

Special thanks are extended to Dr. John A. Wiebelt for his guidance in the study of radiation heat transfer and Dr. Karl N. Reid for his valuable assistance in many ways. Thanks are due to Dr. Dale D. Grosvenor for serving on the advisory committee; Dr. James H. Boggs, the Vice President of the Academic Affairs, and Dr. Olan H. Hamilton, the former members of the advisory committee; Professor Ladislaus J. Fila for his helpful suggestions and comments.

The helps rendered to the author by Mr. George M. Cooper, the M.E. Laboratory technician; Messrs. William Accola and Daniel Mickish, the members of the Computer Center staff are also appreciated.

The author is very grateful to the Harry Diamond Laboratories of the U.S. Army for their financial support and the University Computer Center, under the direction of Dr. Dale D. Grosvenor, for its contribution of countless hours of valuable computer time.

A special recognition is given to the author's mother and brothers for their encouragement and understanding throughout the course of his study in this country and to his late father who made this possible.

To his wife, Su-yu, the author wishes to express his sincere

appreciation of her patience, encouragement and understanding. May this work in some way justify the sacrifices which have been made by those who are concerned with the author.

TABLE OF CONTENTS

LIST OF TABLES

LIST OF FIGURES

NOMENCLATURE

a	reference velocity, defined on page 24
a_1, a_2, a_3	constants
$A(x,y,t)$	blurring term coefficient for x-direction
$b(x)$	width of jet mixing zone
$B(x,y,t)$	blurring term coefficient for y-direction
B_0, B_1, B_2	constants
c	speed of sound
C_a	Crocco number of adjacent stream, defined on page 23
C_v	specific heat at constant volume
D	D.C. voltage reading from anemometer
e	fluid energy per unit volume
f	fluid property or a scalar function
F^x	functional relation defined on page 20
F^y	functional relation defined on page 20
g	fluid property or a scalar function
h	diagonal length of finite difference net
h_1	finite difference net spacing in x-direction
h_2	finite difference net spacing in y-direction
H_1	height of the separation step
H_2	height of the recompression step
K	time parameter defined on page 26
ℓ	net point number in y-direction (also, mixing length in Chapter II)

L	cavity length
m	net point number in x-direction
M	Mach number
M_a	Mach number of adjacent stream
n	time plane number
N	distance in normal direction
p	pressure
p_a	atmospheric pressure
Δp	pressure difference of pitot-static probe
Q	defined on page 55
R	gas constant
t	time
T	absolute temperature
u	velocity component in x-direction
u_a	velocity of adjacent velocity
v	velocity component in y-direction
w	velocity modulus, $(u^2 + v^2)^{1/2}$
W	nozzle width
x,y	cartesian coordinates
Δx	finite difference net spacing in x-direction
Δy	finite difference net spacing in y-direction
α	blurring term defined on page 26
β	blurring term defined on page 26
γ	ratio of specific heats
$\epsilon(x)$	apparent kinematic viscosity
η	dimensionless coordinate, see pages 3, 5, 6
$\Lambda(x)$	momentum transfer length

μ	dynamic viscosity
ν	kinematic viscosity
ρ	density
σ	jet spreading parameter
σ_i	turbulent normal stress in i-direction
σ_o	maximum allowable Courant number
τ	time increment (also, turbulent shearing stress in Chapter II)
τ_{ij}	tangential shearing stresses
τ_t	turbulent shearing stress
τ_{xy}	shearing stress in the y-direction on a plane perpendicular to x-axis or in the x-direction on a plane perpendicular to y-axis
χ	finite difference net diagonal angle (Figure 2)
ω	blurring parameter

Subscripts

c	centerline
i,j	denotes direction
ℓ	y net point location
m	x net point location
o	reference condition
x	y-direction
y	y-direction
max	maximum
min	minimum
noz	nozzle condition

Superscripts

$\bar{}$	time average
$'$	fluctuating component
$*$	dimensionless quantity
n	time plane number

CHAPTER I

INTRODUCTION

It was Henri Coanda who, in 1932, described a fluid flow phenomenon which stimulated the relatively recent development of fluid control devices without moving mechanical parts. Called the Coanda effect, the phenomenon involves the tendency of a fluid stream emerging into a space with a wall located near the stream to attach to the wall and to remain attached if no outside disturbance is imposed. In 1959, a group of scientists and engineers of the U. S. Army's Diamond Ordnance Fuze Laboratories (now Harry Diamond Laboratories) invented the so called "fluid amplifier." Since then there has been an almost explosive increase in activity on this class of fluid devices. In addition to performing flow switching and amplification, these fluid devices having no moving mechanical parts can be used to perform logic and computation functions, even in an adverse environment. The term "Fluidics" has received general acceptance for describing fluid control components and systems containing fluid elements with no moving mechanical parts.

At present the designs of fluid amplifiers rely almost totally on experimental trial and error methods. It would be very desirable to devise an analytical procedure for predicting the performance characteristics of every element in the control system based on the fundamental flow processes involved.

Many investigators have put forth considerable effort to find a method to predict the velocity and pressure distributions in fluid control components. Some empirical velocity distribution equations for different jet mixing models have been derived; however, the prediction of pressure distributions within these devices has been over-simplified and often ignored.

It is well known that the laminar flow of a viscous fluid can be treated with the Navier-Stokes equation. Due to the non-linear nature of the equation, only a few closed form exact solutions have been obtained. Since the high speed electronic computer became available, considerable progress has been made in numerical integration of non-linear differential equations.

The main objective of this study was to examine the possibility of applying an explicit numerical technique introduced by Rusanov (45) to integrate the simplified flow equations for a low speed, two-dimensional, turbulent jet issuing into a partially confined space. The geometrical arrangement selected is not exactly identical to the one used in most fluid control devices; however, it models the first important section of a proportional fluid amplifier. If the flow characteristics of this geometrical arrangement can be successfully predicted by means of numerical techniques, there should not be any difficulty in doing the same for the other cases.

Evaluation of this numerical technique was carried out with the aid of an IBM 7040 computer. Jet velocities of 100, 200, 250, 300 and 2270 fps at the nozzle exit were used in the computation. Experimental results for a nozzle exit velocity of 200 fps were obtained for comparison with the computed results.

CHAPTER II

LITERATURE SURVEY

After Prandtl introduced the mixing length theory, the theoretical study of jet mixing was greatly stimulated. Tollmien (50) made use of Prandtl's turbulent shear hypothesis,

$$\tau = \rho \ell^2 \left| \frac{\partial u}{\partial y} \right| \frac{\partial u}{\partial y} , \tag{2-1}$$

in the study of the free jet boundary, Fig. 1(b), and the free jet, Fig. 1(a). By assuming constant pressure and replacing the viscosity terms by the turbulent shear stresses in the equation of motion in the x-direction, the following is obtained

$$u \frac{\partial u}{\partial x} + v \frac{\partial u}{\partial y} = \frac{1}{\rho} \frac{\partial}{\partial y} \tau_{xy} . \tag{2-2}$$

Tollmien assumed that the mixing length is a function of x (the direction of the mean flow) only and is proportional to the distance from the point where the mixing starts. This relation may be written as

$$\ell = a_1 x , \tag{2-3}$$

where a_1 is a constant found experimentally to be $a_1 = 0.0174$. With the aid of the stream function and the boundary conditions at the centerline and at the edge of the jet Tollmien was able to write u and v in terms of x and η ($\eta = y/x$). From the solution of the

differential equation obtained by substituting equations (2-1) and (2-3) in equation (2-2) he was able to predict the velocity distributions of the jet. By neglecting $\rho\overline{(v')^2}$ in the equation of motion in y-direction, he derived equations for predicting jet centerline pressure. It was also pointed out that the centerline velocity of a free jet is inversely proportional to the square root of x (i.e., $u_c \sim x^{-1/2}$), where x is measured from the point where mixing first extends to the centerline.

Förthmann (18) extended the work of Tollmien by carrying out a series of experiments to study the jet mixing in the configurations shown in Figs. 1(a), (g) and (h).

From the experimental data on free turbulent flows, Reichardt (41) found that the velocity profiles of free jet boundaries, Fig. 1(b), and free jets, Fig. 1(a), could be represented successfully by the Gaussian error function. From the fact that one form of the solutions of the one-dimensional heat conduction equation is the Gaussian error function, he introduced his inductive theory of turbulence. For frictionless, constant pressure, incompressible flow, the time-average equation of motion in x-direction can be written as

$$\frac{\partial}{\partial x}\overline{(u^2)} + \frac{\partial}{\partial y}\overline{(uv)} = 0 \ . \tag{2-4}$$

Upon introducing an empirical "law of momentum transfer"

$$\overline{uv} = - \Lambda(x) \frac{\partial \overline{u^2}}{\partial y} \tag{2-5}$$

and combining this with equation (2-4), Reichardt obtained the equation

$$\frac{\partial \overline{u^2}}{\partial x} = \Lambda(x) \frac{\partial^2 \overline{u^2}}{\partial y^2} \ , \tag{2-6}$$

where $\Lambda(x)$ is called the "momentum transfer length." The solution of equation (2-6) may be written as

$$\bar{u} = \bar{u}_c \, e^{-a_2 \eta^2} \quad , \tag{2-7}$$

where a_2 is a constant, $\eta = y/b(x)$, and

$$b(x) = \int_0^{+\infty} \left(\frac{\bar{u}}{\bar{u}_c} \right)^2 dy \ .$$

If equation (2-7) is substituted in the expression of $b(x)$ and integrated, the constant a_2 in equation (2-7) can be obtained (i.e., $a_2 = \pi/8$).

As mentioned in Schlichting (48), Görtler built upon Prandtl's second hypothesis,

$$\tau = \rho \varepsilon(x) \frac{\partial u}{\partial y} \quad , \tag{2-8}$$

where $\varepsilon(x)$ is the virtual or apparent kinematic viscosity, to study the free jet boundary and the free jet. Assuming a frictionless, constant pressure flow and introducing equation (2-8) into the equation of motion in the x-direction, following differential equation is obtained:

$$u \frac{\partial u}{\partial x} + v \frac{\partial u}{\partial y} = \varepsilon \frac{\partial^2 u}{\partial y^2} \ . \tag{2-9}$$

For a free jet Görtler made use of the relations that the width of the jet is proportional to the distance x (i.e., $b \sim x$) and the jet centerline velocity is inversely proportional to the square root of the distance x (i.e., $u_c \sim x^{-1/2}$). He expressed the apparent kinematic viscosity in the following form:

$$\epsilon = a_3 \, b(x) \, x \, , \tag{2-10}$$

where a_3 is a constant.

If the continuity equation is integrated with the aid of the stream function and substituted in equation (2-9), the velocity profile equation can be obtained from the solution of equation (2-9). That is

$$u_c = u_c \, \mathrm{sech}^2 \, \eta \, , \tag{2-11}$$

where

$$\eta = \sigma \frac{y}{x}$$

and

$$\sigma = 0.5 \left(\frac{u_c x}{\epsilon} \right)^{1/2} \tag{2-12}$$

The value of the constant σ was determined experimentally by Reichardt, who found that $\sigma = 7.67$.

Albertson, et al. (4) studied low speed free jets, Fig. 1(a), both analytically and experimentally. They determined the velocity distribution and the volume, momentum, and energy flux ratios with respect to those of the nozzle exit in fully developed and half-jet regions. In the fully developed regions, the longitudinal component of velocity varies according to the Gaussian error function, the volume-flux ratio is proportional to $x^{-1/2}$, the momentum-flux ratio remains constant, and the energy-flux ratio is proportional to $x^{-1/2}$. They also indicated that the length of the jet potential core extends about 5.2 nozzle widths from the nozzle exit, whereas Miller and Comings (34) said it is about 7 nozzle widths.

Miller and Comings (34) found that the free jet mixing deviated appreciably from isobaric and the deviations were closely related to

the local turbulent stresses. This relation, as proposed by Townsend (51), can be represented by following relation:

$$\overline{p} + \rho\overline{(v')^2} = p_a \quad . \tag{2-13}$$

Despite this finding, they showed that Reichardt's simple error curve, equation (2-7) describes the velocity profile best. The velocity profile equation proposed by Görtler, equation (2-11) was compared with their experimental results. The distributions of $\overline{p}$, $\overline{(u')^2}$, $\overline{(v')^2}$ and τ are presented in their report.

Ginevskii (24) proposed a different approach to solve for the velocity distributions of incompressible, fully developed jets and wakes in the presence of longitudinal pressure gradients. He assumed a polynomial to represent the tangential stress as follows:

$$\tau = B_o + B_1 y + B_2 y^2 \quad . \tag{2-14}$$

The coefficients B_o, B_1, B_2 are determined by utilizing the boundary conditions at the axis and the edges of the jet in the x-direction equation of motion,

$$\rho u \frac{\partial u}{\partial x} + \rho v \frac{\partial u}{\partial y} + \frac{dp}{dx} = \frac{\partial \tau}{\partial y} \quad , \tag{2-15}$$

and combining the relations thus obtained with equation (2-14). The tangential stress so obtained is not connected with any assumptions regarding the mechanism of turbulence. By combining equation (2-14) with Prandtl's formula for tangential stress, equation (2-1), a new differential equation is obtained. For the case of mixing of a jet with a uniform stream, this differential equation was integrated with the aid of the boundary conditions at the jet centerline and the

external flow where the Bernoulli's equation is valid. The longitudinal pressure gradient term is not included in the velocity distribution equation so obtained, indicating that the existence of the longitudinal pressure gradient in the region of the jet mixing does not have any influence on the shape of the velocity profile. The work of Ginevskii has been applied in the work of Zumwalt and Ruo (56) for the case of constant pressure gradient mixing of a jet with a uniform stream, Fig. 1(c).

Pai (38) proposed a method to predict the velocity profiles of the constant pressure, compressible turbulent mixing of a jet with a uniform stream, Fig. 1(c), and the mixing of two uniform streams, Fig. 1(d). By using the method of small perturbations and the turbulent shear stress relation in equation (2-8), he reduced the equation of motion in the x-direction into a form similar to equation (2-6), that is, a form of the well-known equation of heat conduction. An exact solution was obtained by successive approximations starting with the solution of a small perturbation. The velocity distribution can be expressed in terms of Gaussian error integrals.

By using Pai's small perturbation method and the apparent kinematic viscosity relation in the form of equation (2-10), Korst, et al. (29) investigated the free jet boundary under constant pressure. They found that the velocity profile can be represented by

$$u = \frac{u_a}{2} (1 + \text{erf } \eta) , \qquad (2\text{-}16)$$

where u_a = free stream velocity and $\eta = \sigma\, y/x$. According to the experimental results, σ is approximately equal to 12 for an

incompressible flow.

Crane and Pack (16) and Crane (17) combined the equations for laminar and turbulent flows into one by introducing a coefficient of eddy kinematic viscosity in the turbulent flow case. They started with the stream function for laminar, incompressible flow, which yields a velocity distribution equation in the form of equation (2-11), and expanded it in a series in terms of the square of Mach number to include the effect of compressibility and large temperature differences for compressible flow cases. They pointed out that the net effect of compressibility is, respectively, to decrease and to increase the mixing width of laminar and turbulent free jets. The velocity profile for mixing of two uniform streams is tabulated in (17). For this case, the higher the Mach number the narrower the mixing region and the dimensionless velocity profile is same as that obtained in incompressible flow. The value of σ is found to be 12.7 for zero Mach number.

It has been shown by Maydew and Reed (33) that Crane's velocity profile for the half-jet fits extremely well with their measured velocity profile for an axi-symmetric compressible free jet.

Olson and Miller (37) conducted a great number of experiments on two-dimensional, turbulent, compressible (Mach number ranging from 0.66 to 2.0) free jets, wall jets, and reattaching jets, respectively, as shown in Figs. 1(a), 1(g) and 1(f). Corresponding theoretical investigations provided analytical models for those three types of jet flows, procedures for predicting the velocity profile development characteristics for free jets and wall jets, and a procedure for predicting the reattachment location and mean pressure in the

separation bubble for reattaching jets. Constant exchange coefficient mixing theory was used in both half-jet and fully developed jet regions for the free jet and wall jet. The correlation between theory and experiment was very good. The velocity profiles were represented adequately by a form similar to equation (2-7), the Gaussian mean velocity distribution which was derived originally for an incompressible flow. A method for predicting the centerline velocity decay for the free jet and the wall jet was also presented.

Sawyer (46), (47) and Bourque and Newman (8) carried out a series of experiments on the two-dimensional, incompressible, turbulent jet reattaching to a parallel and an inclined plate. By a simple analysis they were able to predict the mean pressure in the separation bubble and the location of jet reattachment. Though the jet is curved, no appreciable velocity deviation from that of a plane jet in the fully developed region was observed. Bourque and Newman (8) indicated that the flow becomes independent of the length of the plate and the Reynolds number when they are sufficiently large. The reattachment of a jet does not occur below a certain minimum Reynolds number; increasing the Reynolds number will cause the reattachment point to move nearer to the nozzle, but it becomes independent of Reynolds number above a value of approximately 10^4, the minimum value being approximately 10^3. Abbott and Kline (1) made a similar conclusion about the Reynolds number effect on the jet reattachment from their extensive experiments on the water table.

Analytical studies of jet mixing yield equations containing one or more constants which must be determined experimentally; the resulting equations for predicting velocity profiles and the turbulent

shear stresses are then empirical. One of those constants is the jet spreading parameter, σ. This parameter is a measure of the rate of increase of the width of the mixing zone in the downstream direction and its value is inversely proportional to the rate of increase of jet width.

According to Tollmien's experimental results, $\sigma = 12$; Crane found it to be 12.7. Maydew and Reed (33) used an axi-symmetric free jet to investigate the change of the σ value with respect to Mach number. By using Crane's velocity profile, they concluded that for subsonic flow the value of σ is 11.0 and somewhat higher for supersonic flow. Zumwalt and Tang (57) suggested the functional forms shown in equations (3-14) to estimate the value of σ for the error function velocity profile.

Channapragada (10) took into account the temperature ratio between the mixing fluids and presented a formula to evaluate σ in terms of Mach number. Bauer (6) used the error function velocity distribution, equation (2-16), for the jet boundary case and Prandtl's mixing length theory for both laminar and turbulent compressible mixing. He formulated the expressions for σ for laminar and turbulent mixing with the aid of Tollmien's experimental results.

Mueller and Olson (35), using their experimental results (37) and the Gaussian distribution of velocity, studied the spreading parameters of the outer and inner mixing zones of the compressible reattaching jet. For subsonic flow the value of σ for the outer mixing zone was about the same as that of the free jet but it was slightly higher for the inner mixing zone; for the region downstream

of reattachment σ is about twice as large as for the free jet mixing.

Roshko (44) used a 42 x 36 inch subsonic wind tunnel to conduct an experimental study of the flow over a cavity. The cavity opening was 4 x 32 inch and its depth was varied from 0 to 10 inches. He used a 75 fps flow velocity for most of his experiments but 210 fps was also used for the purpose of comparison. He observed that the pressures in the cavities with larger L/H_1 ratio, see Fig. 1(k), were higher than those with smaller L/H_1 ratio. He also observed that the jet would no longer reattach to the cavity floor if the L/H_1 ratio became less than 10. The general cavity pressure distribution observed was characterized by a low pressure near the center of the walls and floor and a high pressure at the corners. An intermittent pressure change which occurred at the center of the cavity for the $1.15 < L/H_1 < 2.0$ and $L/H_1 < 0.5$ ranges was also reported.

Charwat, et al. (14), (15), conducted an experimental study of both supersonic (Mach number 2 to 4) and subsonic boundary jets over rectangular cavities (L/H_1 from 1 to 15) in a 3 x 3 inch wind tunnel. Based on whether the flow reattached to the cavity floor or not, they classified a supersonic flow over a cavity in a solid boundary as one of two kinds. A long cavity, where there are two distinct separated regions, one behind the backward facing step and one ahead of the forward facing step, is called a "closed" cavity. A short cavity, where the jet does not reattach to the cavity floor, is called an "open" cavity. They also showed that the pressure distributions in the "open" cavity floor were quite uniform in the small L/H_1 cavity with a pressure minimum near the center. For the large L/H_1 cavity, the minimum moved towards the separation step

and the pressure gradient along the cavity floor increased as the recompression step was approached. The pressure distribution on the recompression face near the floor was fairly uniform but exhibited a gradient at the outer edge of the step. Generally, the higher the L/H_1 ratio, the higher the pressure on the recompression face. For subsonic flow, the cavity floor pressure distribution was very similar to that for supersonic flow.

Fox (20) also conducted an experimental study of the turbulent subsonic flow (160 to 600 fps) in transverse cavities (L/H_1 from 0.25 to 1.75) adjacent to a free stream in a 6 x 9 inch wind tunnel. Cavities spanned the 6-inch width of the tunnel. Based on his pressure distribution measurements, he found that for $L/H_1 \leq 1.25$ and $L/H_1 \geq 1.75$ the gradual change of pressure on the cavity walls was similar to those results obtained by other investigators, but for the cavity with L/H_1 near 1.50, the pressure changed abruptly and no agreement with others' results was found. He stated that this might be caused by the influence of the difference in the boundary layer thickness ahead of the cavities.

Tani, et al. (49) also showed that the maximum pressure on the face of the recompression step was at the top edge when $L/H_1 < 1.4$, but when $L/H_1 > 1.4$ it was slightly below the top edge.

Since high speed electronic computers became available, numerical methods have been used to solve the Navier-Stokes equations for certain laminar flow problems which cannot be solved by closed form analytical methods.

Kawaguti (28) solved a laminar, steady, viscous fluid flow in a channel with a step, Fig. 1(h) and (i), numerically. He assumed

the fluid velocity on the solid boundaries was zero and the flow in the channel far from the step was two-dimensional Poiseulle flow. He used central differences to transform the equations of motion into difference form and used $\Delta x/\Delta y = 2.0$. He pointed out that it became more difficult to integrate the equation for the case with a forward facing step than for the case with a backward facing step as the Reynolds number increased. Velocity distributions, streamlines and equivorticity lines were also shown in the report.

Fromm (23) proposed a method to calculate the flow properties in terms of stream function and vorticity. Time was advanced through the use of a finite difference approximation of the Helmholtz vorticity equation and the stream function was evaluated by a finite difference approximation of Poisson's equation by using the new vorticities obtained. Before advancing in time, the stream function was evaluated by a method of successive approximations over the whole field. A periodic end boundary method was used in the sample calculation of a viscous incompressible flow between two parallel flat plates with one obstacle. The vortex street in the wake of the obstacle was clearly represented. The pressure distribution was evaluated with an equation in the form of Poisson's equation obtained by combining the partial derivatives of the x-momentum equation with respect to x and the y-momentum equation with respect to y. He pointed out that calculation of pressure distributions directly from either of the momentum equations had not been successful.

Walker (55), in the course of investigating the interaction of a moving shock wave with a turbulent mixing region, by means of a numerical technique developed by Rusanov (45), was able to calculate

a supersonic (Mach number = 2.0), two-dimensional, free jet mixing in a double off-set confined space, Fig. 1(j). The continuity, momentum and energy equations in difference form were used to calculate density, velocities and pressure, respectively, at every net point in the field. Since the equations are time dependent it was necessary to carry out the computation until a near steady state was attained. In addition to the turbulent stresses, "blurring" terms were added to the governing equations to make a discontinuities in the fluid properties act as rapidly changing continuous ones. The velocity distributions in the fully developed region agreed very well with the Gaussian profile. Constant pressure lines in the flow field were also shown. Numerical stability of the technique was also discussed.

In solving fluid flow problems, there are usually two possible methods for describing the motion of fluids. First, the method of Euler, which describes the motions of fluids with reference to a fixed point of space and specifies at each instant of time the density, pressure, velocity, etc., of the fluid particle which happens to be at that point. Secondly, the method of Lagrange, which describes the history of individual fluid particles and specifies at each instant of time the location, density, pressure, velocity, etc., of the individual fluid particles of fixed identity.

In most problems Eulerian method proves to be more convenient in describing the fluid motion than the Lagrangian method; many investigators prefer to use the Eulerian method. However, when the Eulerian method is used to treat multi-specie flow problems numerically, it is difficult to keep track of the material interfaces as they move through an Eulerian mesh if the thin shells of the fluid move distances

many times greater than their original thickness. In order to attain good resolution, a large number of Eulerian mesh points may be needed. If the Lagrangian method were used alone, one might encounter a different kind of difficulty if the physical situation involved slip surfaces or other severe distortions of the original mesh. To overcome these difficulties, Harlow (26), Noh (36), and Frank and Lazarus (22) have proposed several combined Eulerian-Lagrangian methods. Some sample calculations of time-dependent, two-dimensional, compressible, inviscid, laminar flow past a rigid disk and over a rigid step have been successfully shown. For turbulent flow, the above methods do not seem to be generally useful at present; however they do appear to be very promising.

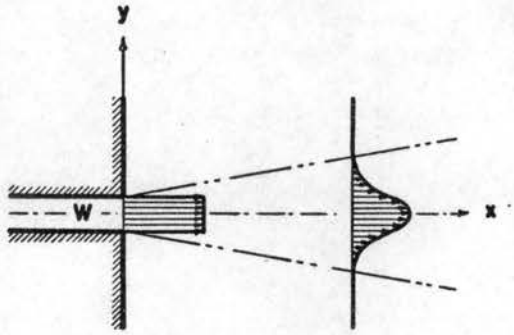

(a) Free Jet

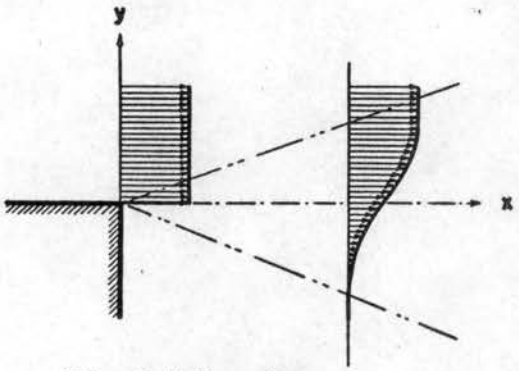

(b) Jet Boundary

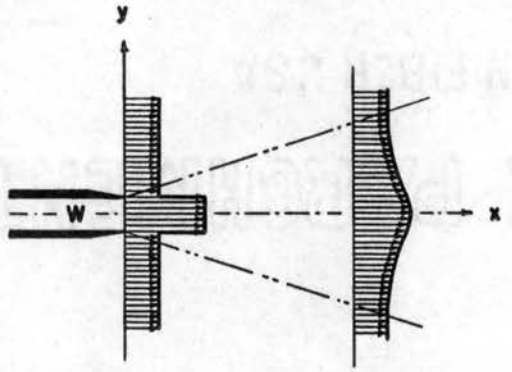

(c) Jet and a Uniform Stream

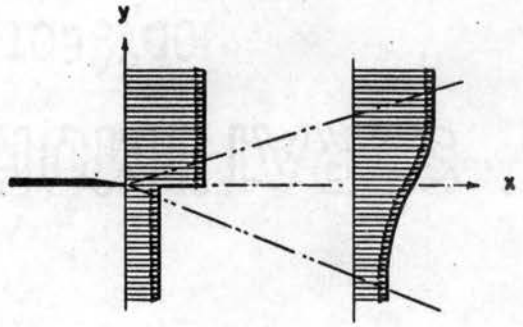

(d) Two Uniform Streams

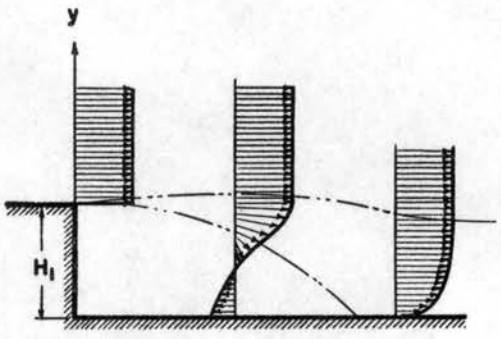

(e) Reattaching Stream

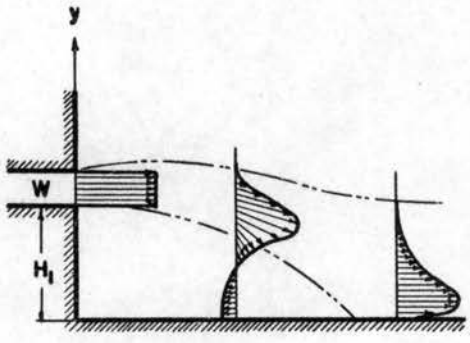

(f) Reattaching Jet

Figure 1. Typical Jet Mixing Configurations

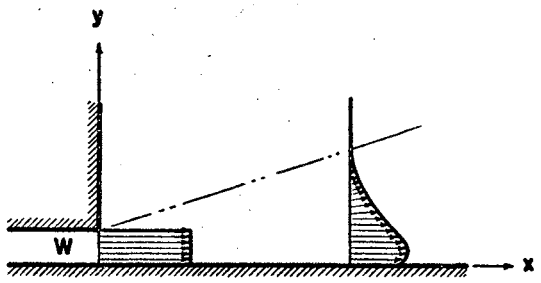

(g) Wall Jet

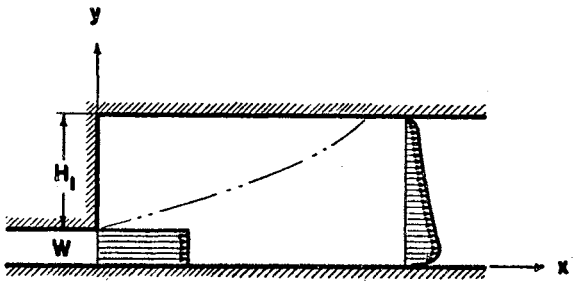

(h) Backward Facing Step

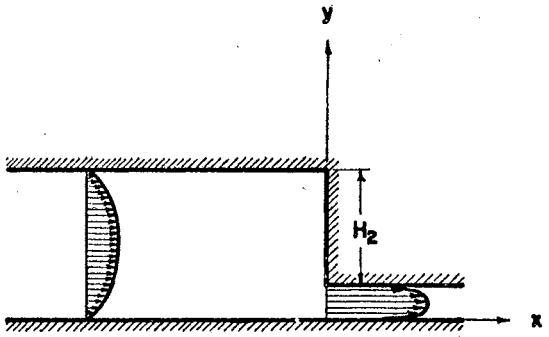

(i) Forward Facing Step

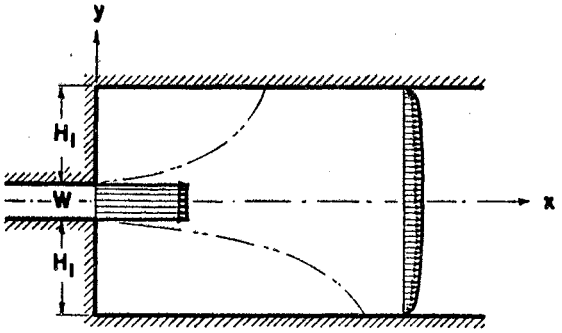

(j) Double Off-Set Jet

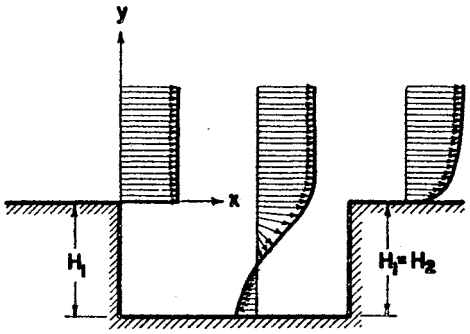

(k) Cavity Flow

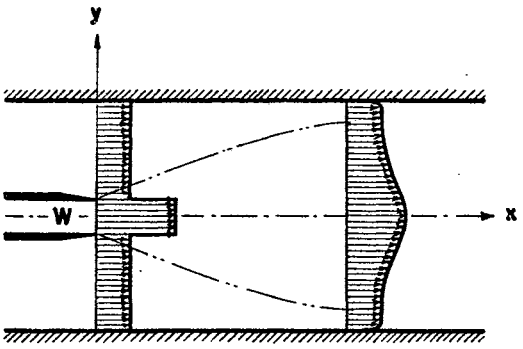

(l) Ejector

Figure 1. (Continued)

CHAPTER III

DERIVATION OF THE GOVERNING EQUATIONS

To represent a compressible flow, one needs the equation of continuity, the equations of motion and the equation of energy. The derivation of these fundamental equations is readily available from any standard fluid mechanics text book. For a turbulent flow with high Reynolds number the effect of molecular transport is negligible compared with the effect of turbulent transport. If the terms including the viscosity effect in the basic hydrodynamic equations are dropped, and it is further assumed that there are no body forces, one obtains the following equations for a two-dimensional, inviscid fluid flow.

Continuity:

$$\frac{\partial \rho}{\partial t} + \frac{\partial}{\partial x}(\rho u) + \frac{\partial}{\partial y}(\rho v) = 0$$

x-Momentum:

$$\frac{\partial}{\partial t}(\rho u) + \frac{\partial}{\partial x}(\rho u^2 + p) + \frac{\partial}{\partial y}(\rho v u) = 0$$

y-Momentum:

$$\frac{\partial}{\partial t}(\rho v) + \frac{\partial}{\partial x}(\rho u v) + \frac{\partial}{\partial y}(\rho v^2 + p) = 0 \qquad (3\text{-}1)$$

Energy:

$$\frac{\partial e}{\partial t} + \frac{\partial}{\partial x}\left[(e + p)u\right] + \frac{\partial}{\partial y}\left[(e + p)v\right] = 0 \ ,$$

where

$$e = \frac{p}{\gamma - 1} + \frac{\rho}{2}(u^2 + v^2) \ . \qquad (3\text{-}2)$$

Equations (3-1) may be written in conservation form as discussed by Tyler (52). The following general equation results:

$$\frac{\partial f}{\partial t} + \frac{\partial F^x}{\partial x} + \frac{\partial F^y}{\partial y} = 0, \tag{3-3}$$

where

$$f = \begin{bmatrix} \rho \\ \rho u \\ \rho v \\ e \end{bmatrix}, \quad F^x = \begin{bmatrix} \rho u \\ \rho u^2 + p \\ \rho uv \\ (e + p)u \end{bmatrix}, \quad F^y = \begin{bmatrix} \rho v \\ \rho vu \\ \rho v^2 + p \\ (e + p)v \end{bmatrix}. \tag{3-4}$$

Derivation of Governing Equations for Turbulent Flow

In the study of turbulence, Reynolds rules of averages are often adopted to carry out the averaging procedure, not only on single quantities but also on products of quantities. These rules, according to Pai (40), are as follows:

$$\begin{aligned} &\text{Rule 1:} && \overline{f + g} = \overline{f} + \overline{g} \\ &\text{Rule 2:} && \overline{cf} = c\overline{f} && (c = \text{constant}) \\ &\text{Rule 3:} && \overline{fg} = \overline{f}\,\overline{g} \\ &\text{Rule 4:} && \overline{\lim f_n} = \lim \overline{f}_n && (f_n = \text{sequence of function}), \end{aligned} \tag{3-5}$$

where f and g are scalar functions and the bar refers to the time average value.

Let the instantaneous fluid properties in the turbulent flow field be represented by the relation $f = \overline{f} + f'$. The prime quantity denotes the fluctuating term and

$$\overline{f} = \frac{1}{t} \int_{t_o}^{t_o + t} f\,dt .$$

From Rule 3 in equations (3-5), if g = 1, then $\overline{\overline{f}} = \overline{f}$. If this relation and Rule 1 are applied to the relation $f = \overline{f} + f'$, it is seen that the time average of the fluctuating component, $\overline{f'}$, is identical to zero. But it must be noted that the time average of the product of fluctuating components is not necessarily zero.

By using the above relations, the basic fluid properties for turbulent flow can be written in the following form:

$$\begin{aligned} \rho &= \overline{\rho} + \rho' \ , & u &= \overline{u} + u' \ , \\ p &= \overline{p} + p' \ , & v &= \overline{v} + v' \ , \\ e &= \overline{e} + e' \ . \end{aligned} \tag{3-6}$$

If the above relations are substituted into equations (3-1) the following set of equations are obtained (see Appendix A for detailed derivation),

Continuity:

$$\frac{\partial}{\partial t}\overline{\rho} + \frac{\partial}{\partial x}(\overline{\rho}\,\overline{u}) + \frac{\partial}{\partial y}(\overline{\rho}\,\overline{v}) = 0 \tag{3-7}$$

x-Momentum:

$$\frac{\partial}{\partial t}(\overline{\rho}\,\overline{u}) + \frac{\partial}{\partial x}\left[\overline{\rho}\,\overline{u}^2 + \overline{p} + \overline{\rho}\,\overline{u'^2}\right] + \frac{\partial}{\partial y}\left[\overline{\rho}\,\overline{v}\,\overline{u} + \overline{\rho}\,\overline{u'v'}\right] = 0$$

y-Momentum:

$$\frac{\partial}{\partial t}(\overline{\rho}\,\overline{v}) + \frac{\partial}{\partial x}\left[\overline{\rho}\,\overline{u}\,\overline{v} + \overline{\rho}\,\overline{u'v'}\right] + \frac{\partial}{\partial y}\left[\overline{\rho}\,\overline{v}^2 + \overline{p} + \overline{\rho}\,\overline{v'^2}\right] = 0$$

Energy:

$$\frac{\partial \overline{e}}{\partial t} + \frac{\partial}{\partial x}\left[(\overline{e} + \overline{p})\overline{u} + \overline{\rho}\,\overline{u}\,(\overline{u'})^2 + \overline{\rho}\,\overline{v}\,(\overline{u'v'})\right]$$

$$+ \frac{\partial}{\partial y}\left[(\overline{e} + \overline{p})\overline{v} + \overline{\rho}\,\overline{v}\,(\overline{v'})^2 + \overline{\rho}\,\overline{u}(\overline{u'v'})\right] = 0 \ ,$$

where

$$\overline{e} = \frac{\overline{p}}{\gamma - 1} + \frac{\overline{\rho}}{2}\left[\overline{u}^2 + \overline{v}^2 + (\overline{u'})^2 + (\overline{v'})^2\right] . \tag{3-8}$$

In place of viscous effects, turbulent effects appear in the momentum equations in equations (3-7). The effects of turbulence also appear in the energy equation. Schlichting (48) showed that those terms can be interpreted as components of a stress tensor due to the turbulent velocity components in two-dimensional flow and they can be represented by

$$\begin{pmatrix} \sigma_x & \tau_{xy} \\ \tau_{xy} & \sigma_y \end{pmatrix} = - \begin{pmatrix} \overline{\rho}\ \overline{(u')^2} & \overline{\rho}\ \overline{u'v'} \\ \overline{\rho}\ \overline{u'v'} & \overline{\rho}\ \overline{(v')^2} \end{pmatrix} . \tag{3-9}$$

They are often known as "apparent stresses of turbulent flow" or "Reynolds stresses". According to Schlichting (48), Boussinesq was first to introduce the idea of apparent kinematic viscosity, ϵ, which is analogous to the kinematic viscosity, ν. Similar to the shearing stress in laminar flow case, the representation of turbulent shearing stress may be written as

$$\tau_t = \overline{\rho}\ \overline{\epsilon}(x) \frac{\partial \overline{u}}{\partial y} . \tag{2-8}$$

In Prandtl's momentum transfer theory, the apparent kinematic viscosity, ϵ, is proportional to the slope of the mean velocity, $d\overline{u}/dy$. This can be seen by comparing equations (2-1) and (2-8). At the jet centerline where $d\overline{u}/dy = 0$, according to equation (2-8), ϵ is also equal to zero; this is incorrect. However, in analogy with Stokes' law, by simply replacing μ by $\overline{\rho}\ \overline{\epsilon}$, the Reynolds stresses can be expressed in the following form

$$\sigma_i = 2\ \overline{\rho}\ \overline{\epsilon} \left(\frac{\partial \overline{u}}{\partial x}\right)_i \tag{3-10}$$

$$\tau_{ij} = \overline{\rho}\ \overline{\epsilon} \left(\frac{\partial \overline{u}_i}{\partial x_j} + \frac{\partial \overline{u}_j}{\partial x_i}\right) . \tag{3-11}$$

Thus, the complete tensor of apparent turbulent stress for two-dimensional flow can be written by substituting equations (3-10) and (3-11) into equation (3-9); yielding

$$\begin{pmatrix} \sigma_x & \tau_{xy} \\ \tau_{xy} & \sigma_y \end{pmatrix} = \epsilon \begin{pmatrix} 2\bar{\rho}\dfrac{\partial \bar{u}}{\partial x} & \bar{\rho}\left(\dfrac{\partial \bar{u}}{\partial y} + \dfrac{\partial \bar{v}}{\partial x}\right) \\ \bar{\rho}\left(\dfrac{\partial \bar{u}}{\partial y} + \dfrac{\partial \bar{v}}{\partial x}\right) & 2\bar{\rho}\dfrac{\partial \bar{v}}{\partial y} \end{pmatrix} = -\begin{pmatrix} \overline{\rho(u')^2} & \overline{\rho\, u'v'} \\ \overline{\rho\, u'v'} & \overline{\rho(v')^2} \end{pmatrix}, \tag{3-12}$$

where $\bar{\epsilon}$, according to Pai (39), can be represented by

$$\bar{\epsilon} = \frac{\bar{u}_a x}{2\sigma^2} \quad , \tag{3-13}$$

in which, $\bar{u}_a$ is the velocity of the free stream adjacent to the mixing zone, x is the distance from the point where mixing starts, and σ is the jet spreading parameter used in equation (2-16). The values of σ can be obtained from the following relationship as suggested by Zumwalt and Tang (57):

$$\begin{aligned} &\sigma = 11.0 \quad \text{for} \quad C_a^2 < 0.23 \qquad (0 < M_a < 1.23) \\ &\sigma = 47.1\, C_a^2 \quad \text{for} \quad C_a^2 > 0.23 \qquad (M_a > 1.23), \end{aligned} \tag{3-14}$$

where C_a is Crocco number and is represented by

$$C_a^2 = \frac{M_a^2}{\dfrac{2}{\gamma - 1} + M_a^2} \quad .$$

If the relations in equation (3-12) are substituted into equations (3-7) and those equations written in the general conservation form of equation (3-3), equations (3-4) become

$$f = \begin{bmatrix} \bar{\rho} \\ \bar{\rho}\,\bar{u} \\ \bar{\rho}\,\bar{v} \\ \bar{e} \end{bmatrix}$$

$$F^x = \begin{bmatrix} \bar{\rho}\,\bar{u} \\ \bar{\rho}\,\bar{u}^2 + \bar{p} - 2\,\bar{\rho}\,\bar{\epsilon}\,\dfrac{\partial \bar{u}}{\partial x} \\ \bar{\rho}\,\bar{u}\,\bar{v} - \bar{\rho}\,\bar{\epsilon}\left(\dfrac{\partial \bar{u}}{\partial y} + \dfrac{\partial \bar{v}}{\partial x}\right) \\ (\bar{e} + \bar{p})\bar{u} - 2\,\bar{\rho}\,\bar{u}\,\bar{\epsilon}\,\dfrac{\partial \bar{u}}{\partial x} - \bar{\rho}\,\bar{v}\,\bar{\epsilon}\left(\dfrac{\partial \bar{u}}{\partial y} + \dfrac{\partial \bar{v}}{\partial x}\right) \end{bmatrix} \qquad (3\text{-}15)$$

$$F^y = \begin{bmatrix} \bar{\rho}\,\bar{v} \\ \bar{\rho}\,\bar{v}\,\bar{u} - \bar{\rho}\,\bar{\epsilon}\left(\dfrac{\partial \bar{u}}{\partial y} + \dfrac{\partial \bar{v}}{\partial x}\right) \\ \bar{\rho}\,\bar{v}^2 + \bar{p} - 2\,\bar{\rho}\,\bar{\epsilon}\,\dfrac{\partial \bar{v}}{\partial y} \\ (\bar{e} + \bar{p})\bar{u} - 2\,\bar{\rho}\,\bar{v}\,\bar{\epsilon}\,\dfrac{\partial \bar{v}}{\partial y} - \bar{\rho}\,\bar{u}\,\bar{\epsilon}\left(\dfrac{\partial \bar{u}}{\partial y} + \dfrac{\partial \bar{v}}{\partial x}\right) \end{bmatrix},$$

where $$\bar{e} = \frac{\bar{p}}{\gamma - 1} + \frac{\bar{\rho}}{2}\left[\bar{u}^2 + \bar{v}^2 - 2\,\bar{\epsilon}\left(\frac{\partial \bar{u}}{\partial y} + \frac{\partial \bar{v}}{\partial x}\right)\right]. \qquad (3\text{-}16)$$

In order to write equations (3-15) in a dimensionless form, the pressure $\bar{p}_{noz}$ and density $\bar{\rho}_{noz}$ at the nozzle exit, $a = \left(\bar{p}_{noz}/\bar{\rho}_{noz}\right)^{1/2}$, $h_2 = \Delta y$ and h_2/a will be used as references to normalize, respectively, pressure, density, velocity, distance and time. They are

$$\bar{p}^* = \frac{\bar{p}}{\bar{p}_{noz}}, \quad \bar{\rho}^* = \frac{\bar{\rho}}{\bar{\rho}_{noz}}, \quad \bar{u}^* = \frac{\bar{u}}{a},$$

$$\bar{v}^* = \frac{\bar{v}}{a}, \quad x^* = \frac{x}{h_2}, \quad y^* = \frac{y}{h_2}, \qquad (3\text{-}17)$$

$$t^* = \frac{ta}{h_2},$$

where the superscript * represents the dimensionless quantity of each corresponding variable. After substituting equations (3-17)

into equations (3-15) and making some rearrangements, one can obtain a set of equations identical to equations (3-15) in dimensionless form and the superscript * can be dropped. It is important to note that if one wants to obtain an exactly identical set of equations in both dimensional and dimensionless form, no other reference velocity can be used than the square root of the quotient of the reference pressure and reference density.

Derivation of Governing Finite Difference Equations

The governing equations derived in previous sections are non-linear partial differential equations and are to be solved by a numerical method. In solving inviscid flow problems involving sudden changes of fluid properties in the flow field, von Neumann (54) altered the inviscid flow equations by adding artificial viscosity terms, so called "blurring" terms, to make discontinuities of the fluid properties become continuous ones in the course of computation. A method with the concept of "blurring" introduced by Rusanov (45) was adopted in this study. If the blurring terms are added to the general first order, non-linear partial differential equation in conservation form, that is equation (3-3), the following equation is obtained:

$$\frac{\partial f}{\partial t} + \frac{\partial F^x}{\partial x} + \frac{\partial F^y}{\partial y} = \frac{\partial}{\partial x}\left[A(x,y,t)\,\frac{\partial f}{\partial x}\right] + \frac{\partial}{\partial y}\left[B(x,y,t)\,\frac{\partial f}{\partial y}\right]. \qquad (3\text{-}18)$$

In writing equation (3-18) in a difference form, forward differences are used for the time derivative and central differences for the spatial derivatives, so that the new f value can be evaluated explicitly from the old values of f, F^x and F^y.

A rectangular net with steps $\Delta x = h_1$ and $\Delta y = h_2$ as shown in Fig. 2 is used and the time increment is denoted by τ. Any quantity f at point (m,ℓ) and the n^{th} time plane or time step is designated by $f^n_{m,\ell}$. After writing equation (3-18) in difference form and rearranging, the following explicit equation is obtained:

$$f^{n+1}_{m,\ell} = f^n_{m,\ell} - \frac{\tau}{2h_1}\left[F^x_{m+1,\ell} - F^x_{m-1,\ell}\right]^n - \frac{\tau}{2h_2}\left[F^y_{m,\ell+1} - F^y_{m,\ell-1}\right]^n$$

$$+ \frac{\tau}{h_1^2}\left[A_{m+\frac{1}{2},\ell}\,(f_{m+1,\ell} - f_{m,\ell}) - A_{m-\frac{1}{2},\ell}(f_{m,\ell} - f_{m-1,\ell})\right]^n$$

$$+ \frac{\tau}{h_2^2}\left[B_{m,\ell+\frac{1}{2}}(f_{m,\ell+1} - f_{m,\ell}) - B_{m,\ell-\frac{1}{2}}(f_{m,\ell} - f_{m,\ell-1})\right]^n . \tag{3-19}$$

Rusanov (45) simplified equation (3-19) by assuming

$$A^n_{m,\ell} = \frac{h_1^2}{2\tau}\,\alpha^n_{m,\ell}$$

$$B^n_{m,\ell} = \frac{h_2^2}{2\tau}\,\beta^n_{m,\ell} , \tag{3-20}$$

and

$$K = \frac{(h_1^2 + h_2^2)^{1/2}}{h_1 h_2}\,\tau ,$$

where

$$\alpha^n_{m,\ell} = \omega K\,(w + c)^n_{m,\ell}\,\sin^2\chi$$

$$\beta^n_{m,\ell} = \omega K\,(w + c)^n_{m,\ell}\,\cos^2\chi . \tag{3-21}$$

The blurring parameter ω is related to K and $(w + c)^n_{m,\ell}$ by the stability condition

$$K^2\left[(w + c)^n_{m,\ell}\right]^2 \le \omega K\,(w + c)^n_{m,\ell} \le 1 , \tag{3-22}$$

which, according to Rusanov, must be satisfied for all (m,ℓ). The quantity $K(w + c)^n_{m,\ell}$ in equation (3-22) is the Courant number at

$$\chi = \tan^{-1} \frac{h_2}{h_1}$$

$$h = (h_1^2 + h_2^2)^{1/2}$$

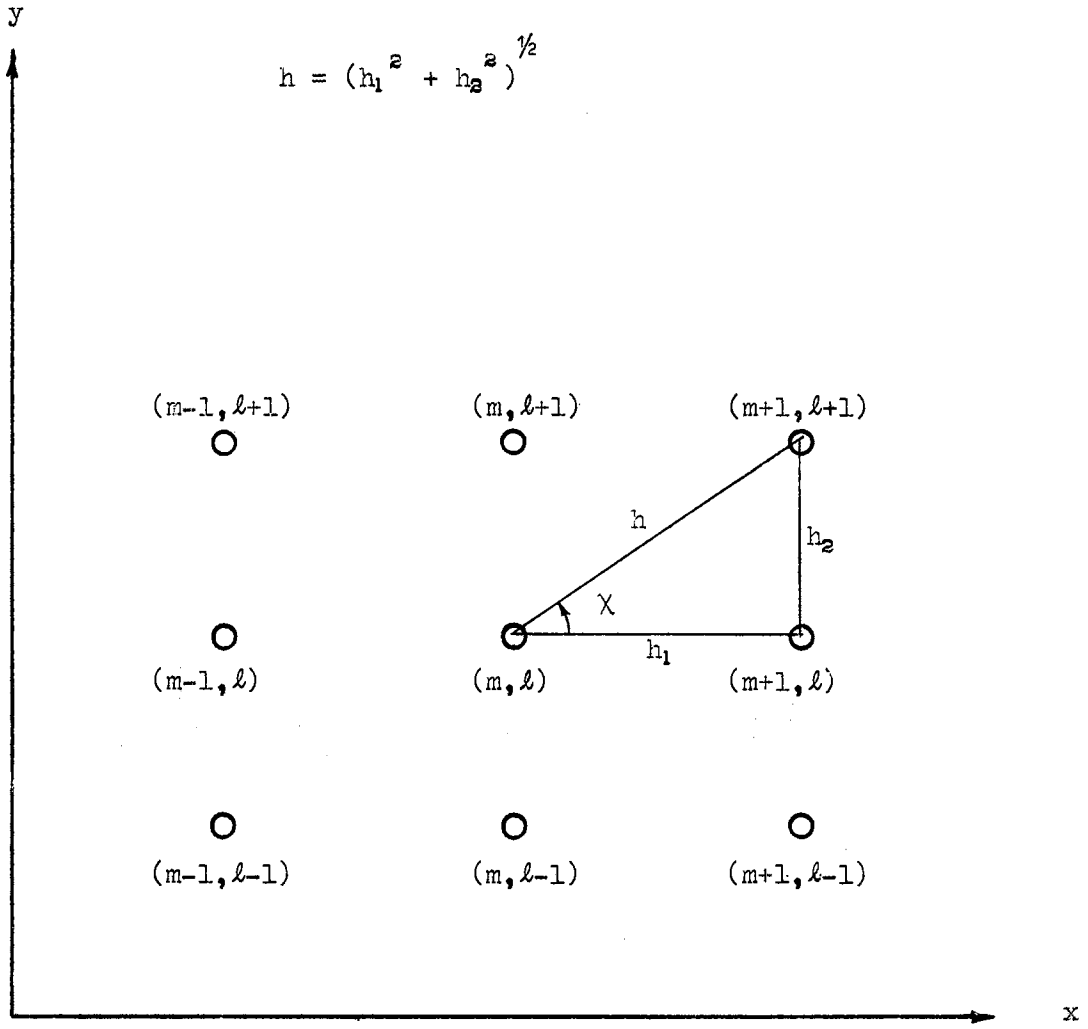

Figure 2. Net Point Notation

point (m,ℓ) of the n^{th} time plane and is designated by $\sigma^n_{m,\ell}$. If σ^r_o represents the maximum allowable Courant number in the flow field under consideration at the n^{th} time plane, then

$$\sigma^n_o = K\ (w + c)^n_{max}\ , \tag{3-23}$$

where σ^n_o is a measure of the time increment. If the blurring parameter ω is chosen according to the relation

$$\sigma^n_o \leq \omega \leq \frac{1}{\sigma^n_o}\ , \tag{3-24}$$

the condition of equation (3-22) is automatically satisfied. Equation (3-24), however, is for the inviscid fluid flow case. It was mentioned by Walker (55) that the lowest acceptable value of ω is about one-tenth of the value calculated from equation (3-24) for a turbulent supersonic jet mixing case. In general, the value of $(w + c)^n_{max}$ differs slightly from time plane to time plane and has to be evaluated in every time plane computation to determine the maximum allowable time increment for the following time step. Walker found this change to be very small, even in a supersonic flow field; this suggests that a constant time step be used at all time.

In the case of a low speed flow, which is the case of interest in this study, the speed of sound, c, is considerably greater than the fluid velocity and stays fairly constant throughout the field since the temperature in the flow field does not change significantly. The quantity $(w + c)$ in the flow field under consideration at any time may be regarded as a constant. Thus, a constant time increment, τ, is used. By the same reasoning, $A(x,y,t)$ and $B(x,y,t)$ in equation (3-18) or equation (3-19) also can be considered as

constants. If the relation of K with σ_o^n and $(w + c)_{max}^n$ is found from equation (3-23) and substituted in equations (3-21), the expressions for $\alpha_{m,\ell}^n$ and $\beta_{m,\ell}^n$, respectively, become

$$\alpha = \omega\sigma_o \sin^2 \chi$$
$$\beta = \omega\sigma_o \cos^2 \chi \ . \tag{3-25}$$

Notice that the superscript n and subscripts m,ℓ are discarded because the values of α and β are no longer dependent on space and time due to the assumption made above. By substituting equations (3-25) into equations (3-20) and introducing the simplified expressions for A and B into equation (3-19), the general explicit difference equation assumes the following form:

$$f_{m,\ell}^{n+1} = f_{m,\ell}^n - \frac{\tau}{2h_1}\left[F_{m+1,\ell}^x - F_{m-1,\ell}^x\right] - \frac{\tau}{2h_2}\left[F_{m,\ell+1}^y - F_{m,\ell-1}^y\right]$$
$$+ \frac{1}{2}\omega\sigma_o \left[(f_{m+1,\ell} - 2f_{m,\ell} + f_{m-1,\ell}) \sin^2 \chi\right.$$
$$\left. + (f_{m,\ell+1} - 2f_{m,\ell} + f_{m,\ell-1}) \cos^2 \chi\right] . \tag{3-26}$$

This general difference equation is valid for the net points lying inside the flow field, i.e., the "interior points".

Representation of Field and Boundary Points

The general difference equation for a two-dimensional, turbulent jet flow, equation (3-26), can be used directly for the interior points of the flow field if the net point in question has only those neighboring points shown in Fig. 2. All quantities needed to estimate the value of the right hand side of equation (3-26) are

readily available from the computed results of the previous time plane. Whereas for those points on the solid boundary or the edge of the flow field under study, equation (3-26) has to be modified slightly or some quantities which are not available from the previous time plane computation have to be assumed according to the boundary conditions. For those points on the solid wall or the plane of symmetry, the following conditions are assumed

$$\frac{\partial \bar{\rho}}{\partial N} = \frac{\partial \bar{p}}{\partial N} = 0,$$

$$\frac{\partial \bar{u}}{\partial N} = 0 \quad \text{and} \quad \bar{v} = 0 \quad \text{for boundary parallel to x-axis,}$$

$$\frac{\partial \bar{v}}{\partial N} = 0 \quad \text{and} \quad \bar{u} = 0 \quad \text{for boundary parallel to y-axis,}$$

where N denotes the direction normal to the boundary under consideration.

The relationship of the interior net point to its neighboring points is shown in Fig. 2. The representations of those points on the different walls are illustrated in Fig. 3. The method used is based upon a reflection technique suggested by Burstein (9). This considers the boundary as a mirror; the image of any interior point has essentially the same properties as the object interior point except the direction perpendicular to the mirror is opposite in sense. Besides the relation of a point to its neighboring points shown in Fig. 2, other representations, such as shown in Figs. 7(a), (c), and (d), are also used. If the relation shown in Fig. 7(d) is used, the representations of the boundary points have to be modified accordingly.

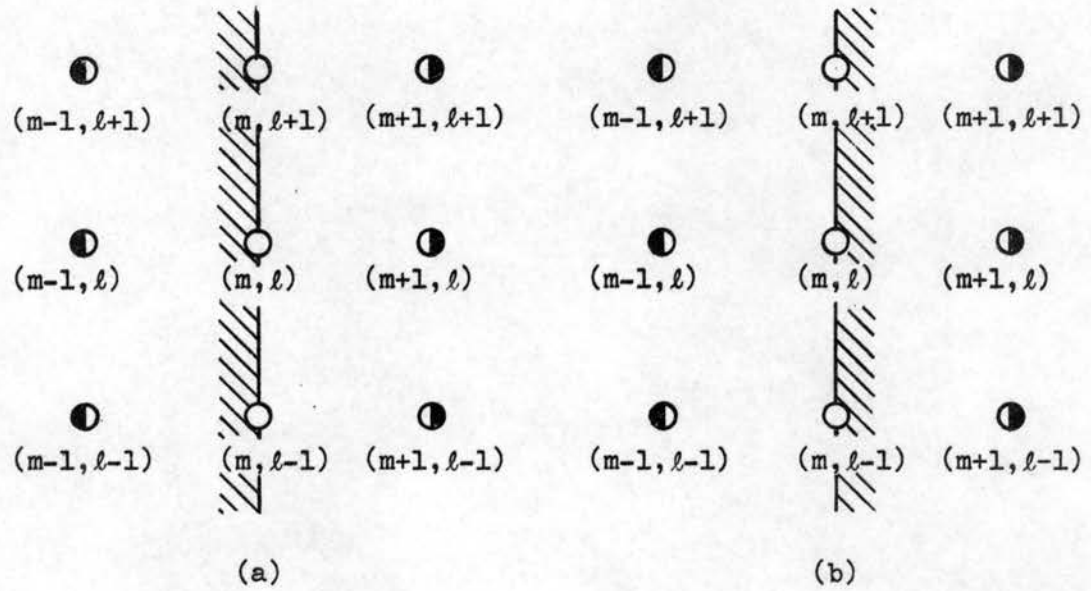

$$
\begin{aligned}
\rho(m-1,\ell+1) &= \rho(m+1,\ell+1) \\
u(m-1,\ell+1) &= -u(m+1,\ell+1) \\
v(m-1,\ell+1) &= v(m+1,\ell+1) \\
p(m-1,\ell+1) &= p(m+1,\ell+1)
\end{aligned}
$$

$$
\begin{aligned}
\rho(m-1,\ell) &= \rho(m+1,\ell) \\
u(m-1,\ell) &= -u(m+1,\ell) \\
v(m-1,\ell) &= v(m+1,\ell) \\
p(m-1,\ell) &= p(m+1,\ell)
\end{aligned}
$$

$$
\begin{aligned}
\rho(m-1,\ell-1) &= \rho(m+1,\ell-1) \\
u(m-1,\ell-1) &= -u(m+1,\ell-1) \\
v(m-1,\ell-1) &= v(m+1,\ell-1) \\
p(m-1,\ell-1) &= p(m+1,\ell-1)
\end{aligned}
$$

$$
\begin{aligned}
\rho(m+1,\ell+1) &= \rho(m-1,\ell+1) \\
u(m+1,\ell+1) &= -u(m-1,\ell+1) \\
v(m+1,\ell+1) &= v(m-1,\ell+1) \\
p(m+1,\ell+1) &= p(m-1,\ell+1)
\end{aligned}
$$

$$
\begin{aligned}
\rho(m+1,\ell) &= \rho(m-1,\ell) \\
u(m+1,\ell) &= -u(m-1,\ell) \\
v(m+1,\ell) &= v(m-1,\ell) \\
p(m+1,\ell) &= p(m-1,\ell)
\end{aligned}
$$

$$
\begin{aligned}
\rho(m+1,\ell-1) &= \rho(m-1,\ell-1) \\
u(m+1,\ell-1) &= -u(m-1,\ell-1) \\
v(m+1,\ell-1) &= v(m-1,\ell-1) \\
p(m+1,\ell-1) &= p(m-1,\ell-1)
\end{aligned}
$$

Figure 3. Representation of Solid Boundary Points

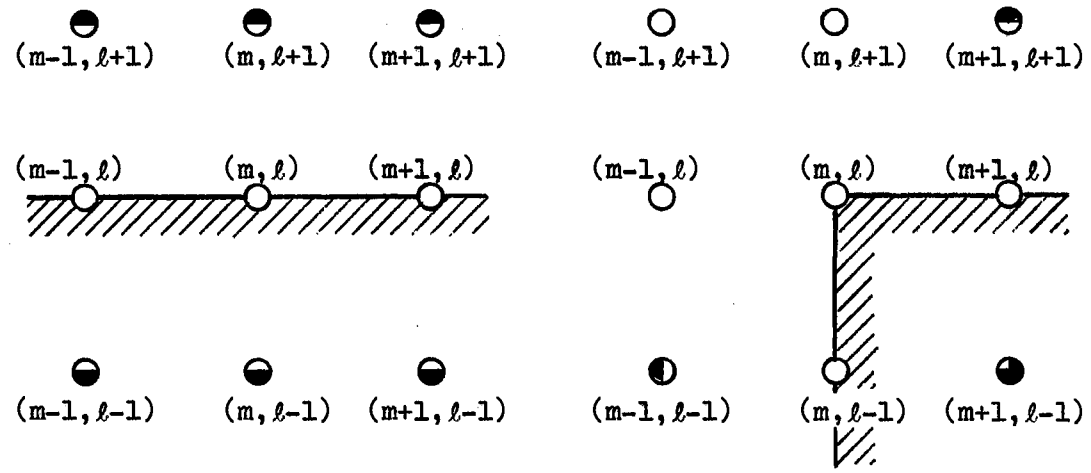

$\rho(m-1,\ell-1) = \rho(m-1,\ell+1)$
$u(m-1,\ell-1) = u(m-1,\ell+1)$
$v(m-1,\ell-1) = -v(m-1,\ell+1)$
$p(m-1,\ell-1) = p(m-1,\ell+1)$

$\rho(m,\ell-1) = \rho(m,\ell+1)$
$u(m,\ell-1) = u(m,\ell+1)$
$v(m,\ell-1) = -v(m,\ell+1)$
$p(m,\ell-1) = p(m,\ell+1)$

$\rho(m+1,\ell-1) = \rho(m+1,\ell+1)$
$u(m+1,\ell-1) = u(m+1,\ell+1)$
$v(m+1,\ell-1) = -v(m+1,\ell+1)$
$p(m+1,\ell-1) = p(m+1,\ell+1)$

$\rho(m+1,\ell-1) = \rho(m-1,\ell-1)$
$u(m+1,\ell-1) = -u(m-1,\ell-1)$
$v(m+1,\ell-1) = v(m-1,\ell-1)$
$p(m+1,\ell-1) = p(m-1,\ell-1)$

Figure 3. (Continued)

$$F^y = \begin{bmatrix} \bar{v} \\ \bar{u}\,\bar{v} - \bar{\epsilon}\left(\frac{\partial \bar{u}}{\partial y} + \frac{\partial \bar{v}}{\partial x}\right) \\ \bar{v}^2 + \bar{p} - 2\,\bar{\epsilon}\,\frac{\partial \bar{v}}{\partial y} \\ (\bar{e} + \bar{p})\bar{v} - 2\,\bar{v}\,\bar{\epsilon}\,\frac{\partial \bar{v}}{\partial y} - \bar{u}\,\bar{\epsilon}\left(\frac{\partial \bar{u}}{\partial y} + \frac{\partial \bar{v}}{\partial x}\right) \end{bmatrix}, \tag{4-1}$$

and

$$\bar{e} = \frac{\bar{p}}{\gamma - 1} + \frac{1}{2}\left[\bar{u}^2 + \bar{v}^2 - 2\bar{\epsilon}\left(\frac{\partial \bar{u}}{\partial x} + \frac{\partial \bar{v}}{\partial y}\right)\right]. \tag{4-2}$$

Although equations (4-1) are said to be valid for incompressible flow, it must be borne in mind that the fluid still has to obey the perfect gas law, otherwise the specific energy cannot be represented by equation (3-2).

There are four equations in (4-1) but the number of unknowns is three; therefore, only three equations from (4-1) or some corresponding supplementary equations are needed to compute the necessary properties $\bar{u}$, $\bar{v}$, and $\bar{p}$. If the general difference equation form, as given in equation (3-26), is used, it is necessary to select the last three equations in (4-1). Generally, for incompressible flow only the continuity and the two momentum equations are needed. Other possible combinations of three-equation sets are listed in Table I.

In the early stages of this study, the expression used for the turbulent shearing stresses was the same as that used by Walker (55). In analogy to equation (2-8), he wrote

$$\tau_{ij} = \bar{\rho}\,\bar{\epsilon}\,\frac{\partial u_j}{\partial x_i}. \tag{4-3}$$

TABLE I

SELECTIONS OF THREE-EQUATION SET

Variable \ Equation Set	1	2	3	4	5	6	7
$\overline{u}^{n+1}$	M_x	M_x	M_x	M_x	M_x	M_x	M_x
$\overline{v}^{n+1}$	M_y	C	C	M_y	C	M_y	C
$\overline{p}^{n+1}$	E	E	M_y	$\frac{D\overline{p}}{Dt} = 0$	$\frac{D\overline{p}}{Dt} = 0$	$\nabla^2\overline{p} = -\overline{Q}$	$\nabla^2\overline{p} = -\overline{Q}$

NOTATION:

M_x ——— momentum equation in x-direction

M_y ——— momentum equation in y-direction

C ——— continuity equation

E ——— energy equation

$\frac{D\overline{p}}{Dt} = 0$ ——— equation (4-11)

$\nabla^2\overline{p} = -\overline{Q}$ ——— equation (4-15)

and if $j = i$, $\tau_{ii} = \sigma_i$. If this relation is used in place of equations (3-10) and (3-11) to represent the turbulent shearing and normal stresses, one obtains a set of equations similar to equations (4-1) as follows:

$$f = \begin{bmatrix} 0 \\ \bar{u} \\ \bar{v} \\ \bar{e} \end{bmatrix}$$

$$F^x = \begin{bmatrix} \bar{u} \\ \bar{u}^2 + \bar{p} - \bar{\epsilon}\dfrac{\partial \bar{u}}{\partial x} \\ \bar{v}\,\bar{u} - \bar{\epsilon}\dfrac{\partial \bar{v}}{\partial x} \\ (\bar{e} + \bar{p})\bar{u} - \bar{\epsilon}\left(\bar{u}\dfrac{\partial \bar{u}}{\partial x} + \bar{v}\dfrac{\partial \bar{v}}{\partial x}\right) \end{bmatrix} \qquad (4\text{-}4)$$

$$F^y = \begin{bmatrix} \bar{v} \\ \bar{u}\,\bar{v} - \bar{\epsilon}\dfrac{\partial \bar{u}}{\partial y} \\ \bar{v}^2 + \bar{p} - \bar{\epsilon}\dfrac{\partial \bar{v}}{\partial y} \\ (\bar{e} + \bar{p})\bar{v} - \bar{\epsilon}\left(\bar{u}\dfrac{\partial \bar{u}}{\partial y} + \bar{v}\dfrac{\partial \bar{v}}{\partial y}\right) \end{bmatrix} ,$$

and

$$\bar{e} = \frac{\bar{p}}{\gamma - 1} + \frac{1}{2}\left[\bar{u}^2 + \bar{v}^2 - \bar{\epsilon}\left(\frac{\partial \bar{u}}{\partial x} + \frac{\partial \bar{v}}{\partial y}\right)\right] . \qquad (4\text{-}5)$$

In place of the forms shown in equations (4-4), the momentum and energy equations may be written in following forms:

x-Momentum: (4-6)

$$\frac{\partial \bar{u}}{\partial t} + \left[2\bar{u}\frac{\partial \bar{u}}{\partial x} + \frac{\partial \bar{p}}{\partial x} - \bar{\epsilon}\frac{\partial^2 \bar{u}}{\partial x^2}\right] + \left[\bar{u}\frac{\partial \bar{v}}{\partial y} + \bar{v}\frac{\partial \bar{u}}{\partial y} - \bar{\epsilon}\frac{\partial^2 \bar{v}}{\partial y^2}\right] = 0$$

y-Momentum:

$$\frac{\partial \bar{v}}{\partial t} + \left[\bar{u}\frac{\partial \bar{v}}{\partial x} + \bar{v}\frac{\partial \bar{u}}{\partial x} - \bar{\epsilon}\frac{\partial^2 \bar{v}}{\partial x^2}\right] + \left[2\bar{v}\frac{\partial \bar{v}}{\partial y} + \frac{\partial \bar{p}}{\partial y} - \bar{\epsilon}\frac{\partial^2 \bar{v}}{\partial y^2}\right] = 0 \qquad (4\text{-}7)$$

Energy:

$$\frac{\partial \bar{e}}{\partial t} + (\bar{e} + \bar{p})\frac{\partial \bar{u}}{\partial x} + \bar{u}\frac{\partial}{\partial x}(\bar{e} + \bar{p}) - \bar{\epsilon}\left[\bar{u}\frac{\partial^2 \bar{u}}{\partial x^2} + \bar{v}\frac{\partial^2 \bar{v}}{\partial x^2} + \left(\frac{\partial \bar{u}}{\partial x}\right)^2 + \left(\frac{\partial \bar{v}}{\partial x}\right)^2\right] \qquad (4\text{-}8)$$

$$+ (\bar{e} + \bar{p})\frac{\partial \bar{v}}{\partial y} + \bar{v}\frac{\partial}{\partial y}(\bar{e} + \bar{p}) - \bar{\epsilon}\left[\bar{u}\frac{\partial^2 \bar{u}}{\partial y^2} + \bar{v}\frac{\partial^2 \bar{v}}{\partial y^2} + \left(\frac{\partial \bar{u}}{\partial y}\right)^2 + \left(\frac{\partial \bar{v}}{\partial y}\right)^2\right] = 0$$

or

$$\frac{\partial \bar{e}}{\partial t} + \frac{\partial}{\partial x}[(\bar{e} + \bar{p})\bar{u}] + \frac{\partial}{\partial y}[(\bar{e} + \bar{p})\bar{v}]$$

$$- \bar{\epsilon}\left[\bar{u}\left(\frac{\partial^2 \bar{u}}{\partial x^2} + \frac{\partial^2 \bar{u}}{\partial y^2}\right) + \bar{v}\left(\frac{\partial^2 \bar{v}}{\partial x^2} + \frac{\partial^2 \bar{v}}{\partial y^2}\right) + \left(\frac{\partial \bar{u}}{\partial x}\right)^2 + \left(\frac{\partial \bar{v}}{\partial x}\right)^2\right.$$

$$\left. + \left(\frac{\partial \bar{u}}{\partial y}\right)^2 + \left(\frac{\partial \bar{v}}{\partial y}\right)^2\right] = 0 . \qquad (4\text{-}9)$$

Equations (4-6) through (4-9) were also used in some of the computations, but the general difference equation for the equations in conservation form, equation (3-26), cannot be used directly. A difference equation was written for each individual equation.

Representation of Initial Conditions

A two-dimensional, low speed, turbulent jet issuing from a nozzle into a cavity was considered. The general configuration of the cavity is shown in Fig. 4. All the properties of the fluid at the nozzle were held constant. In Fig. 4, region ① was assumed initially to have the same velocity as the nozzle exit and regions ② was assumed to be stationary; the dimensionless pressure was assumed to be unity in whole flow field. The representation of the

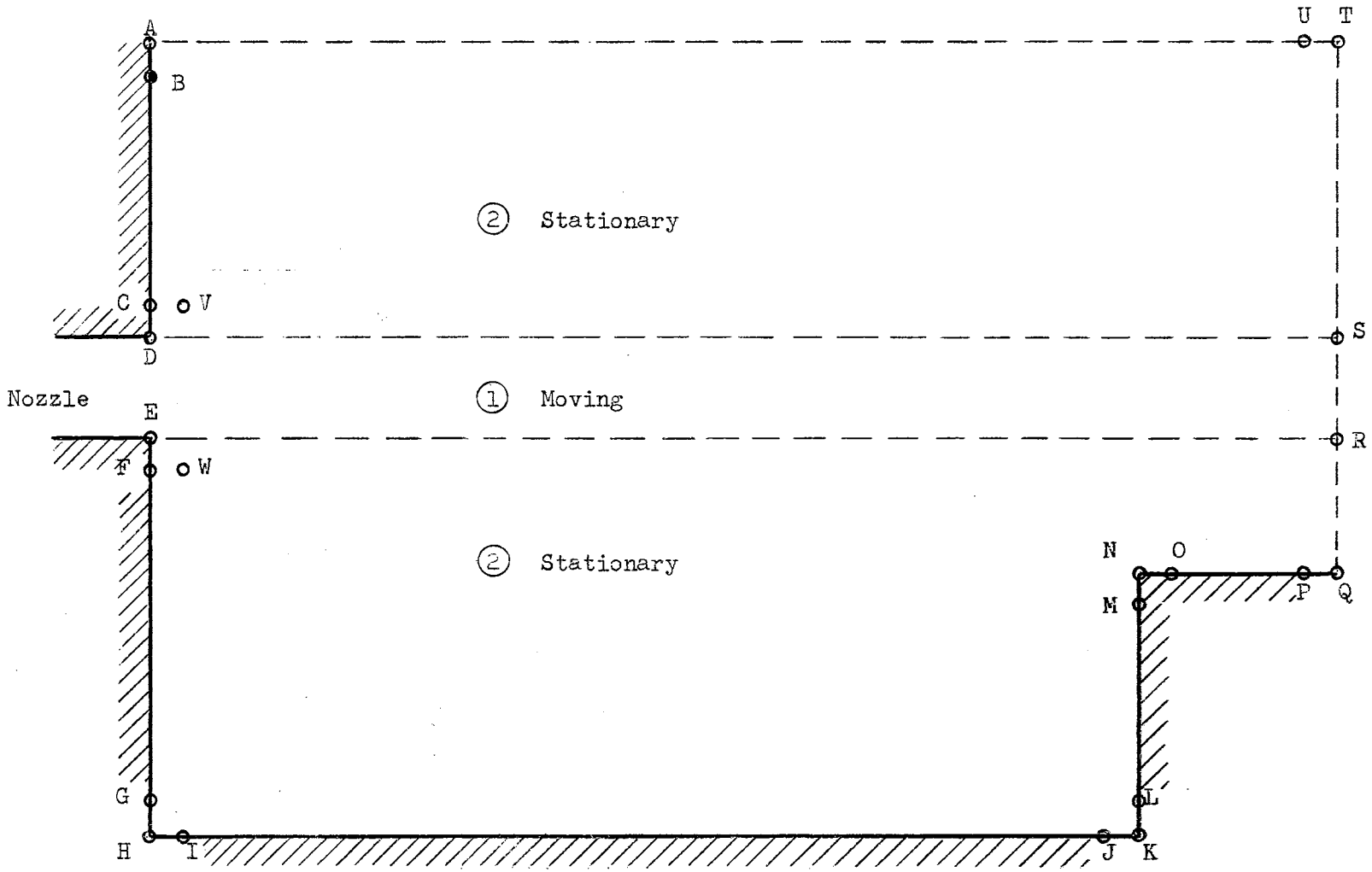

Figure 4. General Configuration of Initial Flow Field and Some Special Boundary Points

initial conditions was immaterial because the asymptotic values of the computed results were mainly dependent on the boundary conditions specified. However, a better representation of initial conditions may shorten the computation time. The initial conditions of some sample points are shown in Fig. 5; those points without velocity vectors are stationary.

Representations of Some Special Boundary Conditions

In addition to the boundary conditions shown in Fig. 3, there are still some other boundaries which need special treatment, such as the corner points and the field boundary points. Some special boundary points are shown in Fig. 4.

The relationship between a point on the solid boundary and its surrounding points is shown in Fig. 3. At those points on the solid walls the flow may be considered either slipping or stagnating on the walls. Slip flow was allowed on walls IJ, LM and OQ in Fig. 4. Both slipping flow and stagnating flow on walls AC and FG were considered. The velocity at corner points H and K was assumed to be zero. The corner point N was considered as one of the field points, this was done so that the fluid would not be forced to stagnate at the corner point N. Because of the cavity, the main jet will bend toward the cavity and the stagnation point may change according to the geometry.

For those points on the field boundaries, AU and QT in Fig. 4, the general technique cannot be applied due to the lack of information of the surrounding points. Some special method has to be used to provide the best estimated information on those boundaries, so that

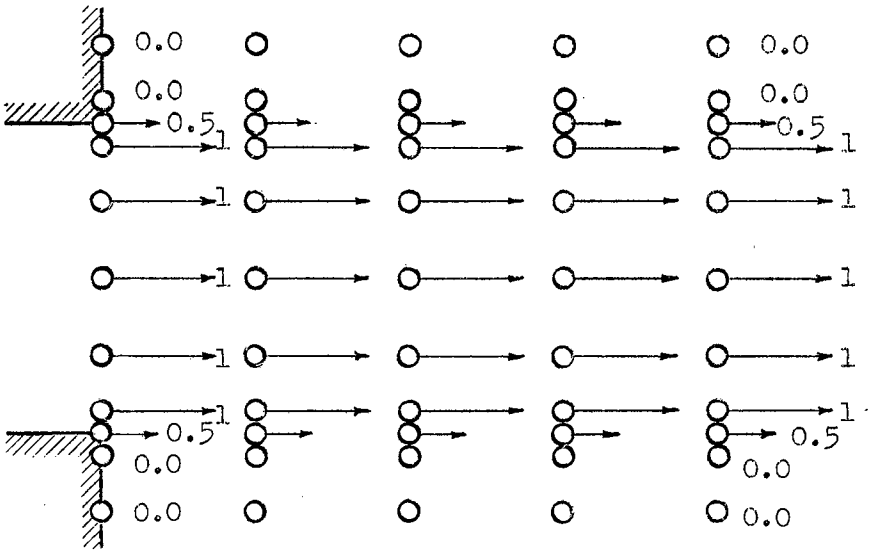

Figure 5. Initial Condition of the Triple Value Net Points

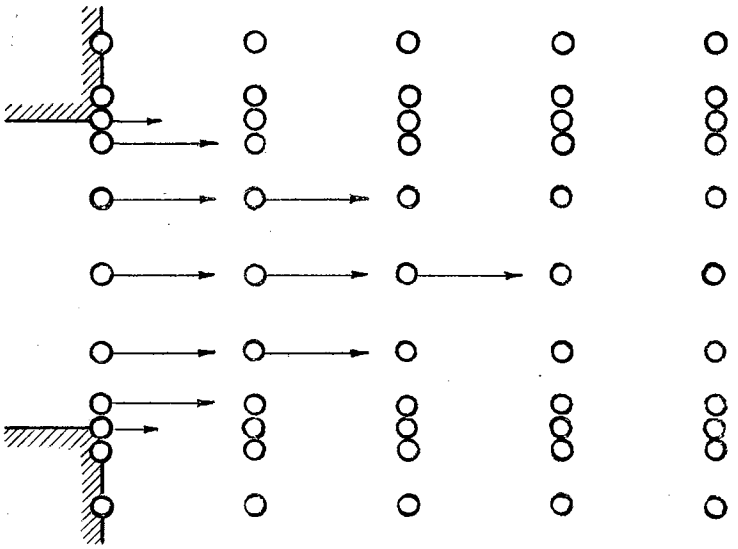

(Vectors shown are held constant for all time)

Figure 6. Typical Representation of Simulated Jet Potential Core

the computation can be continued. Four methods were tried, namely: 1) linearly extrapolating from two nearby points, 2) assuming the property of the flow is identical to the next point inside the field for the same time plane, 3) assuming the property of the flow is identical to the next point inside the field for the previous time plane, and 4) averaging the first and the second methods. If the property of a point on the field boundary QT is designated by $f_{m,\ell}$, the above methods can be written in following forms:

$$
\begin{aligned}
&1. \quad f^n_{m,\ell} = 2f^n_{m-1,\ell} - f^n_{m-2,\ell} \\
&2. \quad f^n_{m,\ell} = f^n_{m-1,\ell} \\
&3. \quad f^n_{m,\ell} = f^{n-1}_{m-1,\ell} \\
&4. \quad f^n_{m,\ell} = \frac{1}{2}\left[f^n_{m-1,\ell} + (2f^n_{m-1,\ell} - f^n_{m-2,\ell})\right] .
\end{aligned}
\tag{4-10}
$$

For the points on the boundary AU, similar relations can be written by interchanging the indices m and ℓ. If the computation is continued to such a point that steady state is established, it would be hoped that all methods in equations (4-10) would give the same results. However, since the flow is subsonic, boundary influences propagate throughout the field and the results prior to steady-state are not the same for the various relations in equations (4-10).

Walker (55) found that the blurring was too great at small values of x and suggested a method to reduce this excessive blurring by forcing the velocity at points, C, V, F and W (see Fig. 4) to be zero. Because of the representation of the initial conditions of the flow field, Walker also suggested that triple values be assigned to all properties along DS and ER to retard the rate of the artificial

blurring. The relation of the triple-value points to the other net points is shown in Fig. 5. For the net point above a triple-value point, the upper value was used and for the net point below it, the lower value was used in computations. The triple-value net point was treated as a triple point in the computations but the middle value was used to represent the properties of the fluid at that particular point.

In free jet mixing, there exists a potential core which usually extends 5 to 7 nozzle widths from the nozzle exit. In some cases of this numerical study, the potential core was simulated by holding the velocity of a few points near the nozzle identical to that of the nozzle exit at all time. One of such cases is shown in Fig. 6. The velocities of those points with velocity vectors shown, were held constant and the rest of the points were allowed to vary according to the equations used. In this way the rate of decay of jet centerline velocity is retarded. Instead of assuming some artificial potential core near the nozzle exit, different values of the blurring coefficient ω were also tried for the first three columns to retard the blurring rate of the jet.

An Early Attempt to Solve for $\overline{u}$, $\overline{v}$ and $\overline{p}$

Selection of Equations

As mentioned previously, three independent equations are needed to solve for $\overline{u}$, $\overline{v}$ and $\overline{p}$ in an incompressible flow field. In addition to the continuity, momentum and energy equations, another equation which may be used to solve for $\overline{p}$ explicitly was derived by combining

the momentum equations and the energy equation (see Appendix B for the derivation), that is

$$\frac{D\overline{p}}{Dt} = \frac{\partial \overline{p}}{\partial t} + \frac{\partial}{\partial x}(\overline{p}\,\overline{u}) + \frac{\partial}{\partial y}(\overline{p}\,\overline{v}) = 0 \ . \qquad (4\text{-}11)$$

The possible combinations of the three-equation set are listed in Table I. Sets 1 through 5 were tried in this part of study.

Evaluation of Apparent Kinematic Viscosity

The apparent kinematic viscosity, $\overline{\epsilon}$, is assumed to be independent of y and can be estimated by equation (3-13). The value of u_a in equation (3-13) is the free stream velocity for half-jet mixing. For a full jet, it has been common practice to use the maximum velocity in the velocity profile at a given x distance as u_a, whereas for a mixing of two streams u_a may be represented by $\overline{u}_{max} - \overline{u}_{min}$; e.g., see Schlichting (48). The value of x in equation (3-13) is not always measured from the nozzle exit because it is not necessary that the mixing starts at the nozzle exit.

The value of u_a was first set equal to the nozzle exit velocity, $\overline{u}_{noz}$, because the maximum velocity at any section in the flow field under consideration should not be very different from that of the nozzle exit; secondly, the local maximum velocity, $\overline{w}_{max}$, was used; and thirdly, the local maximum x-component velocity, $\overline{u}_{max}$, was used because the y-component velocity was known to be small at the location of the maximum velocity. These assumptions can be expressed in the following forms:

$$\overline{\epsilon} = \frac{\overline{u}_{noz} x}{2\sigma^2} \qquad (4\text{-}12)$$

$$\bar{\epsilon} = \frac{\bar{w}_{max} x}{2\sigma^2} \tag{4-13}$$

$$\bar{\epsilon} = \frac{\bar{u}_{max} x}{2\sigma^2} \tag{4-14}$$

The results of computations showed that there is little difference among these choices.

Methods of Taking Finite Differences

In general, the method of central differences yields better accuracy than either backward or forward differences. Here, the forward difference was used to evaluate the derivatives with respect to time. For the space derivative terms, central, backward and forward difference methods were all used.

Depending on the number of the neighboring points around the point (m,ℓ) under consideration, different methods may be used for expressing the space derivative terms in equations (4-4), (4-6), (4-7), (4-8) and (4-9) in difference form. The net point relations are shown in Fig. 7, and the space derivatives in difference form are listed in Table II.

If the relation of the neighboring points used in the computation is like the one shown in Fig. 7(d), the treatment of the solid wall and field boundaries has to be slightly modified. On the solid wall boundary, $(m-2,\ell)$ and $(m+2,\ell)$ were considered as images of each other if the point (m,ℓ) was on the vertical wall, and $(m,\ell-2)$ and $(m,\ell+2)$ were images of each other if point (m,ℓ) is on the horizontal wall. For a point on the field boundary, methods similar to those

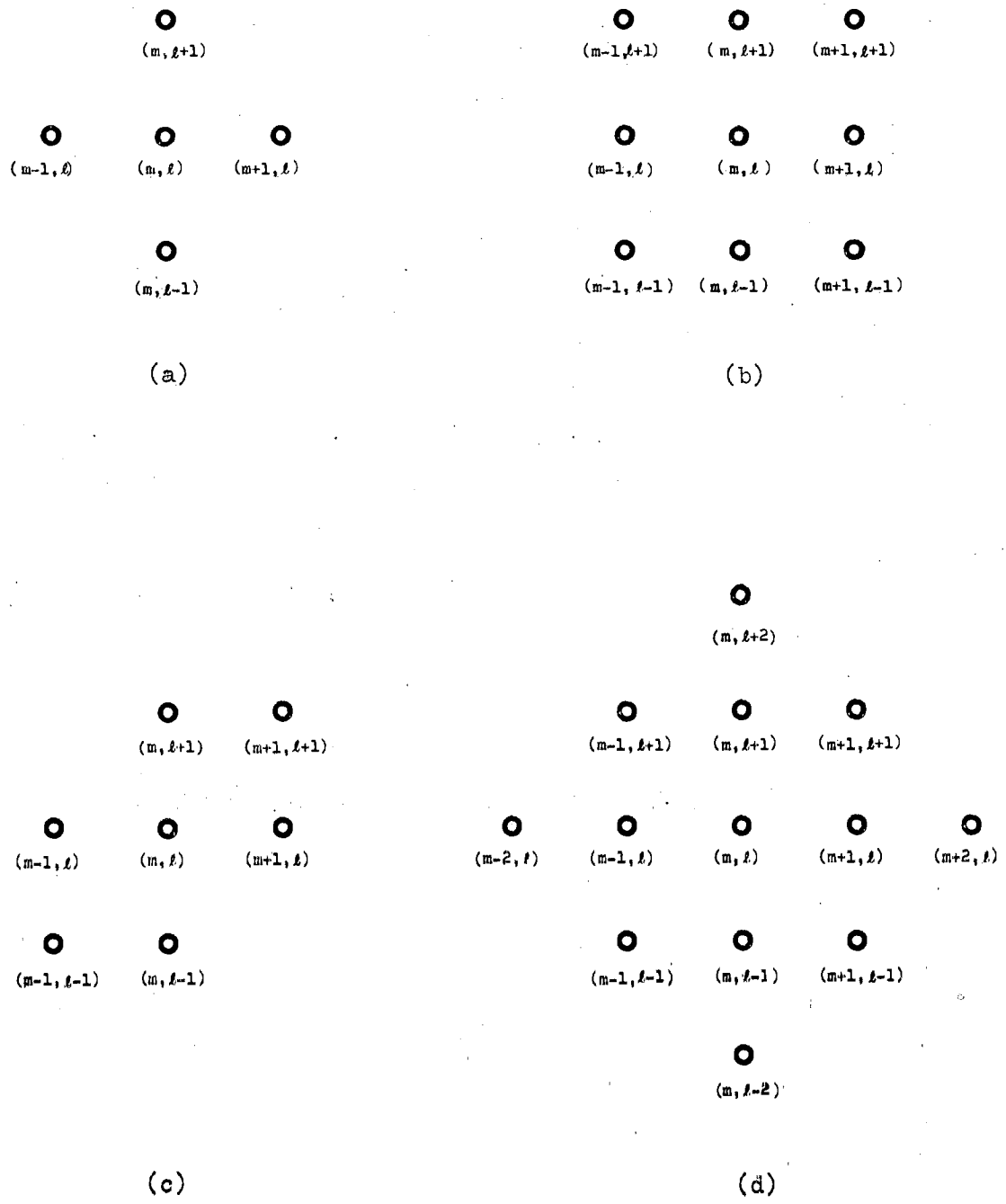

Figure 7. Net Point Relation for the Evaluation of Space Derivative Terms

TABLE II

FOUR METHODS OF REPRESENTING DERIVATIVES BY FINITE DIFFERENCES

Derivative	Figure 7(a)	Figure 7(b)	Figure 7(c)	Figure 7(d)
$\left.\frac{\partial f}{\partial x}\right\|_{m+1,\ell}$	$\frac{1}{\Delta x}(f_{m+1,\ell} - f_{m,\ell})$	$\frac{1}{\Delta x}(f_{m+1,\ell} - f_{m,\ell})$	$\frac{1}{\Delta x}(f_{m+1,\ell} - f_{m,\ell})$	$\frac{1}{2(\Delta x)}(f_{m+2,\ell} - f_{m,\ell})$
$\left.\frac{\partial f}{\partial x}\right\|_{m-1,\ell}$	$\frac{1}{\Delta x}(f_{m,\ell} - f_{m-1,\ell})$	$\frac{1}{\Delta x}(f_{m,\ell} - f_{m-1,\ell})$	$\frac{1}{\Delta x}(f_{m,\ell} - f_{m-1,\ell})$	$\frac{1}{2(\Delta x)}(f_{m,\ell} - f_{m-2,\ell})$
$\left.\frac{\partial f}{\partial x}\right\|_{m,\ell+1}$		$\frac{1}{2(\Delta x)}(f_{m+1,\ell+1} - f_{m-1,\ell+1})$	$\frac{1}{\Delta x}(f_{m+1,\ell+1} - f_{m,\ell+1})$	$\frac{1}{2(\Delta x)}(f_{m+1,\ell+1} - f_{m-1,\ell+1})$
$\left.\frac{\partial f}{\partial x}\right\|_{m,\ell-1}$		$\frac{1}{2(\Delta x)}(f_{m+1,\ell-1} - f_{m-1,\ell-1})$	$\frac{1}{\Delta x}(f_{m,\ell-1} - f_{m-1,\ell-1})$	$\frac{1}{2(\Delta x)}(f_{m+1,\ell-1} - f_{m-1,\ell-1})$
$\left.\frac{\partial f}{\partial y}\right\|_{m+1,\ell}$		$\frac{1}{2(\Delta y)}(f_{m+1,\ell+1} - f_{m+1,\ell-1})$	$\frac{1}{\Delta y}(f_{m+1,\ell+1} - f_{m+1,\ell})$	$\frac{1}{2(\Delta y)}(f_{m+1,\ell+1} - f_{m+1,\ell-1})$
$\left.\frac{\partial f}{\partial y}\right\|_{m-1,\ell}$		$\frac{1}{2(\Delta y)}(f_{m-1,\ell+1} - f_{m-1,\ell-1})$	$\frac{1}{\Delta y}(f_{m-1,\ell} - f_{m-1,\ell-1})$	$\frac{1}{2(\Delta y)}(f_{m-1,\ell+1} - f_{m-1,\ell-1})$
$\left.\frac{\partial f}{\partial y}\right\|_{m,\ell+1}$	$\frac{1}{\Delta y}(f_{m,\ell+1} - f_{m,\ell})$	$\frac{1}{\Delta y}(f_{m,\ell+1} - f_{m,\ell})$	$\frac{1}{\Delta y}(f_{m,\ell+1} - f_{m,\ell})$	$\frac{1}{2(\Delta y)}(f_{m,\ell+2} - f_{m,\ell})$
$\left.\frac{\partial f}{\partial y}\right\|_{m,\ell-1}$	$\frac{1}{\Delta y}(f_{m,\ell} - f_{m,\ell-1})$	$\frac{1}{\Delta y}(f_{m,\ell} - f_{m,\ell-1})$	$\frac{1}{\Delta y}(f_{m,\ell} - f_{m,\ell-1})$	$\frac{1}{2(\Delta y)}(f_{m,\ell} - f_{m,\ell-2})$
$\left.\frac{\partial^2 f}{\partial x^2}\right\|_{m,\ell}$	$\frac{1}{(\Delta x)^2}(f_{m+1,\ell} - 2f_{m,\ell} + f_{m-1,\ell})$	$\frac{1}{(\Delta x)^2}(f_{m+1,\ell} - 2f_{m,\ell} + f_{m-1,\ell})$	$\frac{1}{(\Delta x)^2}(f_{m+1,\ell} - 2f_{m,\ell} + f_{m-1,\ell})$	$\frac{1}{(\Delta x)^2}(f_{m+1,\ell} - 2f_{m,\ell} + f_{m-1,\ell})$
$\left.\frac{\partial^2 f}{\partial y^2}\right\|_{m,\ell}$	$\frac{1}{(\Delta y)^2}(f_{m,\ell+1} - 2f_{m,\ell} + f_{m,\ell-1})$	$\frac{1}{(\Delta y)^2}(f_{m,\ell+1} - 2f_{m,\ell} - f_{m,\ell-1})$	$\frac{1}{(\Delta y)^2}(f_{m,\ell+1} - 2f_{m,\ell} + f_{m,\ell-1})$	$\frac{1}{(\Delta y)^2}(f_{m,\ell+1} - 2f_{m,\ell} + f_{m,\ell-1})$

shown in equations (4-10) were used, except for method 3. If method 3 were to be used, it would require storage of the data of three consecutive time planes in the computer memory. This, in turn, would reduce the available storage locations and the number of net points in the flow field would have to be reduced.

Methods of Computation

The computation was carried out columnwise and always started from the lower left corner. A field layout similar to that of Fig. 13 was used. The first time plane computation was based on the assumed initial conditions. Thereafter the computed values for a given time plane were used to compute the values for the following time plane. A rectangular field was defined in the computer program rather than the actual field shape, as shown in Fig. 13. No computation was required for those points inside the solid wall because the fluid properties at those points were preassigned to be zero. In most cases, a $\Delta x/\Delta y = 2$ mesh spacing was used. The field size was 32 columns by 41 rows or 35 columns by 55 rows, depending on the cavity dimensions.

If any computed pressure was above or below the limits given (normally $\pm$ 50% of the nozzle pressure), the job would be terminated automatically. The last set of the computed values was stored on a magnetic tape which could be used as the input if it was found necessary to do further computation.

In general, $\overline{u}$ was computed first, then $\overline{v}$, and then $\overline{p}$. As can be seen in Table I, the momentum equation in x-direction was always used for solving $\overline{u}$. If the energy equation was used to solve for $\overline{p}$

according to equation (4-5), $\overline{u}$ and $\overline{v}$ values had to be known at every point in the field before $\overline{p}$ could be computed because the velocity gradients had to be evaluated in the same time plane. For this case, the computation of each time plane was accomplished by going through the field twice. Alternately, one computation was sufficient if backward differences were used to evaluate the velocity gradients either by assuming both $\overline{u}$ and $\overline{v}$ were zero on the vertical walls of the nozzle exit plane or by approximating the velocity gradient terms at the net points in the first column with the values of the previous time plane. When the continuity equation was used to solve for $\overline{v}$, backward differences were used to write the continuity equation in difference form. Evaluation of $\overline{v}$ for each net point in the first column was made by either assuming zero velocity on the walls or, as an approximation, the values computed in the previous time plane.

Although the equations used in the computation and the output data were in dimensionless form, the input data such as the nozzle exit velocity, temperature and gas constant of the fluid, width of nozzle, dimension of the cavity, Δx and the reference length Δy were all entered with physical dimensions; conversion to dimensionless form was accomplished within the program.

Results and Findings

In this part of the study, mainly equation set 1 in Table I was used. That is, momentum equations were used in the x and y directions to solve for $\overline{u}$ and $\overline{v}$, respectively, and the energy equation was used to solve for $\overline{p}$. The continuity equation was only used implicitly in

these equations.

Different methods of representing the governing equations in difference form and the boundary conditions, and imposing different constraints near the nozzle exit were tried, but it was found that the value of the blurring parameter ω had the most influence on the computed results. If a small ω value was used, the computation became unstable for all methods of representing equation set 1 in difference form, neighboring points, triple-value points, artificial potential core, etc. With a large value of ω, stability was maintained but excessive blurring resulted; eventually large sinks were created in the flow field. The stability of the computation depends almost exclusively on the selection of the values of ω and σ_o. The estimated effect of ω and σ_o on solution stability is shown in Fig. 8.

When the representation of the initial conditions of the triple-value net points (see Fig. 5) was used, the triple values would become essentially identical in the region some distance from the nozzle after a period of computation time. For those triple-value points near the nozzle, there was no convergence to a single value because the triple-value at the nozzle exit was constrained at all time; however, there was a tendency to approach the middle value. From the nozzle plane to the following column, the values of the triple-value point changed considerably, especially the upper and lower values. The higher value decreased and the lower value increased, this, in turn, caused some difference in pressure among the triple values. When the zero velocity constraint at net points V and W in Fig. 4 was applied, the pressure at these points increased

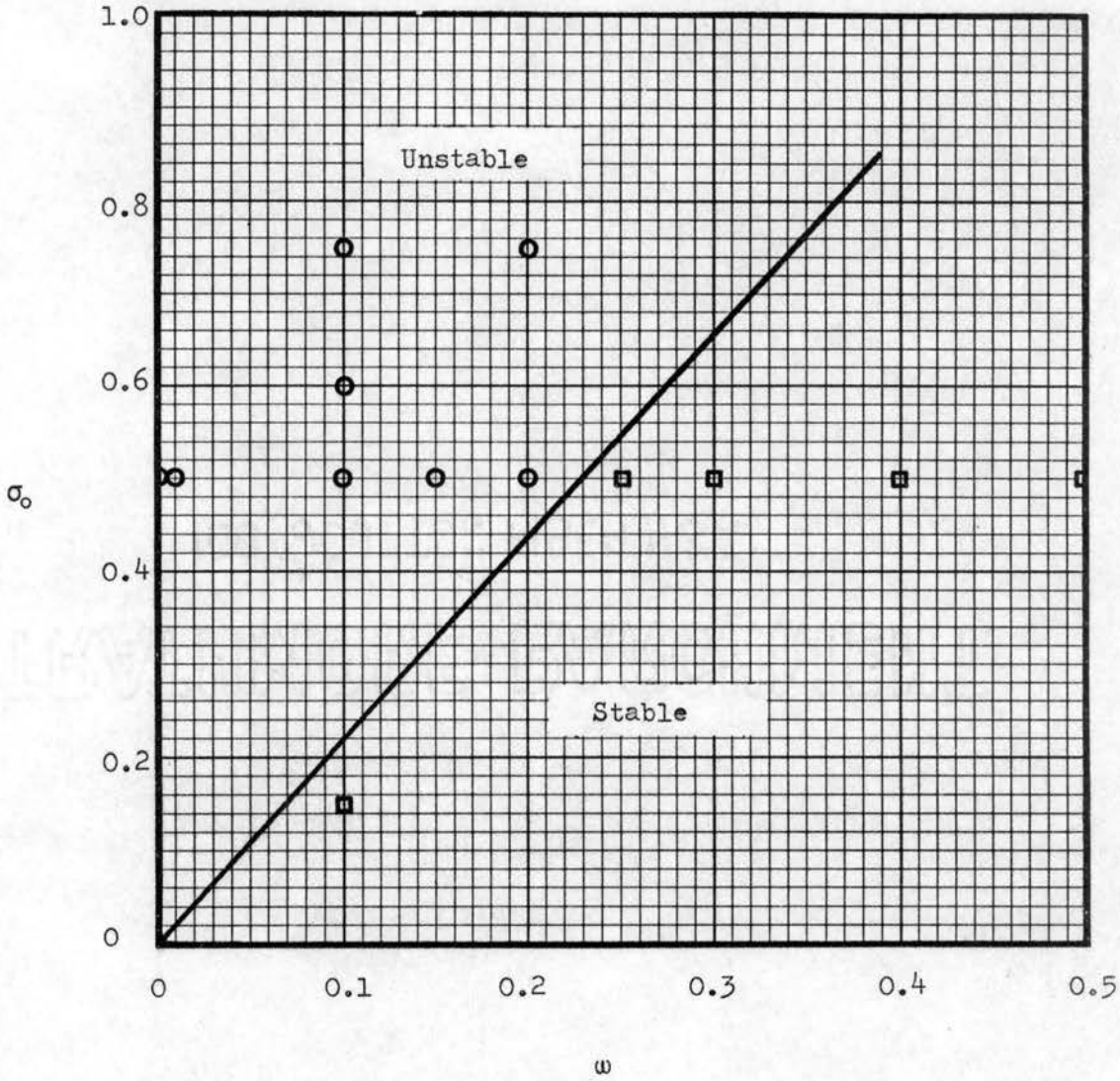

Figure 8. Effect of ω and σ_o Values on Numerical Stability for Subsonic Jets

to some extent, thereby causing a higher pressure increase near the nozzle than would occur without this constraint. These jumps in pressure are not favorable to the computation. If the jump is large, the resulting pressure pulse can propagate throughtout the field as the computation proceeds; this pulse may be amplified or damped depending on the other conditions and the values of ω and σ_o used.

Instead of imposing the constraints mentioned above, an artificial potential core was added to some of the computations (e.g. see Fig. 6). A large value of ω must be used to keep the computation stable; however this causes the jet centerline velocity to decrease too rapidly, especially near the nozzle. The pressure of the net point downstream of the last point of the artificial potential core had an unusually high pressure rise due to the sudden decrease in velocity. This pressure jump may have the same effect as mentioned in the preceding paragraph. Without the assumption of an artificial potential core, the rate of jet velocity decay was the highest in the region near the nozzle. In order to retard the rate of jet velocity decay near the nozzle, smaller values of ω were used on the second and the third columns than for the rest of the field. But then instability set in very quickly. The use of larger ω values in the second and the third columns did not improve the results.

Methods of estimating the field boundary conditions used are shown in equations (4-10). The first method tended to enlarge the existing gradient; the third one tended to create a suction effect if the product of flow velocity and time increment did not match the space increment; the fourth one slightly reduced the enlargement

effect of the first method. Consequently, more time planes are required to obtain a steady state result using the time dependent method if instability is to be avoided. The second method in equations (4-10) was found to be most satisfactory. It helped to suppress the end effect and to force the solution to reach an asymptotic value faster than with the other methods.

In general, a large ω value was required to stabilize the computation; this also created sinks in the computation field and the mass rate of flow decreased steadily as the computation continued. For this reason, equation sets 2 and 3 in Table I were tried with the hope that the mass rate of flow might be conserved. However, these approaches were not successful either; instability resulted even earlier. The results obtained with equation set 4 were similar to those of equation set 1. Although a larger ω value was used in equation set 5 in the computation, the results were not stable.

No noticeable difference was found from the alternate use of equations (4-12), (4-13) or (4-14) to evaluate the apparent kinematic viscosity.

Solving for $\overline{p}$ by Iteration

It was realized that for an incompressible flow, any pressure in the flow field would influence the whole field and it might be preferable to use an iteration method to find the pressure at every net point by using the known velocities $\overline{u}$ and $\overline{v}$. The numerical method thus becomes implicit rather than explicit. Fromm (23) suggested this method and used it in a study of the wake structure of an incompressible, viscous fluid flow behind an obstacle. The

equation used to iterate for the pressure was obtained by differentiating the x- and y-momentum equations with respect to x and y, respectively, and then combining the results. Since the iteration was to be done on a fixed time plane, the time derivative terms were ignored. The necessary equation for an incompressible turbulent flow is as follows (see Appendix C for derivation):

$$\frac{\partial^2}{\partial x^2}\overline{p} + \frac{\partial^2}{\partial y^2}\overline{p} = -\overline{Q} \quad , \tag{4-15}$$

where

$$\overline{Q} = \frac{\partial^2}{\partial x^2}\left[(\overline{u})^2 + \overline{(u')^2}\right] + \frac{\partial^2}{\partial y^2}\left[(\overline{v})^2 + \overline{(v')^2}\right]$$

$$+ 2\frac{\partial^2}{\partial x \partial y}\left[\overline{u}\,\overline{v} + \overline{u'v'}\right] . \tag{4-16}$$

The initial condition used was similar to the one shown in Fig. 4, but no triple-value and zero velocity constraints were imposed. No artificial potential core was added. The points originally represented by triple values were represented initially by a single value, namely, one-half of the nozzle exit velocity (see Fig. 14). Blurring terms were dropped completely. Turbulent shearing stresses were estimated according to equations (3-9) and (3-11), and the turbulent normal stresses σ_i were neglected because the $\partial\overline{u}_i/\partial x_i$ terms were assumed to be small. Evaluation of the apparent kinematic viscosity $\overline{\epsilon}$ was modified by using a different origin of the turbulent jet mixing. Miller and Comings (34) found that the starting point of the turbulent jet mixing is about 1.572 nozzle widths upstream from the nozzle exit plane. The value of u_a in equation (3-13) was represented by $(\overline{u}_{max} - \overline{u}_{min})$. Because of the reverse flow in the

cavity, the jet mixing was considered to be similar to the mixing of two streams. The apparent kinematic viscosity was correspondingly expressed by

$$\bar{\epsilon} = \frac{1}{2\sigma^2} (\bar{u}_{max} - \bar{u}_{min}) \cdot (1.572\ W + x), \qquad (4\text{-}17)$$

where W is the nozzle width.

The neighboring net point relation as shown in Fig 7(b) was used. In order to use central differences to write the simplified momentum equations in equations (4-1) and equations (4-15) in difference form, the properties at $(m + \frac{1}{2}, \ell + \frac{1}{2})$, $(m + \frac{1}{2}, \ell - \frac{1}{2})$, $(m - \frac{1}{2}, \ell + \frac{1}{2})$ and $(m - \frac{1}{2}, \ell - \frac{1}{2})$ points were approximated by the following relations

$$\begin{aligned}
f_{m+\frac{1}{2},\ell+\frac{1}{2}} &= (f_{m,\ell} + f_{m,\ell+1} + f_{m+1,\ell+1} + f_{m+1,\ell})/4 \\
f_{m+\frac{1}{2},\ell-\frac{1}{2}} &= (f_{m,\ell} + f_{m+1,\ell} + f_{m+1,\ell-1} + f_{m,\ell-1})/4 \\
f_{m-\frac{1}{2},\ell+\frac{1}{2}} &= (f_{m,\ell} + f_{m-1,\ell} + f_{m-1,\ell+1} + f_{m,\ell+1})/4 \\
f_{m-\frac{1}{2},\ell-\frac{1}{2}} &= (f_{m,\ell} + f_{m,\ell-1} + f_{m-1,\ell-1} + f_{m-1,\ell})/4 .
\end{aligned} \qquad (4\text{-}18)$$

The space derivative terms appearing in equations (4-1) (i.e., the second order derivatives), were written in difference form by considering $(m+\frac{1}{2},\ell)$, $(m-\frac{1}{2},\ell)$, $(m,\ell+\frac{1}{2})$ and $(m,\ell-\frac{1}{2})$ as reference points rather than $(m+1,\ell)$, $(m-1,\ell)$, $(m,\ell+1)$ and $(m,\ell-1)$, respectively. These terms are listed in Table III.

Backward differences were used to write the continuity equation in difference form when it was used to solve for $\bar{v}$. As before, forward differences were used for the time derivative terms.

The flow field considered in this example is shown in Fig. 13. Square mesh spacing with $\Delta x = \Delta y = 0.15625$ inches was used, and the nozzle width was 0.625 inches. The separation step and the recom-

TABLE III

FIFTH METHOD OF REPRESENTING DERIVATIVES BY FINITE DIFFERENCES

Derivative	Finite Difference
$\left.\frac{\partial f}{\partial x}\right\|_{m+\frac{1}{2},\,\ell}$	$\frac{1}{\Delta x}\left(f_{m+1,\,\ell} - f_{m,\,\ell}\right)$
$\left.\frac{\partial f}{\partial x}\right\|_{m-\frac{1}{2},\,\ell}$	$\frac{1}{\Delta x}\left(f_{m,\,\ell} - f_{m-1,\,\ell}\right)$
$\left.\frac{\partial f}{\partial x}\right\|_{m,\,\ell+\frac{1}{2}}$	$\frac{1}{\Delta x}\left(f_{m+\frac{1}{2},\,\ell+\frac{1}{2}} - f_{m-\frac{1}{2},\,\ell+\frac{1}{2}}\right)$
$\left.\frac{\partial f}{\partial x}\right\|_{m,\,\ell-\frac{1}{2}}$	$\frac{1}{\Delta x}\left(f_{m+\frac{1}{2},\,\ell-\frac{1}{2}} - f_{m-\frac{1}{2},\,\ell-\frac{1}{2}}\right)$
$\left.\frac{\partial f}{\partial y}\right\|_{m+\frac{1}{2},\,\ell}$	$\frac{1}{\Delta y}\left(f_{m+\frac{1}{2},\,\ell+\frac{1}{2}} - f_{m+\frac{1}{2},\,\ell-\frac{1}{2}}\right)$
$\left.\frac{\partial f}{\partial y}\right\|_{m-\frac{1}{2},\,\ell}$	$\frac{1}{\Delta y}\left(f_{m-\frac{1}{2},\,\ell+\frac{1}{2}} - f_{m-\frac{1}{2},\,\ell-\frac{1}{2}}\right)$
$\left.\frac{\partial f}{\partial y}\right\|_{m,\,\ell+\frac{1}{2}}$	$\frac{1}{\Delta y}\left(f_{m,\,\ell+1} - f_{m,\,\ell}\right)$
$\left.\frac{\partial f}{\partial y}\right\|_{m,\,\ell-\frac{1}{2}}$	$\frac{1}{\Delta y}\left(f_{m,\,\ell} - f_{m,\,\ell-1}\right)$

pression step heights were respectively 4 and 3 nozzle widths, and the cavity length was 10 nozzle widths. The nozzle exit velocity was 200 fps and the reference velocity was 958.23 fps (= acoustic velocity/$\sqrt{\gamma}$).

The evaluation of $\bar{u}$ and $\bar{v}$ was identical to that used previously. Pressure was computed by the procedure discussed below. After computing $\bar{u}$ and $\bar{v}$ at each new time plane, the value of $\bar{Q}$ was computed according to equation (4-16) with the $\overline{(u_i')^2}$ terms neglected and the $\overline{u'v'}$ term expressed in the form shown in equation (3-11). After all $\bar{u}$, $\bar{v}$ and $\bar{Q}$ values for every point in the field were computed, the pressure at each point in the field was estimated from equation (C-6), the difference form of equation (4-15). Before proceeding to the new time plane, the pressure at every net point was iterated by the same method until the difference between the old and new values at every point was smaller than a specified limit. After this condition was satisfied at every net point, a set of new $\bar{u}$ and $\bar{v}$ values was computed based on the latest values of pressure; the entire procedure was then repeated.

The dimensionless pressure at the nozzle exit was held at unity. With equation set 6 in Table I and σ_o = 0.5, for the first 300 time planes less than 6 iterations always satisfied the given limits of ± 0.00001 between two iterations. The rate of the $\bar{u}$ velocity decay on the nozzle centerline is plotted in Fig. 9. The disturbances built up from the end of the field and were moving upstream with increasing strength at the end as the computation continued. Thus the representation of the field boundary by the second equation of equations (4-10) is not valid here. At the 300th time plane, the

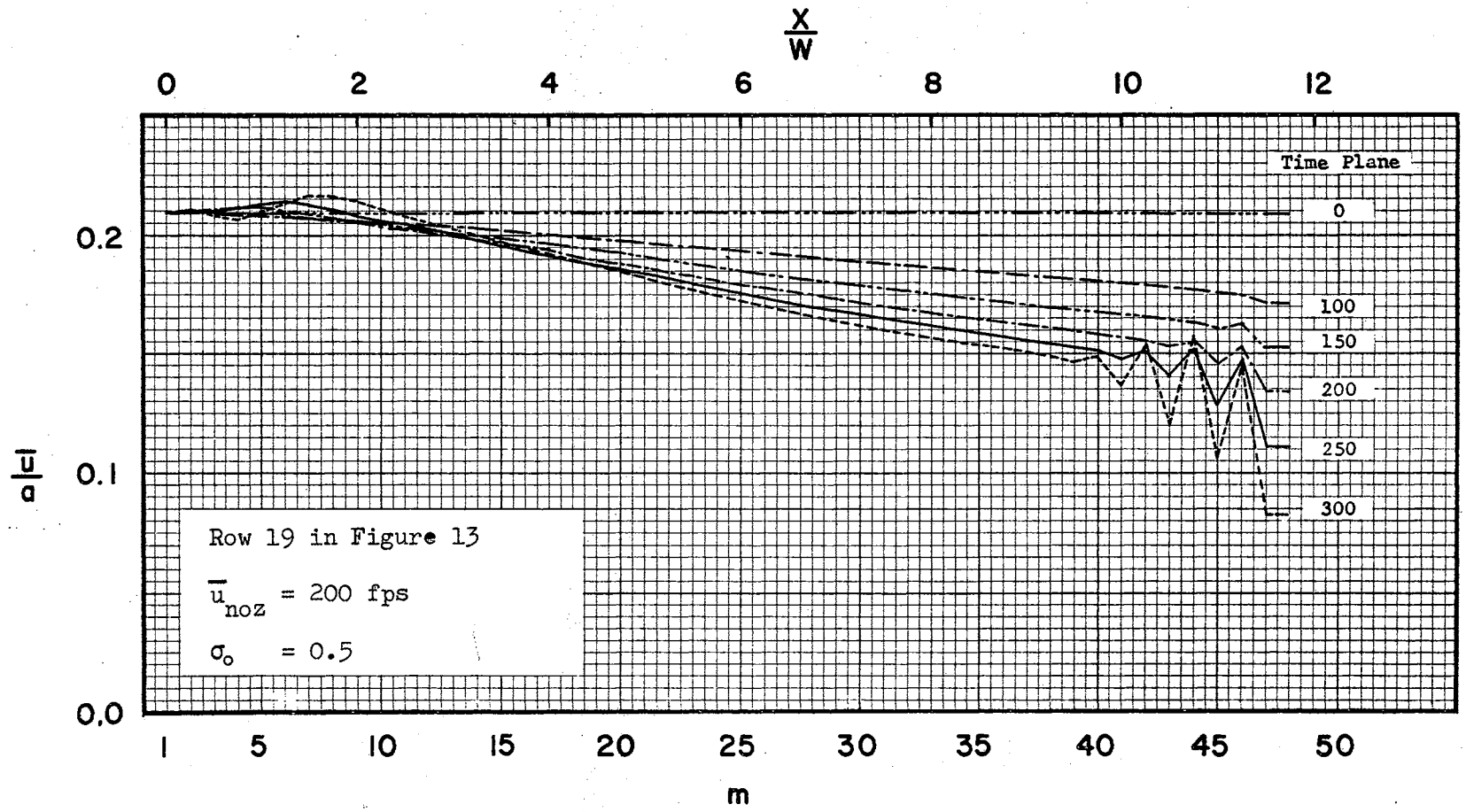

Figure 9. Decay of Nozzle Centerline x-Component Velocity of a Subsonic Incompressible Jet Computed by the Iteration Method

pressure was still very close to 1 except for those points in the vicinity of the disturbed region. The pressure in the cavity was, in general, smaller than that in the region of the open side. Predictions of the velocity field showing reverse flow in the cavity and the pressure distribution on the cavity walls were not very successful.

With equation set 7 in Table I, the computation became unstable at an early time plane. It can be concluded that use of the continuity equation to solve for $\overline{v}$ is not a good technique in the methods of this study.

The Later Attempts to Solve for $\overline{u}$, $\overline{v}$ and $\overline{p}$

This part of the study was done after the computations shown in Chapter V were completed. In this way, the results of computations based on incompressible and compressible flow assumptions could be compared. The method of computation was identical to the similar one discussed in Chapter V. The field of computation was identical to the one shown in Fig. 13. The nozzle exit velocity was 200 fps and the values of ω and σ_o were, respectively, 0.10 and 0.15. The computed results of the velocity profiles at the 2000th time plane are plotted in Fig. 10. It is seen that the jet centerline stays almost horizontal in spite of the existence of the cavity, and the jet centerline velocity decay is too great; at the 2000th time plane, the maximum jet velocity at 12 nozzle widths downstream of the nozzle is only about 33% of the nozzle exit velocity instead of 78%, as found in a typical experiment. The strength of the reverse flow in the cavity is unusually low, and the y-component

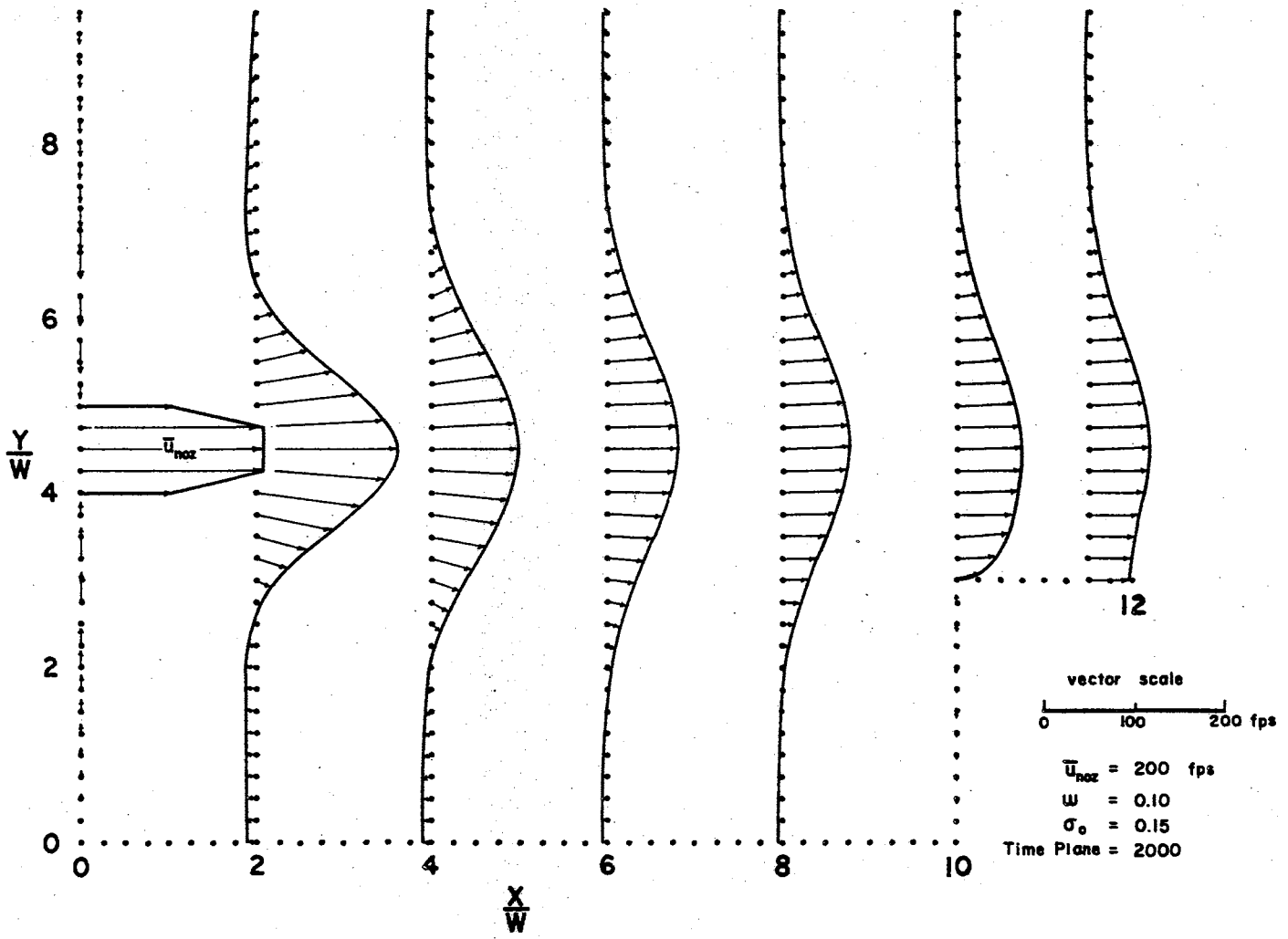

Figure 10. Computed Velocity Distribution of the Low Speed Incompressible Flow Case

velocity is negligibly small everywhere in the field.

The relation of the nozzle centerline x-component velocity change to the time plane of computation is shown in Fig. 11. The velocity converges slowly to an asymptotic value. However, the velocity near the nozzle has started to recover, but it decreases steadily in the downstream region.

The computed pressure throughout the field is not very different from the pressure at the nozzle exit, that is, unity. The pressure fluctuates from point to point in the fourth decimal place. Consequently, the constant pressure lines are not plotted; however, the average pressures in the cavity and in the open side are shown in Fig. 12. The solid line shows the average pressures on the open side (simple average of values from 22nd to 37th rows) and the broken line shows those in the cavity (simple average of values from 1st to 16th rows). The values of pressure from the 17th to 21st rows were not taken into account because this region was considered as the dividing zone of the cavity and the open side. Up to about 4 nozzle widths downstream from the nozzle, the average pressure in the cavity is slightly lower than that of the open side, whereas from 4 to 10 nozzle widths, the trend is reversed.

With an IBM 7040 computer system, it took about 27 seconds to compute one time plane with a flow field size of 48 columns by 39 rows. With an on-line printer printing out every 100 time planes, an average of 47.31 minutes was required to compute 100 time planes.

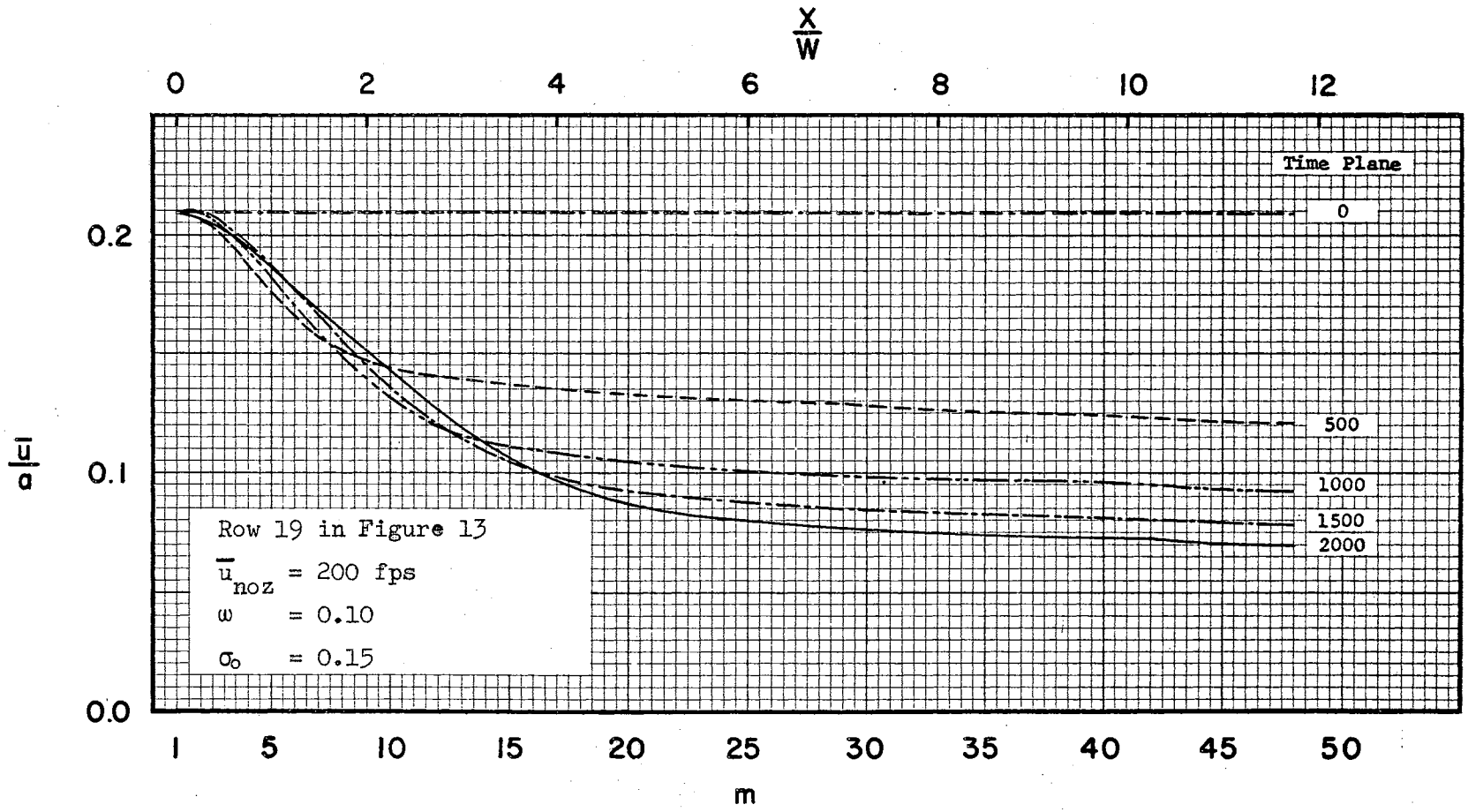

Figure 11. Rate of Nozzle Centerline x-Component Velocity Decay for Incompressible Subsonic Jet

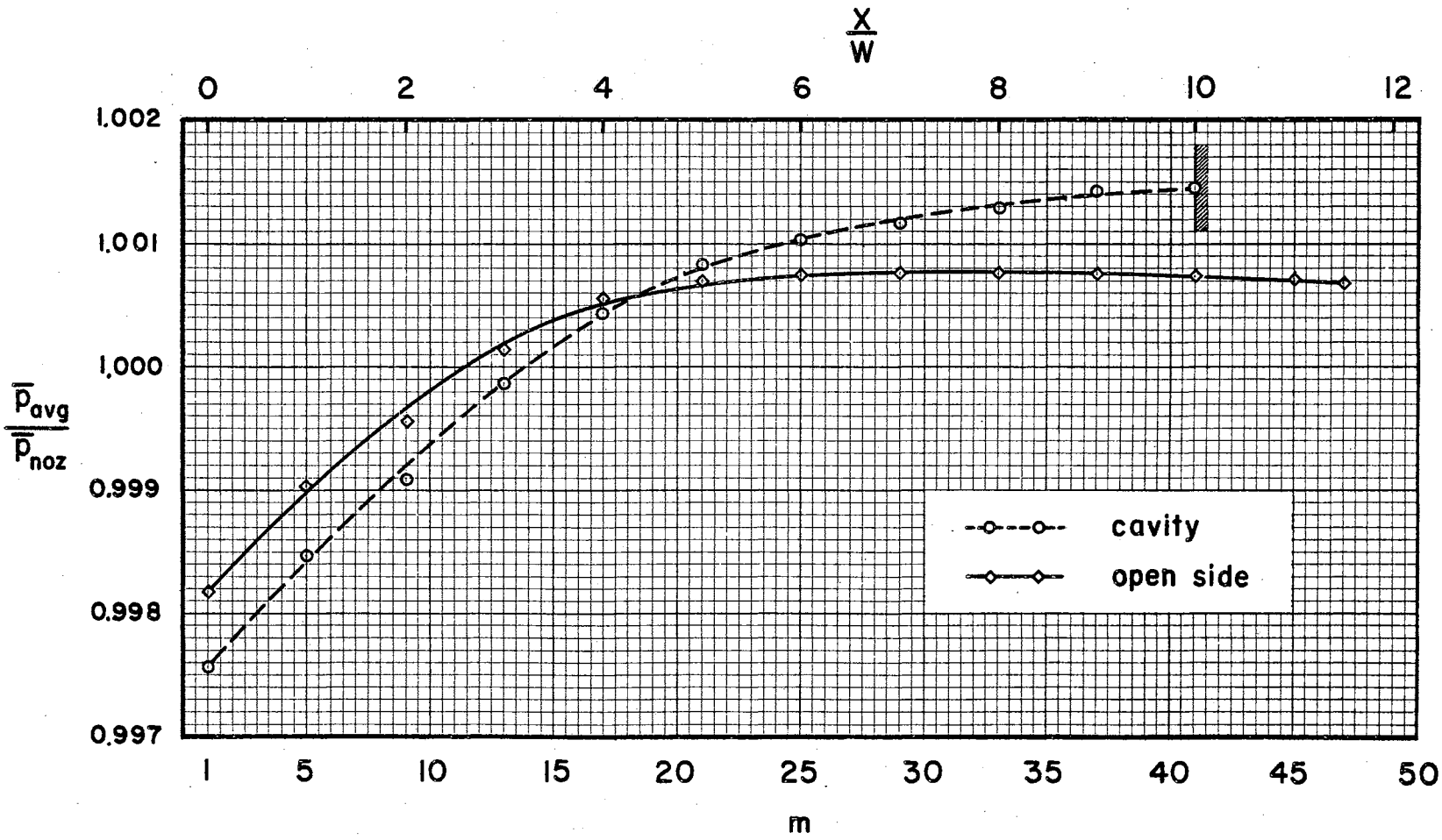

Figure 12. Average Pressure in the Cavity and the Open Side of the Low Speed Incompressible Flow Case

CHAPTER V

NUMERICAL SOLUTION OF THE GOVERNING FINITE DIFFERENCE EQUATIONS FOR COMPRESSIBLE FLOW

In Chapter IV, attempts were made to solve the flow characteristics of a low velocity, incompressible, plane, turbulent jet issuing from a nozzle over a cavity by means of the numerical technique. It was felt that the mass rate of flow was not conserved and it might be necessary to include continuity equation explicitly in the computation with the hope that this shortcoming could be overcome. In order to use the continuity equation in the computation, the density $\overline{\rho}$ has to be allowed to change, which makes the flow a compressible one. Even though the flow speed is still low, the above allowance is permissible. The governing equations derived in Chapter III, equations (3-15), can be applied directly here. The basic method used in this chapter is identical to that in Chapter IV. The basic programming logic is presented in Appendix D.

Description of the Methods Used

The methods used in this chapter were generally similar to those used in Chapter IV. The representation of the initial conditions was similar to that shown in Fig. 4. The representation of triple-value net points was also similar but the density had to be adjusted according to the velocities assigned to each of the

triple points. Pressure at the nozzle exit was held constant at all time and the densities at the triple-value net points there were adjusted by assuming all fluid issuing from the nozzle had the same total energy and the products of densities and temperatures of the three points were equal. This means that at the lower value of velocities the density must be lower also. The initial density of regions ② in Fig. 4 was adjusted by assuming the temperature of those regions was the stagnation temperature of the fluid from the nozzle.

After several computations, it was found that the value of ω had to be large to keep the computation stable, but this, in turn, increased the rate of jet centerline velocity decay. The addition of a blurring term in the continuity equation caused an apparent "loss" in mass rate of flow. In an attempt to eliminate the computational "leakage", the blurring term was dropped from the continuity equation but retained in the remaining equations. However, the computation became unstable quite early. When the blurring term was eliminated from the energy equation, the results were not favorable either.

In order to see the effects of the blurring term and the turbulent shearing stress on the results of the computation, the value of the turbulent shearing stress was artificially increased or decreased by the multiplication factors of 20, 10, 5, and 0. It was found that the relation of ω and σ_o to the stability of computation was unaffected by the change of the amount of the turbulent shearing stress. However, with a higher multiplication factor, the jet spread slightly faster. This showed that the

turbulent shearing stress appeared to have the same effect as the blurring term on the jet mixing, but of much smaller magnitude.

In addition to the assigned velocities at the triple-value net points shown in Fig. 5, two other combinations of nozzle-exit velocities were also tried. With a combination of assigned velocities of $0.2\ \bar{u}_{noz}$, $0.5\ \bar{u}_{noz}$, $0.8\ \bar{u}_{noz}$, the jet spread faster than with the combination $0.0\ \bar{u}_{noz}$, $0.5\ \bar{u}_{noz}$, $1.0\ \bar{u}_{noz}$ (see Fig. 5). Similarly, the one using $0.5\ \bar{u}_{noz}$, $0.5\ \bar{u}_{noz}$, $0.5\ \bar{u}_{noz}$ combination had the greatest jet spread rate. The selection of the velocity combination of the triple-value net point did not seem to have any influence on the stability of computation.

The method of taking finite differences did not significantly affect the computed results, regardless whether Fig. 7(b) or Fig. 7(d) was chosen to represent the relation of the point (m,ℓ) with its neighboring points. The finite differences were taken according to each corresponding column in Table II. When the finite differences were taken according to the method shown in Table III, the rate of jet spread was found to be slightly greater than that of the other two methods tried.

It should be noted that the representation of the turbulent normal stress, σ_i, as described by equation (3-12), that is,

$$\sigma_i = 2\,\bar{\rho}\,\bar{\epsilon}\left(\frac{\partial \bar{u}}{\partial x}\right)_i = -\,\bar{\rho}\,\overline{(u_i')^2}\ , \qquad (5\text{-}1)$$

may not be valid. Physically the turbulent normal stress can be either positive or negative depending on the value of $\left(\frac{\partial \bar{u}}{\partial x}\right)_i$, and the quantity $\bar{\rho}\,\overline{(u_i')^2}$ is always positive. If the relation in equation (5-1) is used, the turbulent normal stress can only be

negative. In order to determine if the $\overline{\rho}\ \overline{(u_i')^2}$ terms could be neglected, the values of $\overline{\rho}\ \overline{(u_i')^2}$ were estimated by following relations:

$$\overline{\rho}\,\overline{(u_i')^2} = 2\,\overline{\rho}\,\overline{\epsilon}\left(\frac{\partial \overline{u}}{\partial x}\right)_i \tag{5-2}$$

$$\overline{\rho}\ \overline{(u_i')^2} = 2\,\overline{\rho}\,\overline{\epsilon}\left|\frac{\partial u}{\partial x}\right|_i \tag{5-3}$$

$$\overline{\rho}\ \overline{(u_i')^2} = 0\ . \tag{5-4}$$

No significant difference in the computed results was observed regardless which relation was used. Though the differences were very small, equation (5-3) gave the lowest and equation (5-4) the highest rate of jet spread. From this exploratory computation it was decided to neglect the $\overline{\rho}\ \overline{(u_i')^2}$ terms completely in the computation to save computer time.

Neglecting the turbulent normal stress, the governing equations become:

$$\frac{\partial \overline{\rho}}{\partial t} + \frac{\partial}{\partial x}(\overline{\rho}\ \overline{u}) + \frac{\partial}{\partial y}(\overline{\rho}\ \overline{v}) = 0$$

$$\frac{\partial}{\partial t}(\overline{\rho}\ \overline{u}) + \frac{\partial}{\partial x}\left[\overline{\rho}\ \overline{u}^2 + \overline{p}\right] + \frac{\partial}{\partial y}\left[\overline{\rho}\ \overline{v}\ \overline{u} - \overline{\rho}\ \overline{\epsilon}\left(\frac{\partial \overline{u}}{\partial y} + \frac{\partial \overline{v}}{\partial x}\right)\right] = 0$$

$$\frac{\partial}{\partial t}(\overline{\rho}\ \overline{v}) + \frac{\partial}{\partial x}\left[\overline{\rho}\ \overline{u}\ \overline{v} - \overline{\rho}\ \overline{\epsilon}\left(\frac{\partial \overline{u}}{\partial y} + \frac{\partial \overline{v}}{\partial x}\right)\right] + \frac{\partial}{\partial y}\left[\overline{\rho}\ \overline{v}^2 + \overline{p}\right] = 0 \tag{5-5}$$

$$\frac{\partial \overline{e}}{\partial t} + \frac{\partial}{\partial x}\left[(\overline{e} + \overline{p})\overline{u} - \overline{\rho}\ \overline{v}\ \overline{\epsilon}\left(\frac{\partial \overline{u}}{\partial y} + \frac{\partial \overline{v}}{\partial x}\right)\right]$$

$$+ \frac{\partial}{\partial y}\left[(\overline{e} + \overline{p})\overline{v} - \overline{\rho}\ \overline{u}\ \overline{\epsilon}\left(\frac{\partial \overline{u}}{\partial y} + \frac{\partial \overline{v}}{\partial x}\right)\right] = 0\ ,$$

and

$$\bar{e} = \frac{\bar{p}}{\gamma - 1} + \frac{1}{2}\left[\bar{\rho}\,\bar{u}^2 + \bar{\rho}\,\bar{v}^2\right]. \qquad (5\text{-}6)$$

Computed Results for the Subsonic Flow Case

The geometrical arrangement of the cavity used in this chapter was similar to Case 1 of Fig. 27. If a square mesh of $\Delta x = \Delta y = 0.15625$ inches is used, the flow field under consideration can be represented by a net point field as shown in Fig. 13. The data used in the computations are listed in Table IV and the nozzle exit velocity was represented by the relation shown in Fig. 14. The procedure of computation is presented in Appendix D. Equations (5-5) and (5-6) were used in this example. The apparent kinematic viscosity was evaluated with equation (4-17) and the finite differences were taken according to the relation shown in Table III. The relation between the point under consideration and its neighboring points was established as shown in Fig. 7(b).

The value of ω was 0.10 at the beginning and was reduced to 0.05 after computing 1119 time planes in this example; this reduced the excessive blurring effect. The computed velocity profiles at the 2000th time plane are plotted in Fig. 15. By comparing the velocity profiles plotted in Figs. 10 and 15, almost the same conclusions can be made for this example as for the example shown in Fig. 10. Fig. 16 shows the x-component velocity distributions at the 1000th time plane for both incompressible and compressible cases under the same conditions. It is concluded that the computation method is more significantly affected by the presence of the

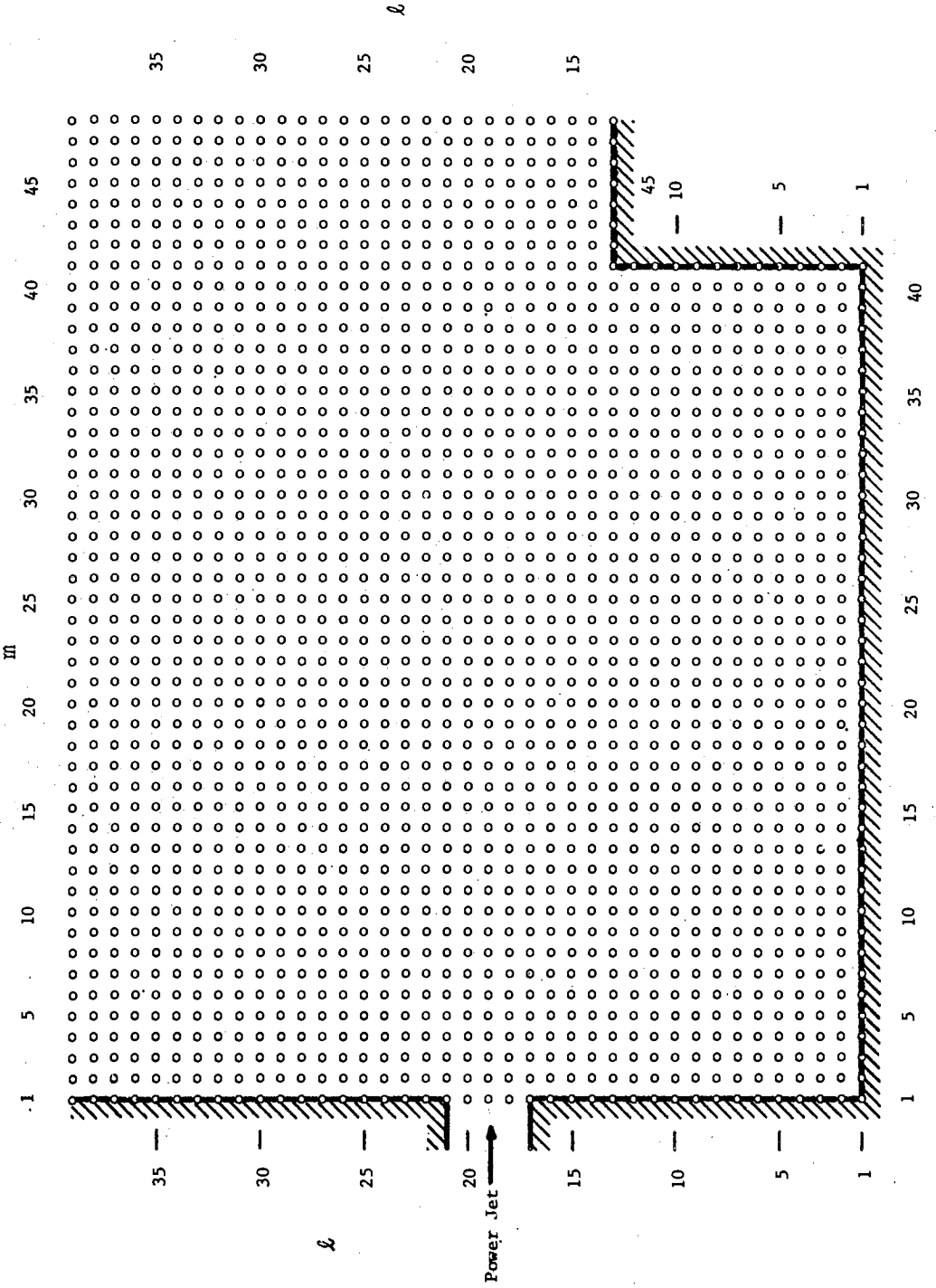

Figure 13. Computation Net Point Field

TABLE IV

FIXED VALUES FOR THE COMPUTATIONS

	Subsonic Flow Case	Supersonic Flow Case
$\bar{u}_{noz}$ (fps)	200.0	2270.0
$\bar{v}_{noz}$ (fps)	0.0	0.0
a (fps)	958.23	958.23
T_{noz} (°R)	535.0	535.00
$\bar{p}^*_{noz}$	1.0	1.0
$\bar{\rho}^*_{noz}$	1.0	1.0
$\bar{\rho}^*_{\frac{1}{2}\bar{u}_{noz}}$	0.9954029	0.6667467
γ	1.4	1.4
R $\frac{lb_f - ft}{lb_m - {}^\circ R}$	53.3	53.3
σ	11.0	29.3
σ_o	0.15	0.5
ω	0.10 (0.05)	0.2

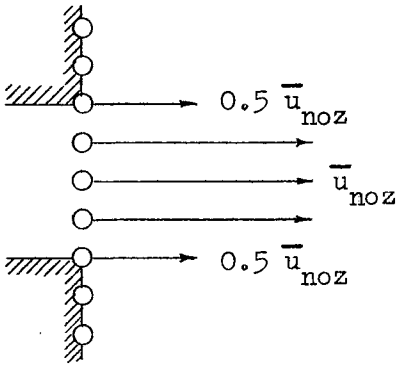

Figure 14. Velocity Distribution at the Nozzle Exit

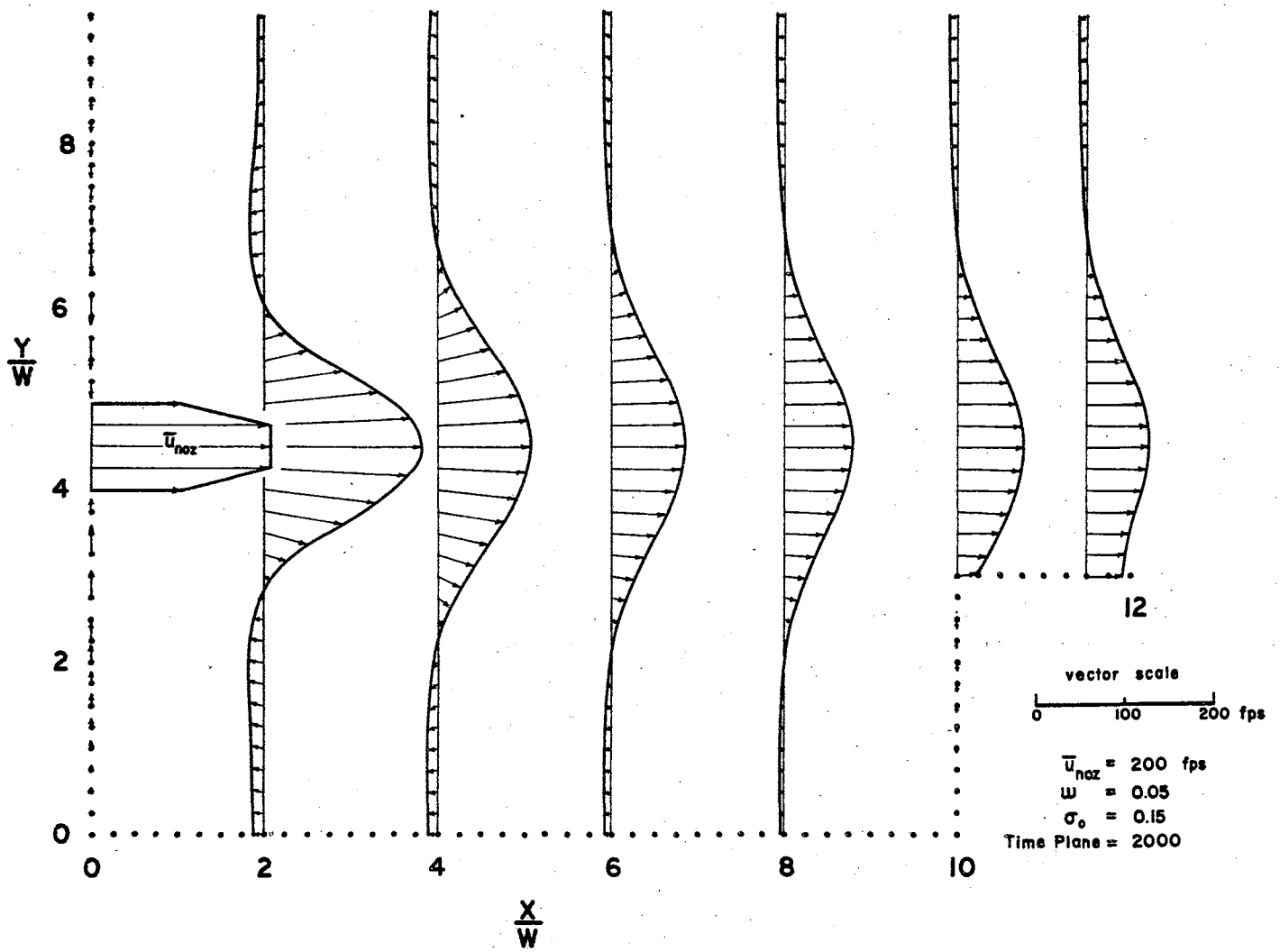

Figure 15. Computed Velocity Distribution of the Low Speed Compressible Flow Case

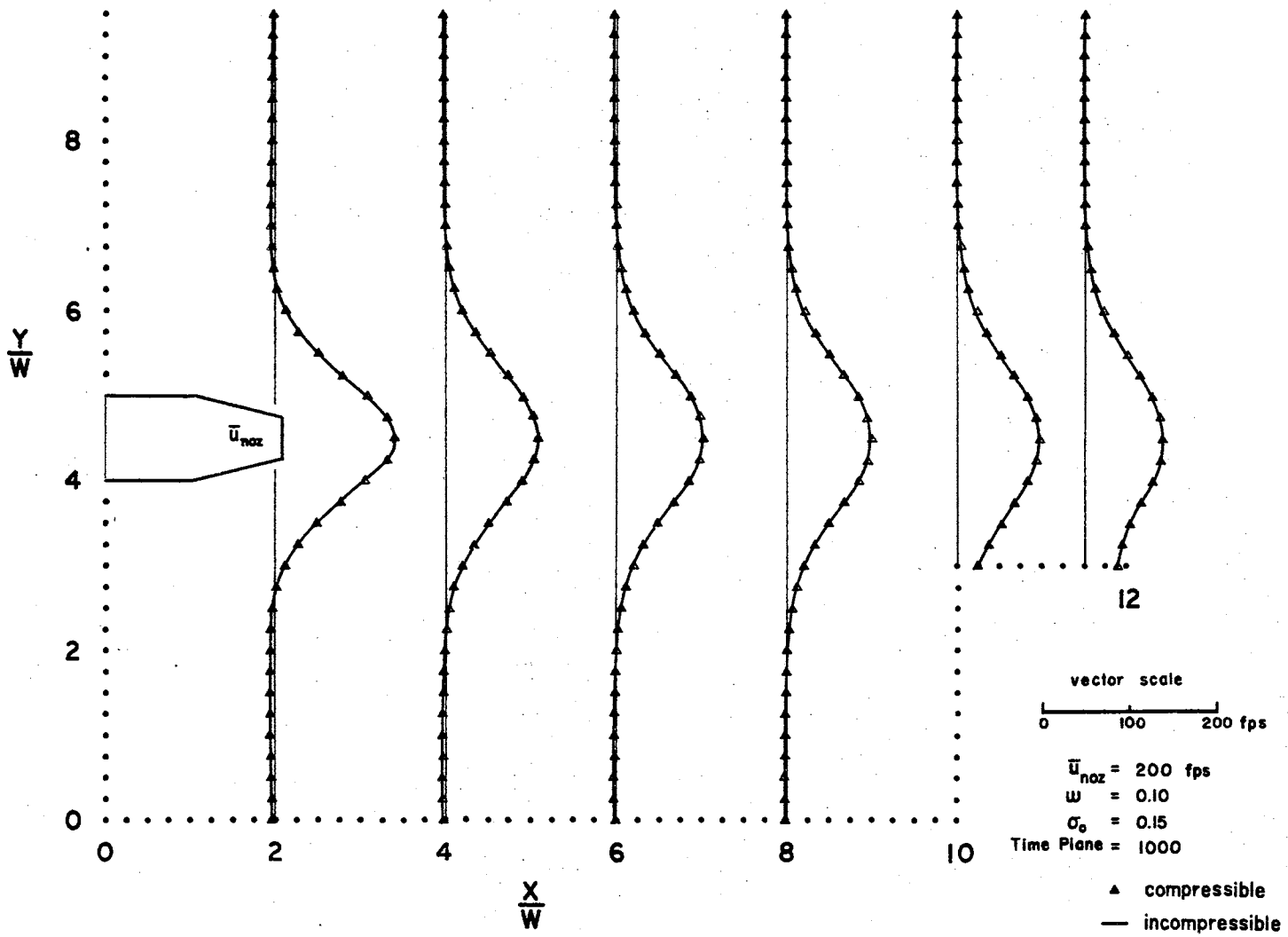

Figure 16. x-Component Velocity Distributions of the Low Speed Incompressible and Compressible Flows

blurring terms than the assumption of incompressible or compressible flow.

The computed pressure over the field was in general very close to the nozzle pressure, that is, the reference pressure. Due to fluctuations from point to point in the fourth decimal place it was not meaningful to plot the pressure distribution; some average pressures are shown in Fig. 17. The average pressure was estimated by a method similar to the one shown in Fig. 12. In Fig. 17, the average pressure in the cavity is always lower than that of the open side and the average pressure gradient in the x-direction is far greater than the ones shown in Fig. 12. The difference between Figs. 12 and 17 might be due to the different ω values used in the computations.

With print-out every one hundred time planes it took about 58.42 minutes with an IBM 7040 system to perform these computations.

Solving for $\overline{p}$ by Iteration

As in one of the examples in Chapter IV, an iteration method was also used to solve for $\overline{p}$ for the compressible flow case. The method and the governing equations were identical except for the inclusion of the continuity equation. Density was obtained from the continuity equation, x- and y-component velocities were solved for using the x- and y-momentum equations respectively, and pressure was computed according to equations (4-15) and (C-5) by iteration. The rate of nozzle centerline x-component velocity decay is plotted in Fig. 18. A comparison of Figs. 9 and 18 shows a stronger disturbance at the nozzle exit and a weaker one at the downstream

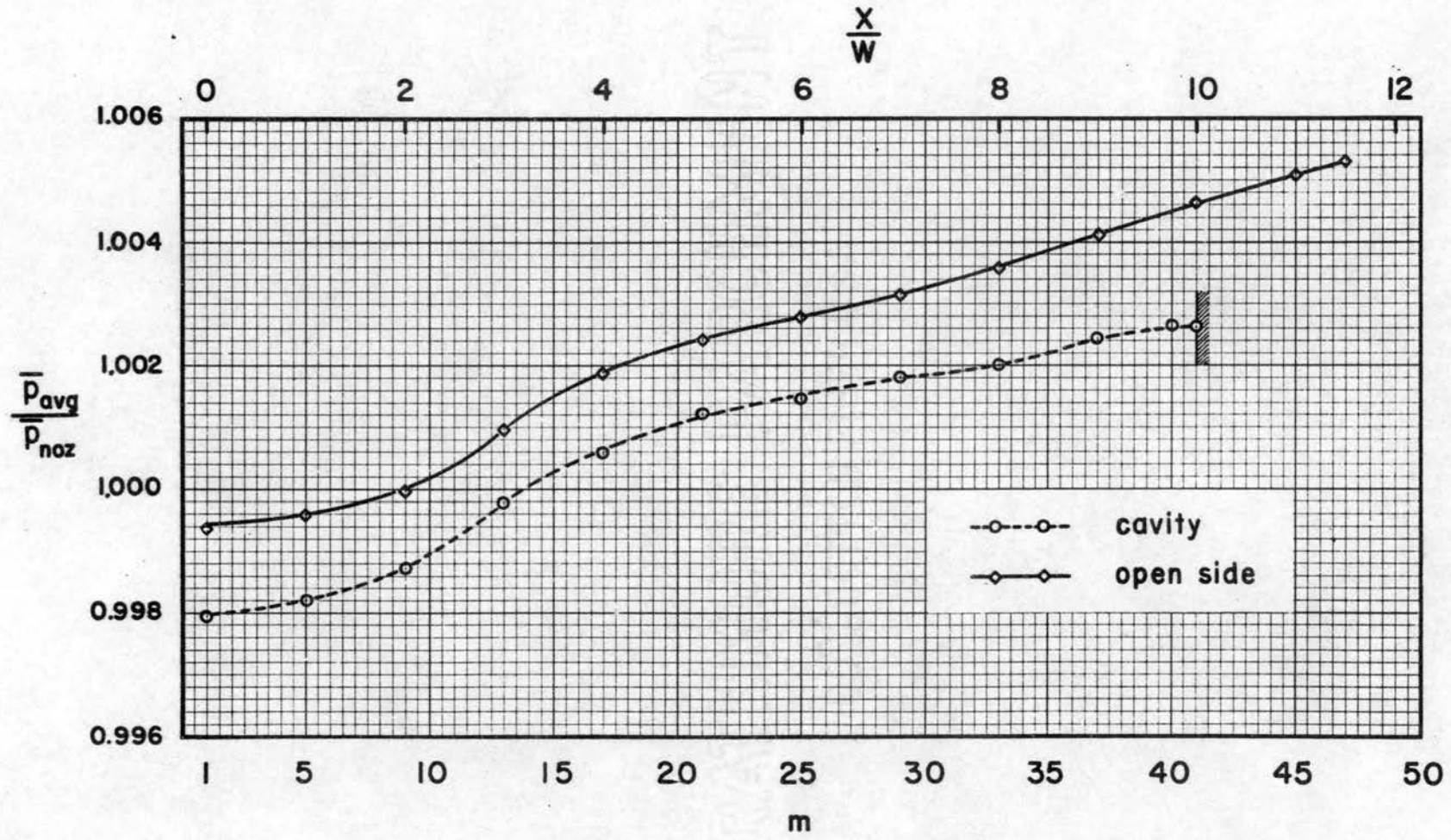

Figure 17. Average Pressure in the Cavity and the Open Side of the Low Speed Compressible Flow Case

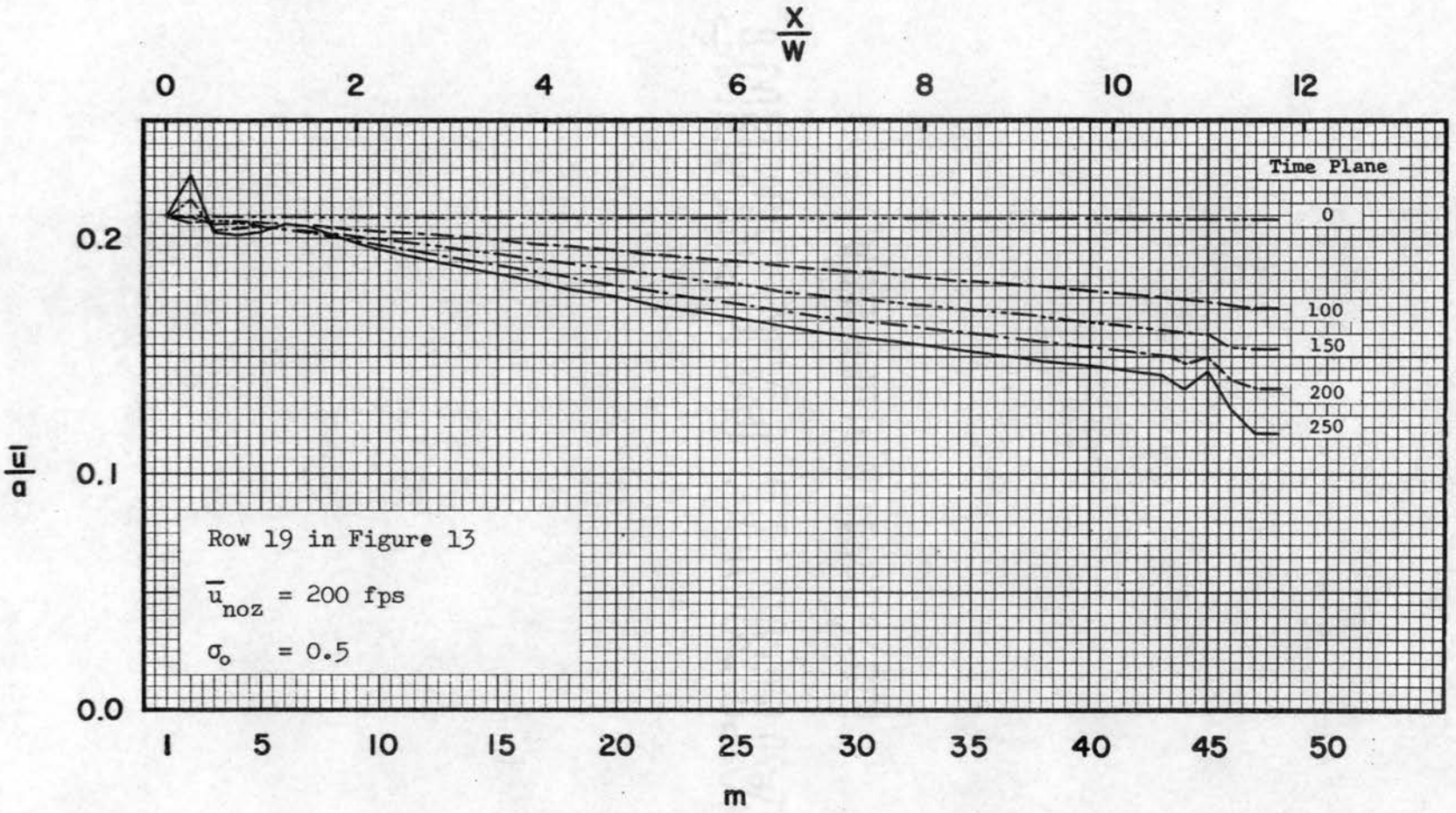

Figure 18. Decay of Nozzle Centerline x-Component Velocity of a Subsonic Compressible Jet Computed by the Iteration Method

end for the present example. Except for this difference, the same conclusions drawn for the previous example can be equally applied here. Similar to the preceding example in this chapter, the addition of the continuity equation to the set of governing equations gave no improvement.

Computed Results for the Supersonic Flow Case

Because the prediction of velocity and pressure distributions of the low speed jet by the methods described above were not successful, a supersonic flow jet mixing problem with the same geometrical arrangement as for the subsonic flow case was solved for comparison. The data used for the computation are shown in Table IV, the representation of the nozzle exit velocity is shown in Fig. 14, and the net point field is shown in Fig. 13. The method of computation is exactly identical to the one used for the subsonic flow case. The velosity and pressure distributions of the computed results of the 1000th time plane are plotted respectively in Figs. 19 and 20. At the 1000th time plane, the computed values have not yet reached their asymptotic values but are converging slowly.

Fig. 19 shows clearly the entrainment of fluid from the open side of the cavity and a fairly strong reverse flow in the cavity itself. The jet bends toward the cavity first and then outward. The jet reattaches to the upper part of the recompression step, as can be seen from the high concentration of constant pressure lines near the downstream upper corner in Fig. 20. The local low pressure in the cavity is located near the center of the cavity and the trend of the pressure distribution on the cavity walls is similar to that

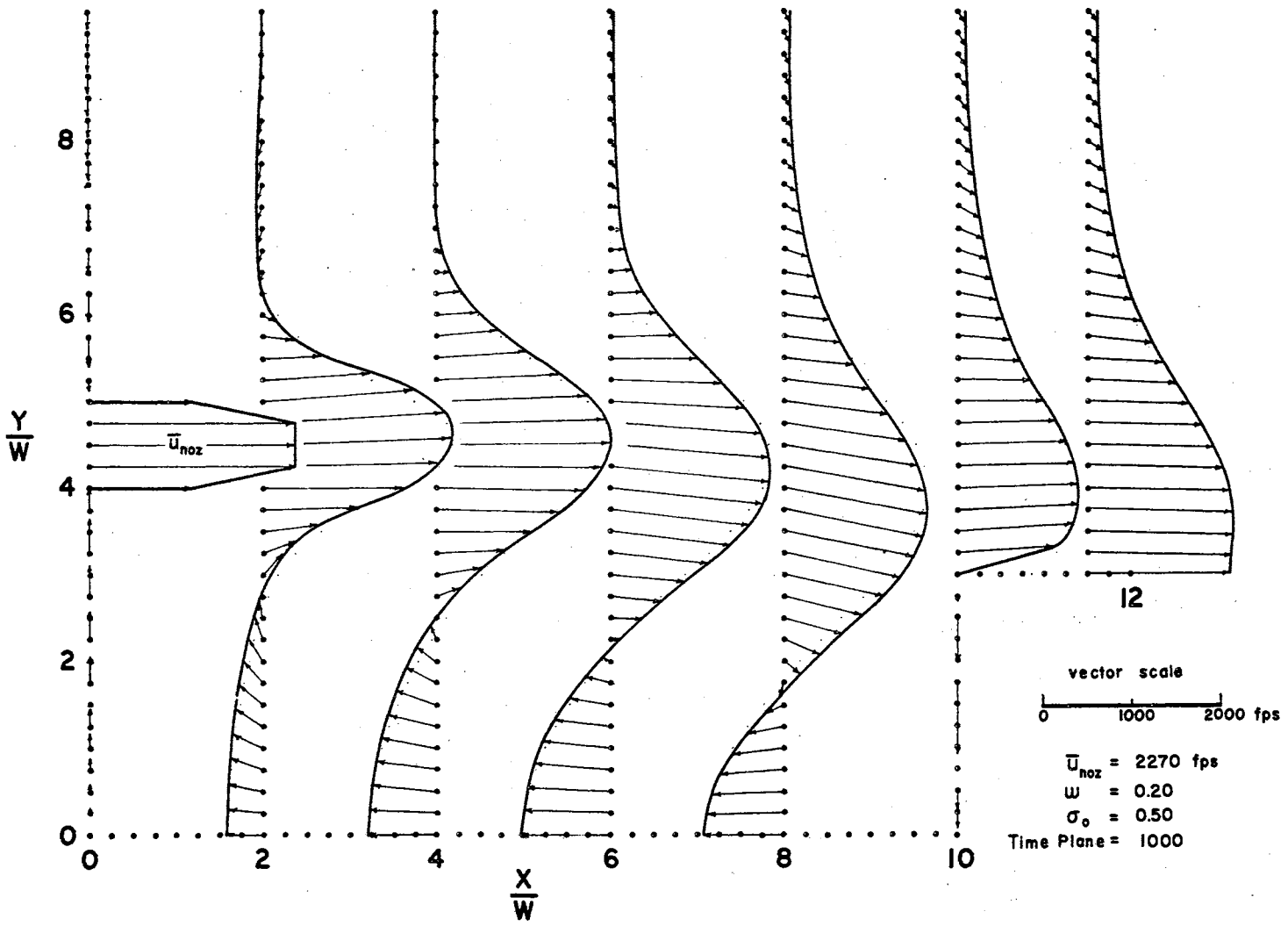

Figure 19. Computed Velocity Distribution of the Supersonic Flow Case

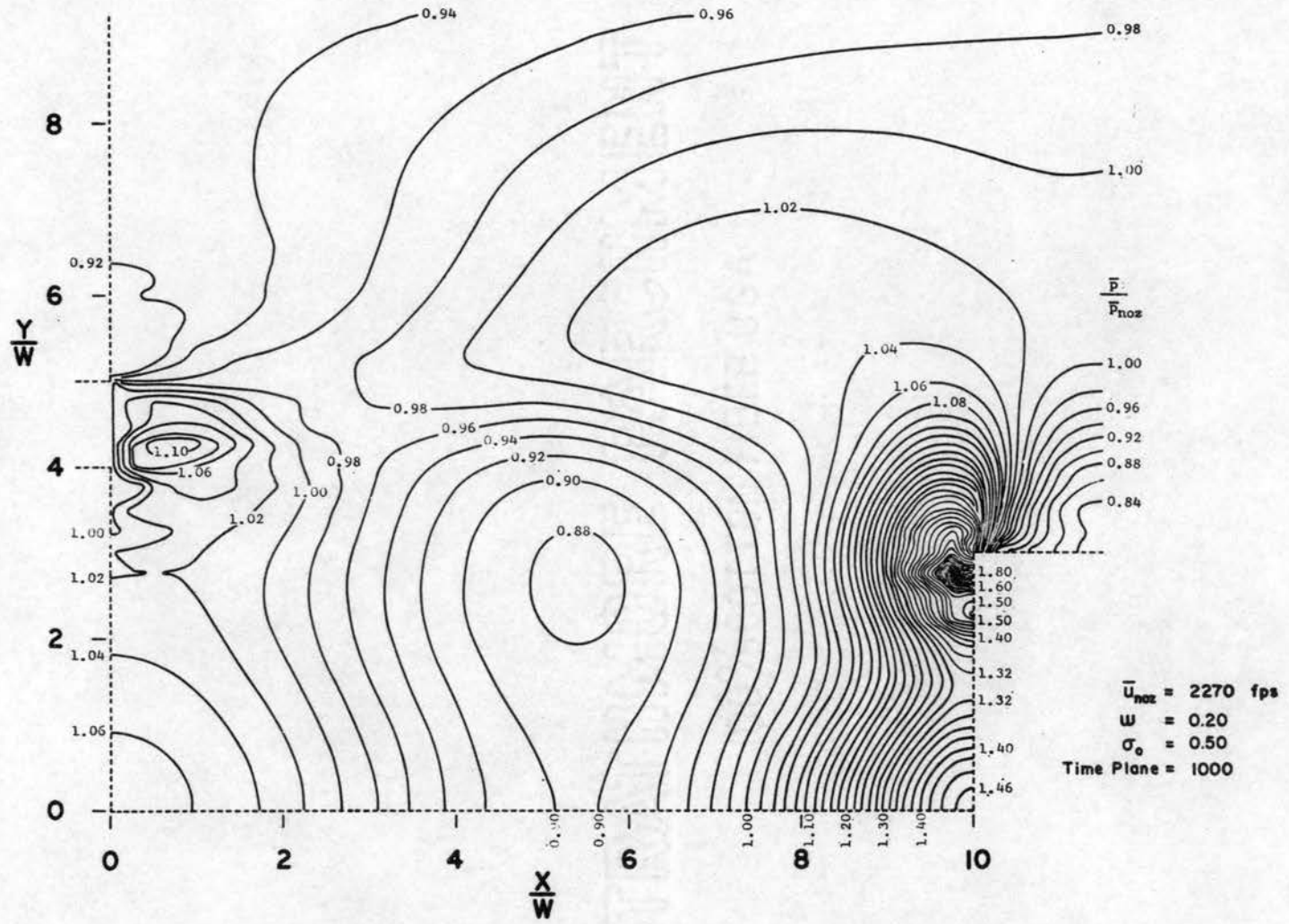

Figure 20. Computed Constant Pressure Lines for the Supersonic Flow Case

measured by Charwat, et al. (14) for a different cavity and jet arrangement (see Fig. 1(k)). The application of this method in the solution of the supersonic flow jet mixing problem looks fairly promising.

About 58.68 minutes were required to compute 100 time planes and one print-out of the results.

CHAPTER VI

EXPERIMENTAL STUDY

The major objective of this experimental study was to obtain qualitative information about the partially confined, two-dimensional, turbulent jet, so that comparison between the computed and experimental results can be made. The experimental apparatus, however, was so designed that it can be used to study a wide variety of jet flow problems such as the effects of side walls, receivers, receiver-diffusers and cavities on the main jet and the flow characteristics in these elements.

Description of General Apparatus

A 3-hp, 1 to 7 ratio variable drive motor was connected directly to a blower. The supply air pressure was adjusted by regulating the motor speed. The output of the blower was passed through a 6-inch flexible hose to a plenum chamber. A schematic drawing of the test setup is shown in Fig. 21.

The first section of the plenum chamber was a 6 to 12 inch conical diffuser with a 18-degree included angle. This was followed by five 12-inch diameter cylindrical sections. According to the original designer, K. N. Reid (42), the first section contained in succession, 4 inches of fiberglas, 3 inches of rubberized packing material, and approximately 5000 paper soda straws. A taut 30 mesh

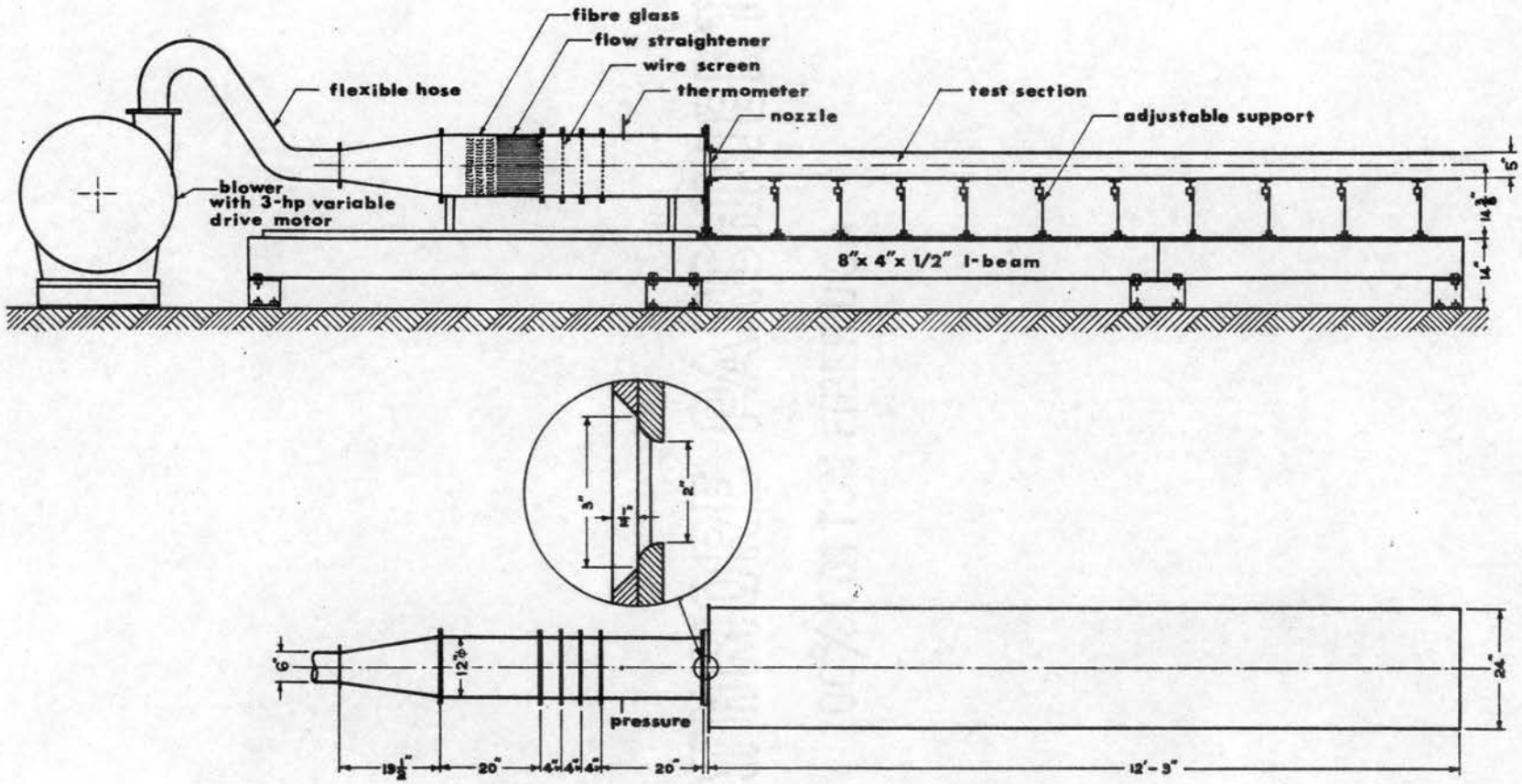

Figure 21. Experimental Flow Channel

copper wire screen was soldered to the rear end of the first section. This was followed by three intermediate, 5-inch long cylinders each with a taut 30 mesh copper wire screen soldered to its rear end. After this, a final 20-inch long section of cylinder followed. The downstream end of this last section was joined to the nozzle assembly. The supply air pressure and temperature were measured 16 inches upstream of the nozzle assembly. Having passed through this plenum chamber, the supply flow entering the nozzle could be considered to be uniform and steady.

The nozzle assembly is shown in Fig. 22. It consisted of a nozzle block (¾" aluminum stock) with a rectangular opening and two sliding plates (½" aluminum stock). The nozzle height was fixed at 5 inches and the maximum opening of the nozzle was 2½ inches.

A ¼-inch deep, 5-inch wide groove was cut horizontally across the nozzle block on one side and 3 x 5-inch rectangular opening was cut at the middle of the groove. Four sides of the opening were ground to an angle of 45-degree on the upstream side and polished. This design served to reduce the possible disturbance caused by the area reduction from the plenum chamber to the nozzle opening. One end of each of the nozzle sliding plates (12" x 5") was rounded off with an ½-inch radius circular arc and polished. Four slots were made on the nozzle sliding plates, so that they could be fastened to the grooves of the nozzle block. The nozzle plates could be adjusted to give a maximum nozzle opening of 2½ inches. Two rows of screw holes on the face of the sliding plates were made for the purpose of the addition of side walls or a cavity assembly with different separation offsets and angles. The maximum

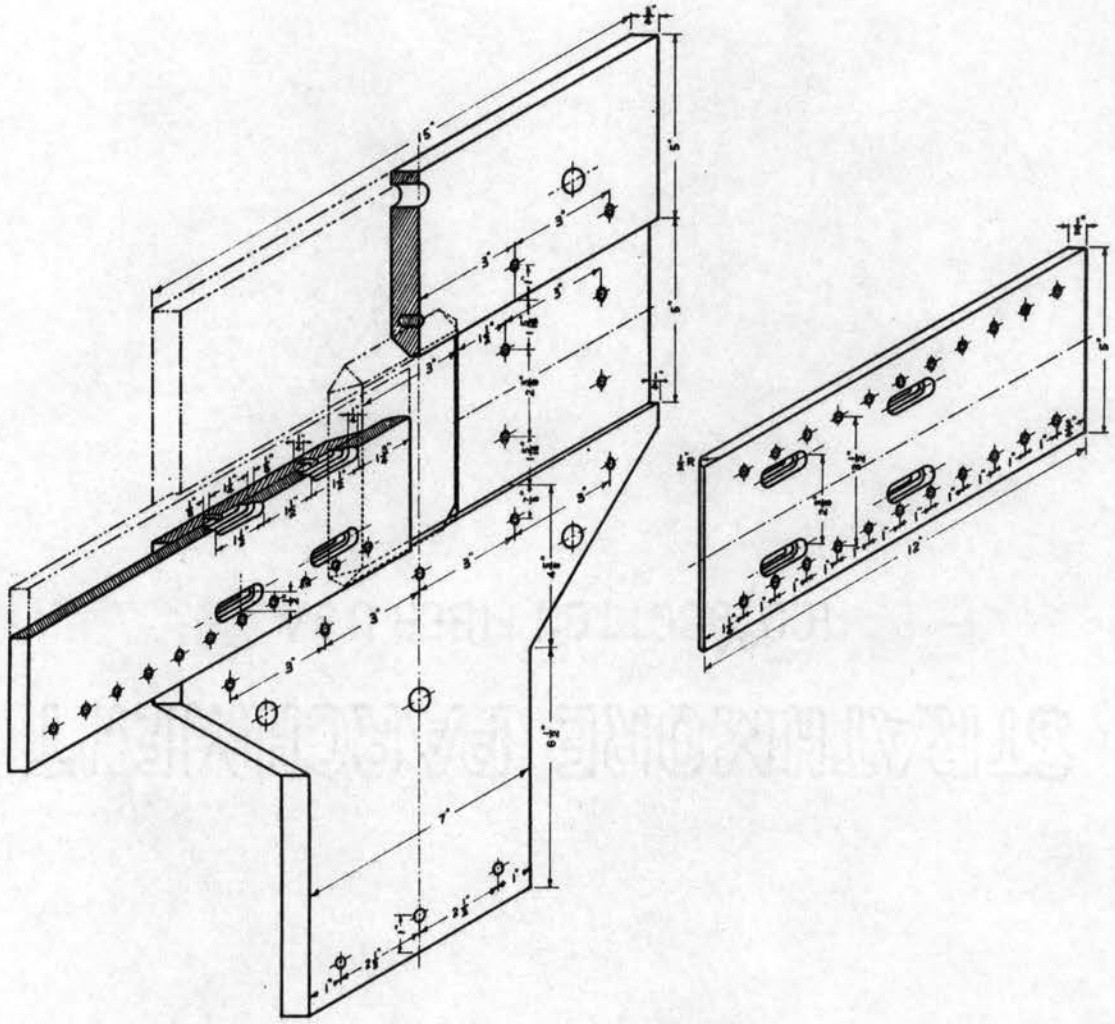

Figure 22. Nozzle Assembly

allowable offset from the tip of the nozzle plate was 10 inches. A small amount of silicon grease was spread over the groove as a sealant before the nozzle plates were fitted to it.

The bottom plate of the flow channel was a 24-inch wide, 57-inch long, ¼-inch thick aluminum plate and was extended to a total length of 12 feet, 3 inches. One end of the bottom plate was attached to the nozzle block. The whole span of the bottom plate was set on ten adjustable supports. The top plate of the flow channel was not a single piece. Several different lengths of 3/8-inch thick plexiglas pieces, ranging from 2 to 20 inches, were made, so that, a probe traverse unit could be placed at the desired location to make velocity profile measurement. In addition to these, one extra long piece (6 ft) was made to cover the unused part of the flow channel. All plexiglas pieces were 24 inches in width, excluding the flanges. Those pieces, including the probe traverse unit, were joined together with threaded rods and nuts. One end of the assembled top plate was fastened to the nozzle block.

Depending on the kind of experiment to be made, different means of support for the top plate were used. The height of all the side walls, receivers, diffuser and cavity assembly was 5 inches. Different test geometries could be easily set up on the bottom plate and the whole assembly covered with the top plate. The resulting flow channel was sandwiched between a series of parallel bar clamps, as can be seen from the Figs. 23 and 26.

On the bottom plate of the flow channel, there were 204 pressure taps with a high concentration near the nozzle exit. The holes were made with a No. 54 drill (0.055" diameter) and an 1-inch long No. 17

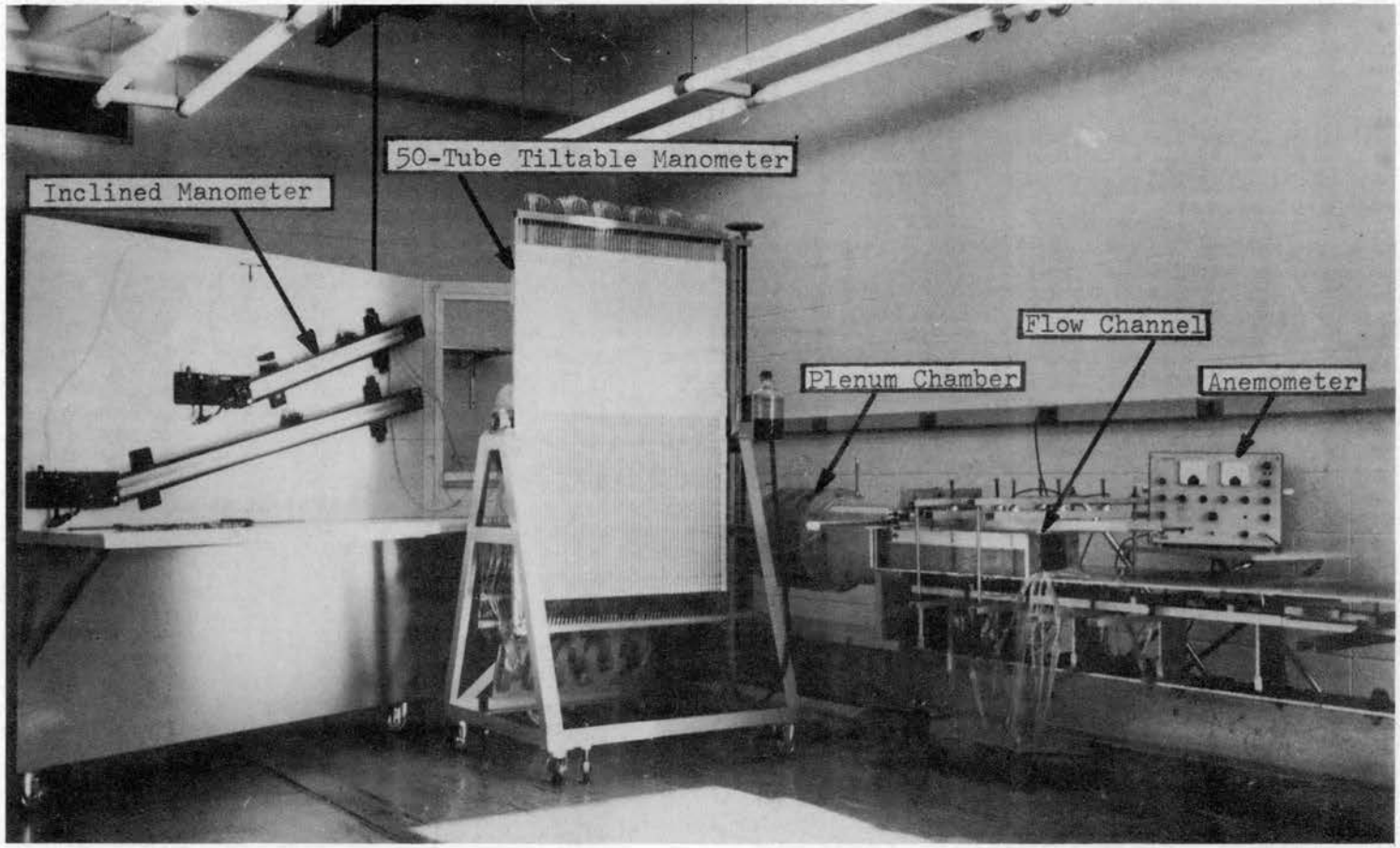

Figure 23. Photograph of Apparatus and Test Section

(0.059" O.D.) stainless steel hypodermic tubing was driven into each hole. After insertion of the hypodermic tubing, each hole was checked carefully at the face of the bottom plate and made as uniform as possible by a hand drill if the hole was not round. Clear plastic spray was applied around the hypodermic tubings from the other side of the bottom plate to eliminate possible clearance between the hole and tubing. Leakage was thoroughly checked and eliminated. Depending on the region of interest in the flow field, 147 pressure taps could be selected and connected to a tiltable 50-tube manometer. The unused taps were plugged.

In order to make this 50-tube manometer applicable for a greater number of pressure measurements, a guillotine switch system was constructed. This made it possible to measure up to 147 pressure readings without changing the pressure tap connections. One tube among the 50 tubes was left open to the atmosphere for reference. The guillotine switch system consisted of a three-way adapter and three sets of guillotines (see Fig. 24). The manometer board could be tilted to any desired angle from 0 to 90 degrees; three pre-fixed positions were provided to give multiplication ratios of 1:2, 1:4, and 1:5. Two additional inclined manometers were used with the pitot-static probe.

The probe traverse unit included a base plate (26" x 4 15/16" x 3/8"), two guiding pieces and a sliding probe carrier (46 1/2" x 2 5/8" x 3/4") and a probe carrier advancing gear unit which consisted of a worm (single thread), worm gear (30 teeth), pinion (12 teeth) and rack (2 feet), all of 24 pitch. A slot, ¼-inch in

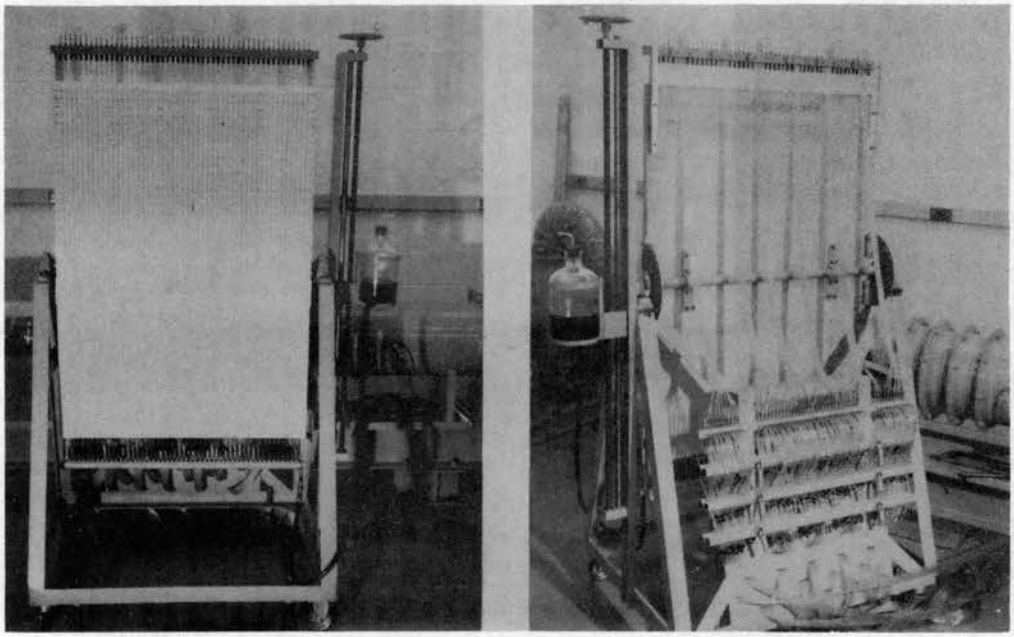

(a) (b)

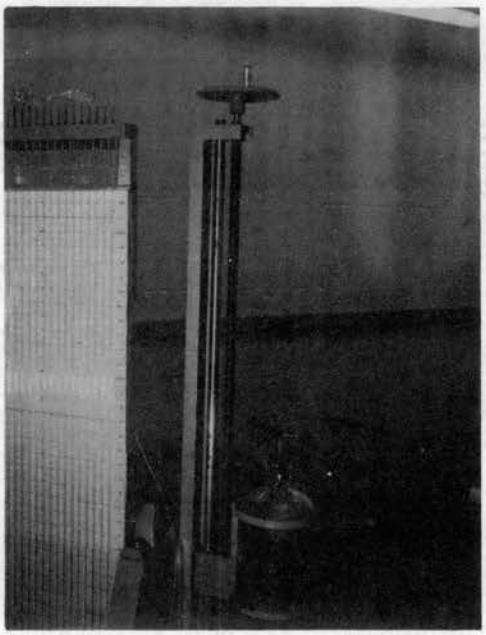

(c)

Figure 24. Photographs of the 50-Tube Tiltable Manometer

width and 20½-inches in length was milled from the base plate so that the probe could travel across the flow channel. An O-ring groove was cut around the slot and a 1/8-inch O-ring was laid in the groove; a small amount of silicon grease was applied to the O-ring to aid in sealing.

A rectangular groove was milled on one side of each of the guiding pieces and the two sides of the sliding probe carrier were milled to match them. The rectangular groove of one of the guiding pieces was deeper than needed to match the probe carrier. This space was provided so that the rack could be mounted on the probe carrier. At the mid-way point of the probe carrier, a hole with a 3/8-inch normal pipe thread was made to enable one to use different kinds of probes, such as pitot-static probes, directional probes and hot-wire probes, all with the same traverse unit. Worm gears driving a rack-and-pinion were assembled at the end of the rear guiding piece and the rack was fastened to the downstream edge of the probe carrier, see Fig. 25. The worm gear and pinion were mounted on the same shaft (3/16" diameter). Each revolution of the worm made the probe travel 0.0523 inches.

For velocity distribution measurements, a DISA (DISA ELEKTRONIK A/S, Herlev, Denmark) Constant Temperature Anemometer, Type 55A01, and a pitot-static probe (0.060" diameter, United Sensor & Control Corp., No. PAA-5-J) was used.

Procedure and Results

The nozzle opening was set at 5/8-inch (i.e., a nozzle aspect ratio of 8) throughout the tests. Due to the size of the probe, it

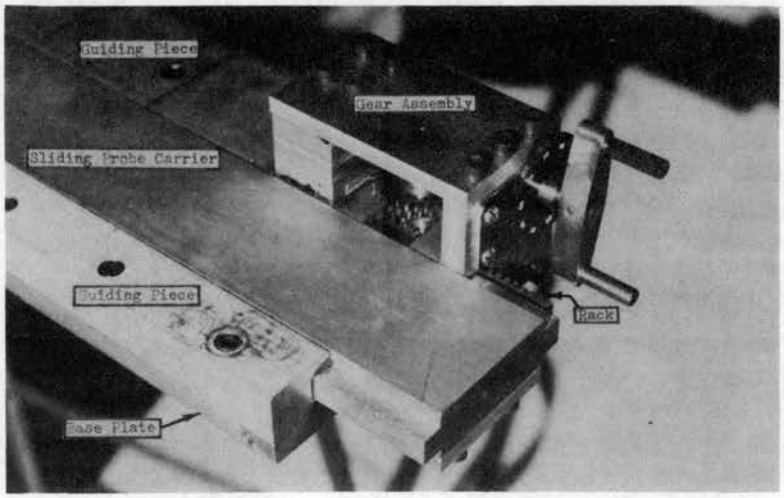

Figure 25. Photograph of Gear Assembly for Probe Traverse Unit

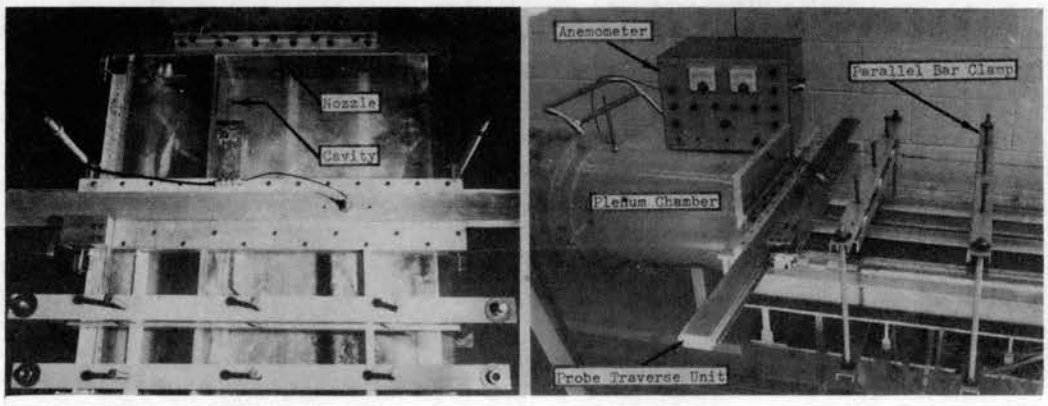

(a) (b)

Figure 26. Photographs of Test Section

was preferable to use a bigger nozzle opening. On the other hand, it was desirable to have a smaller nozzle opening from the viewpoint of obtaining two-dimensional flow. With an aspect ratio of 8, the flow was no longer two-dimensional but it had been found, according to some previous experiments conducted for the study of jet reattachment, that the deviation from two-dimensional flow was still within the tolerance of engineering accuracy.

Due to the configuration of the flow field of this study, shown in Fig. 27, the flow directions varied. In most cases there was a reverse flow in the cavity. The orientation of the hot-wire probe was difficult since it had to be placed in the flow field with its axis perpendicular to the flow direction. Before the calibration of the hot-wire probe was made, the hot-wire anemometer was calibrated according to the instruction manual supplied by the manufacturer.

A DISA miniature hot-wire probe type 55A25 (45 mm long), with type 55A21 (91 mm long) probe support, was calibrated by comparing measurements with the hot-wire probe and a pitot-static probe, at a location 0.5 inches away from the nozzle and 2.5 inches from the flow channel bottom plate.

Nozzle openings of 5/8 inches and 1 inch were used for the hot-wire probe calibration. A warm up period was allowed before any data were taken. The estimated error in the calibration was 7% of full scale. The air velocity was calculated from following equation

$$u_{noz} = 2.94528 \sqrt{(\Delta p)\ T} \quad \text{fps} , \qquad (6\text{-}1)$$

where Δp is the difference between total and static pressure in inches of water and T is absolute temperature in degrees Rankine. The pressure at the point of measurement was assumed equal to the

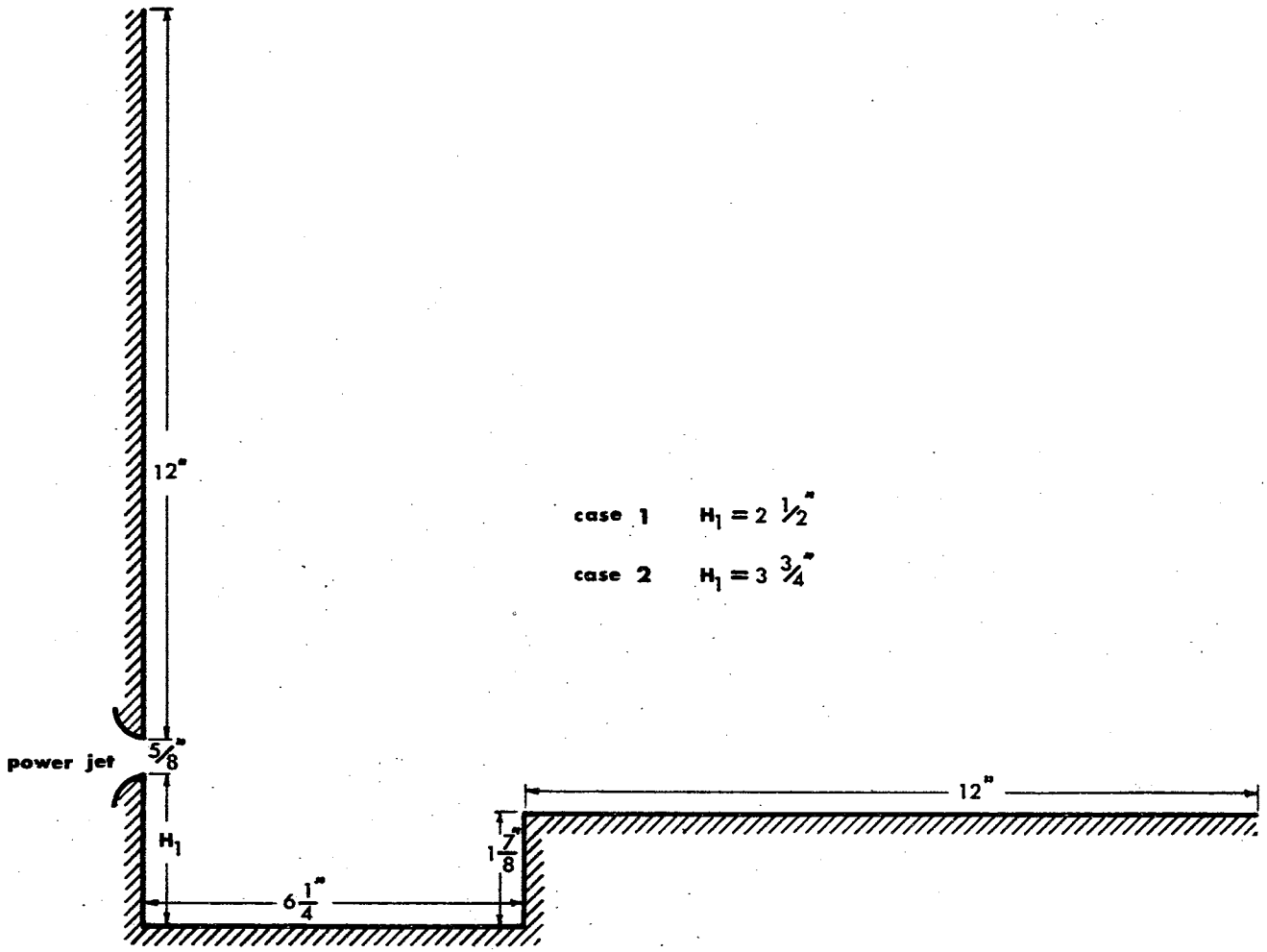

Figure 27. Dimensions of the Test Section

atmospheric pressure and the temperature was assumed to be stagnation temperature as measured in the plenum chamber.

Calibration data for the hot-wire probe are plotted in Fig. 28. The best straight line fit of the data in the range of the flow velocities used was found to be

$$D^2 - D_o^2 = 6.4795\, \bar{u}^{-0.48} \quad . \tag{6-2}$$

The configuration of the test setup is shown in Fig. 27. All dimensions except H_1 were held constant for all tests. H_1 for case 1 and case 2 were 2 1/2 inches and 3 3/4 inches respectively. For every setup, two different supply pressures, 9 inches and 1 3/4 inches of water, were used. In addition to those pressure taps on the bottom plate of the flow channel, some more pressure taps were made along the middle plane of the walls of the cavity assembly. Typical pressure distributions are shown in Figs. 31(a) and (b).

The wire of the hot-wire probe was placed at the middle plane of the flow channel, that is 2 1/2 inches from the bottom plate. To measure x-component velocity, the wire of the probe was placed in parallel with the y-axis, and it was placed in parallel with the x-axis for y-component velocity measurements. The walls of the cavity assembly were actually used as a reference for measurements. Hot-wire readings in the region of the vortex in the cavity were quite unstable, indicating that the flow in the cavity was not actually very stable. However, the average readings were taken from the anemometer to compute the average velocity.

The measured y-component of velocity was not used to plot the velocity distribution because the calibration curve was not

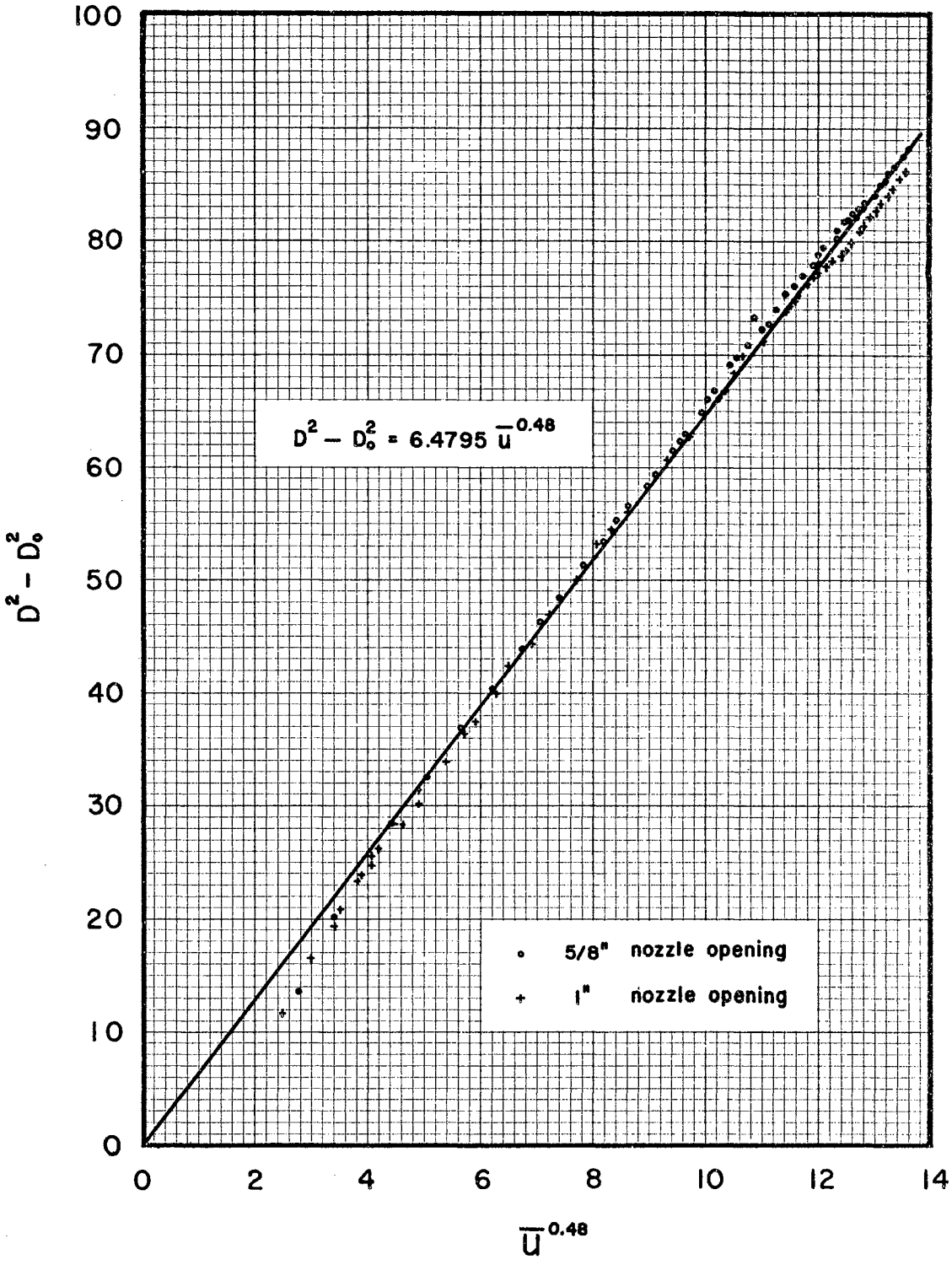

Figure 28. Calibration Curve for DISA 55A25 Hot-Wire Probe

satisfactory due to the fact that the y-component velocity was always low. The hot-wire anemometer could not give accurate measure of $\overline{v}$ when it was much less than $\overline{u}$, locally. Attempts were made to compensate for the $\overline{u}$ effect, but this could not be done with precision.

The approximate flow direction was found by placing a sharp edged, 1/32-inch thick, flat aluminum sheet cut to fit the flow field in the same plane as the probe wire had been. As can be seen in Figs. 29, about a 1/4-inch space existed between the contour of the cavity walls and the edges of the plate to eliminate possible three dimensional effects near the walls. The plate was supported by three piano wires through the pressure taps on the cavity wall and the open side was supported at four locations by C-clamps. A thin layer of lampblack and kerosene mixture was uniformly painted on the surface of the plate and the top plate was replaced in position. The blower was turned on for 5 to 10 minutes, depending on the supply pressure, to form a steady flow pattern. Typical flow patterns are shown in Figs. 29. These pictures were taken with the top plate removed and a transparency with 1/2-inch grid lines placed on the plate. Figs. 29 (a) and (b) are the flow patterns for the same geometry (H_1 = 2.5") and for supply pressures of 9 inches and 1.75 inches of water, respectively. Figs. 29 (c) and (d) are for a geometry having H_1 = 3.75 inches and for supply pressures of 9 inches and 1.75 inches of water, respectively.

It is seen that a small difference in supply pressure does not actually change the flow pattern but a difference in geometry has considerable effect. With a separation step of 2.5 inches, the main jet reattached to the upper portion of the vertical wall at the

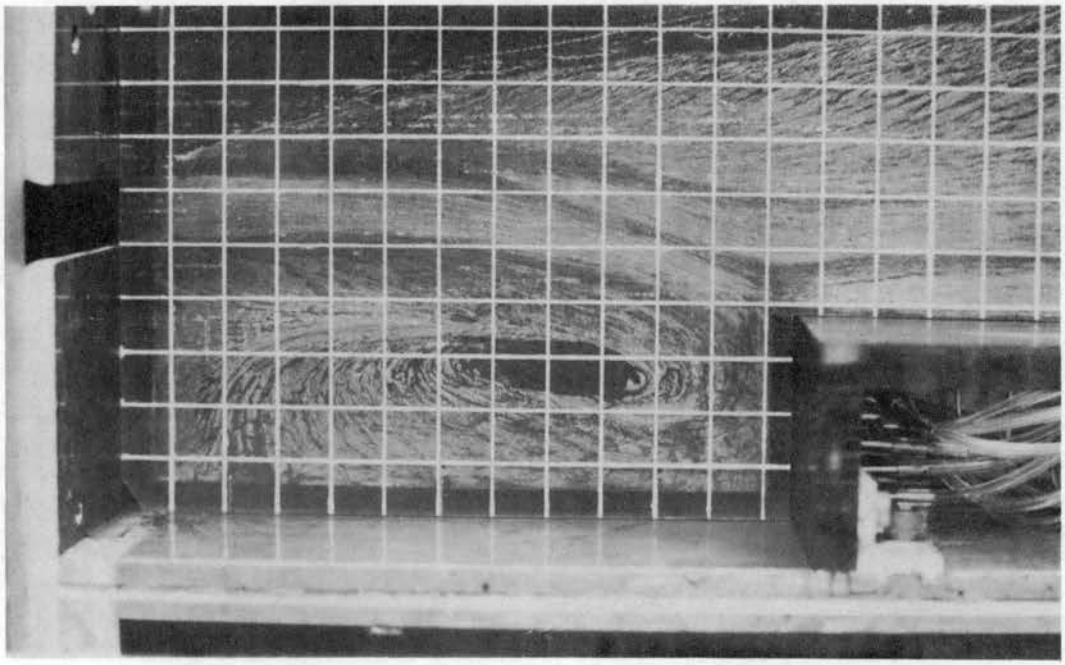

(a) H_1 = 2.5", Supply Pressure = 9" Water

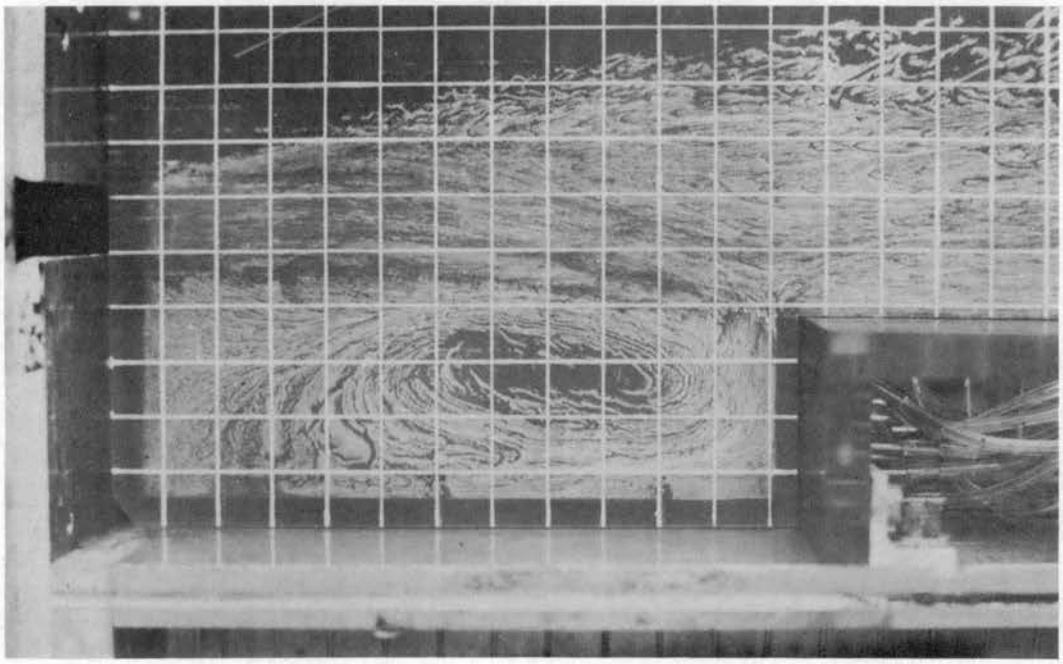

(b) H_1 = 2.5", Supply Pressure = 1.75" Water

Figure 29. Typical Flow Patterns

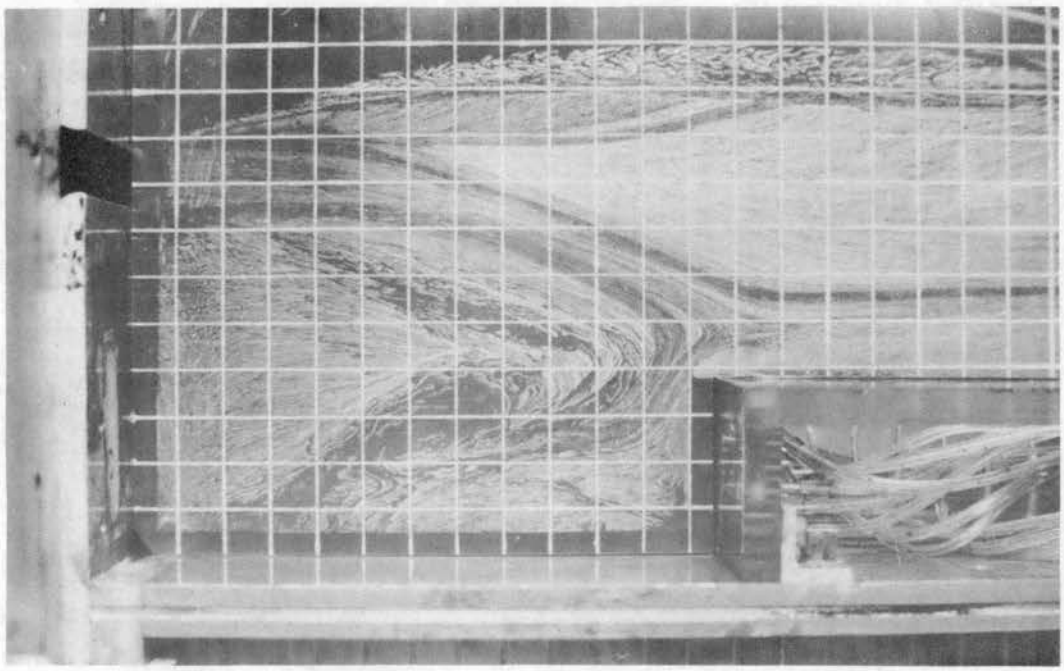

(c) H_1 = 3.75", Supply Pressure = 9" Water

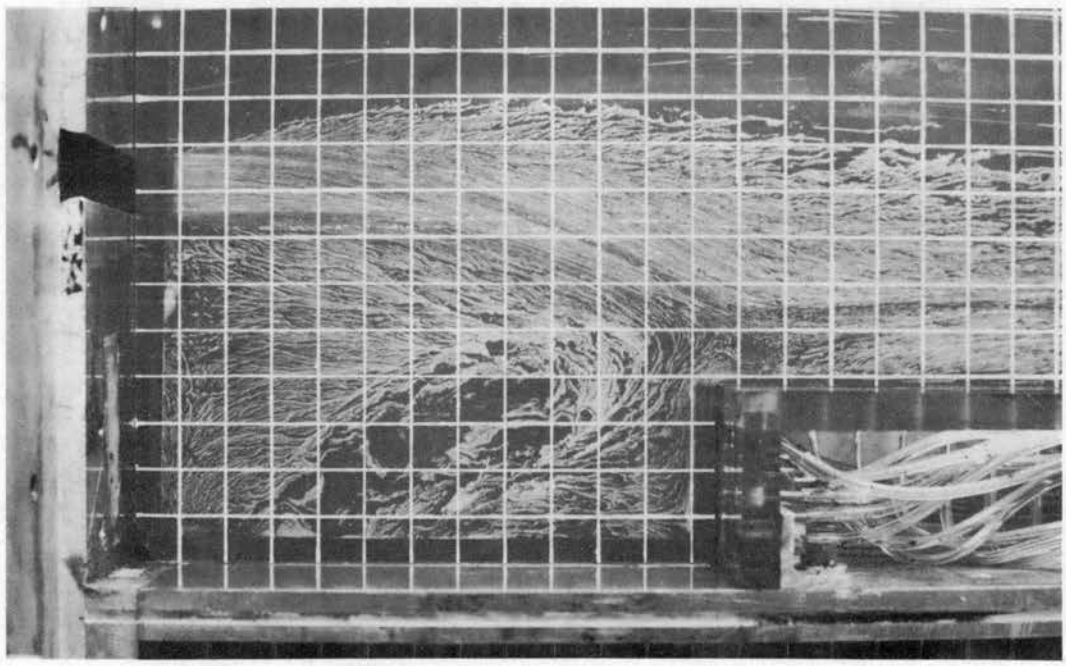

(d) H_1 = 3.75", Supply Pressure = 1.75" Water

Figure 29. (Continued)

end of the cavity. With a separation step of 3.75 inches, the jet reattached to the horizontal wall near the corner of the recompression step. The difference in the formation of reverse flow in the cavity also can be seen in Figs. 29.

The velocity profiles shown in Figs. 30 (a) and (b) were determined from the x-component velocities as measured with the hot-wire probe and the flow angles as measured from the flow pattern pictures for the cases shown in Figs. 29 (a) and (c). The estimated pressure distributions for the same geometries are shown in Figs. 31 (a) and (b).

In general, high pressure regions were located at the upper and lower corners of the recompression step and low pressure regions were located at the central portion of the horizontal wall in the cavity and the vertical wall of the recompression step. Low pressure also existed in the location of the vortex center; this is not shown in the figures due to the lack of data. Besides those few particular regions, the pressure was atmospheric. Both pressure and velocity distributions some distance downstream of the recompression step became similar.

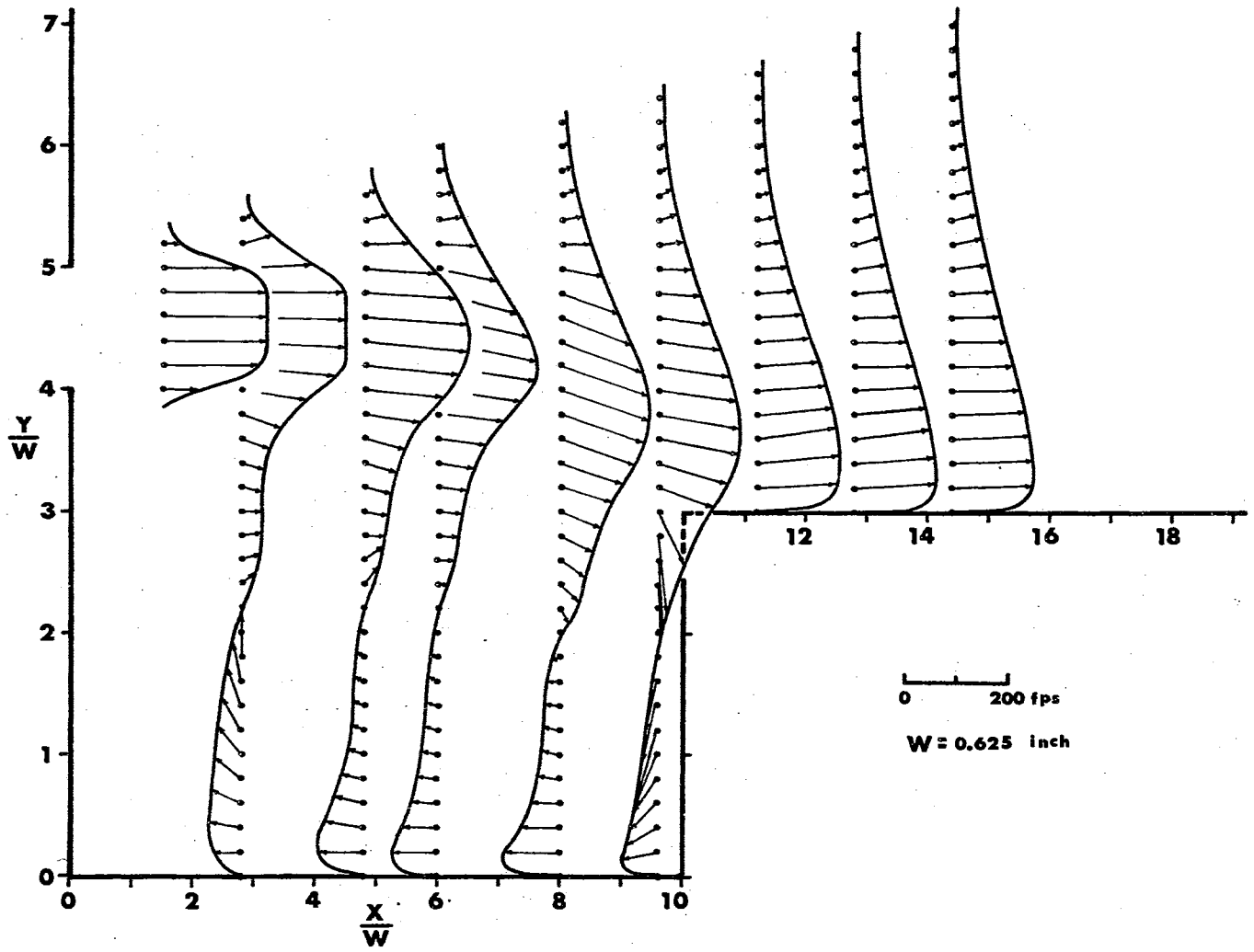

(a)

Figure 30. Measured Velocity Distributions

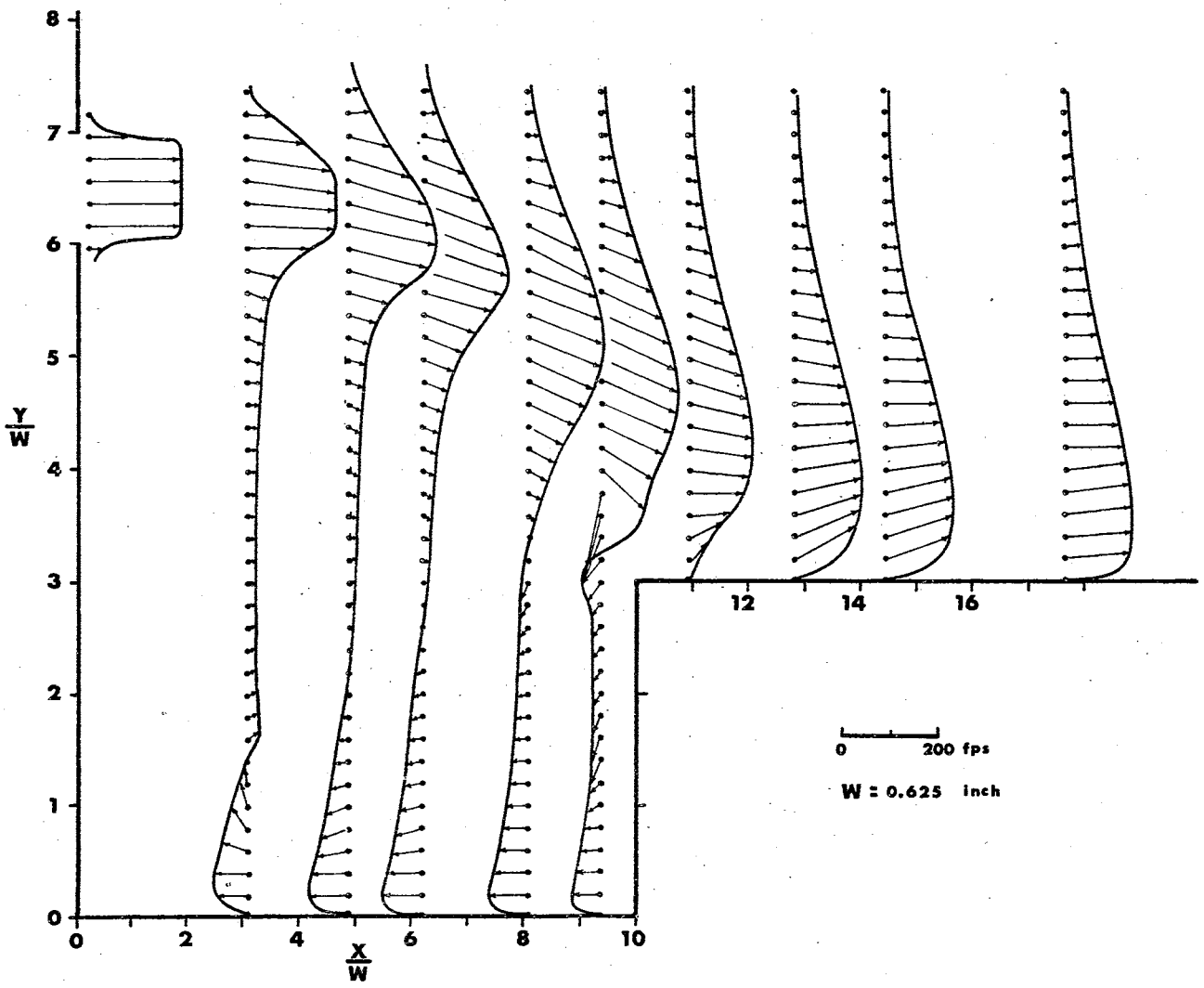

(b)

Figure 30. (Continued)

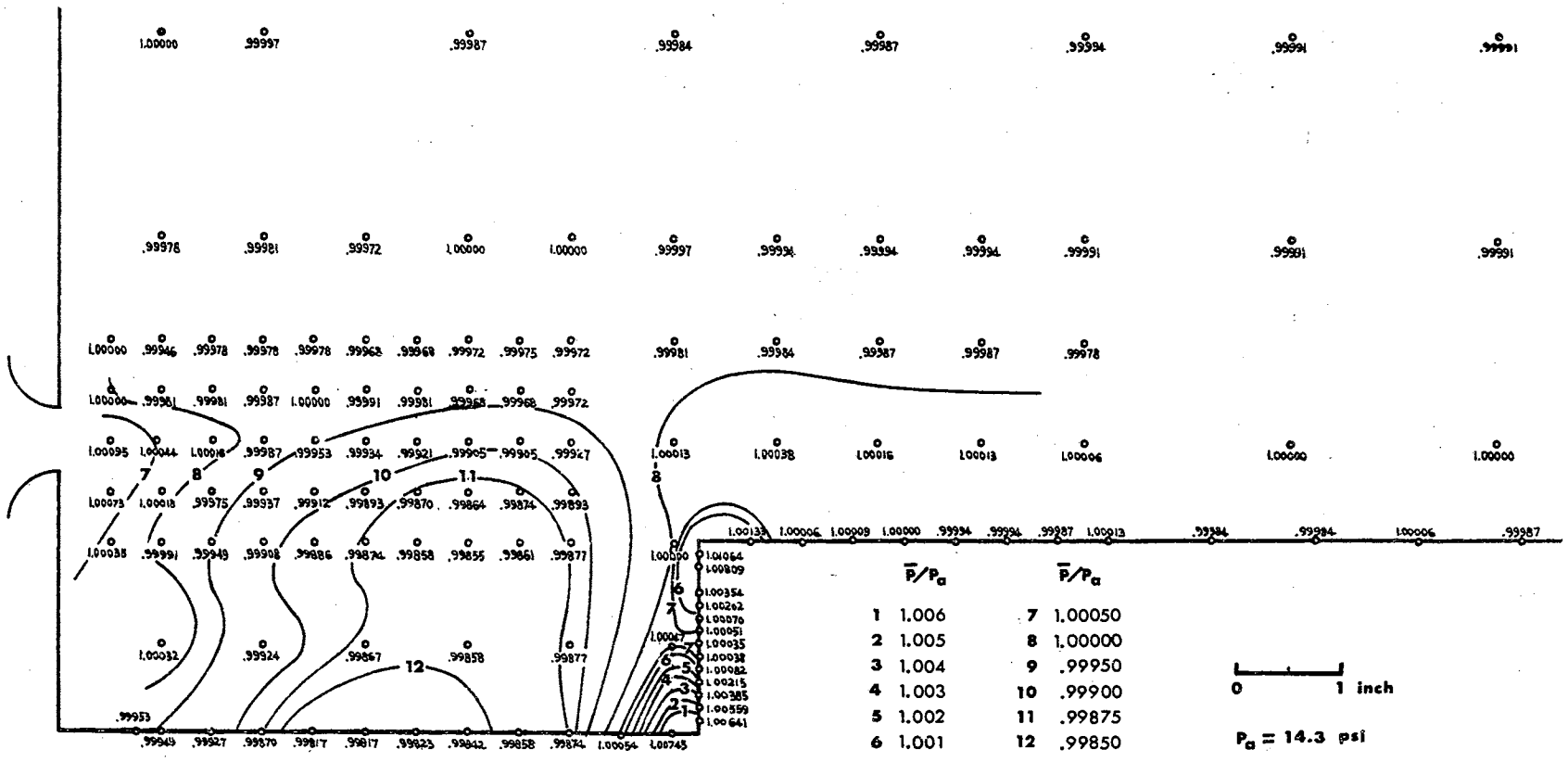

(a)

Figure 31. Estimated Constant Pressure Lines Based on Experimental Data

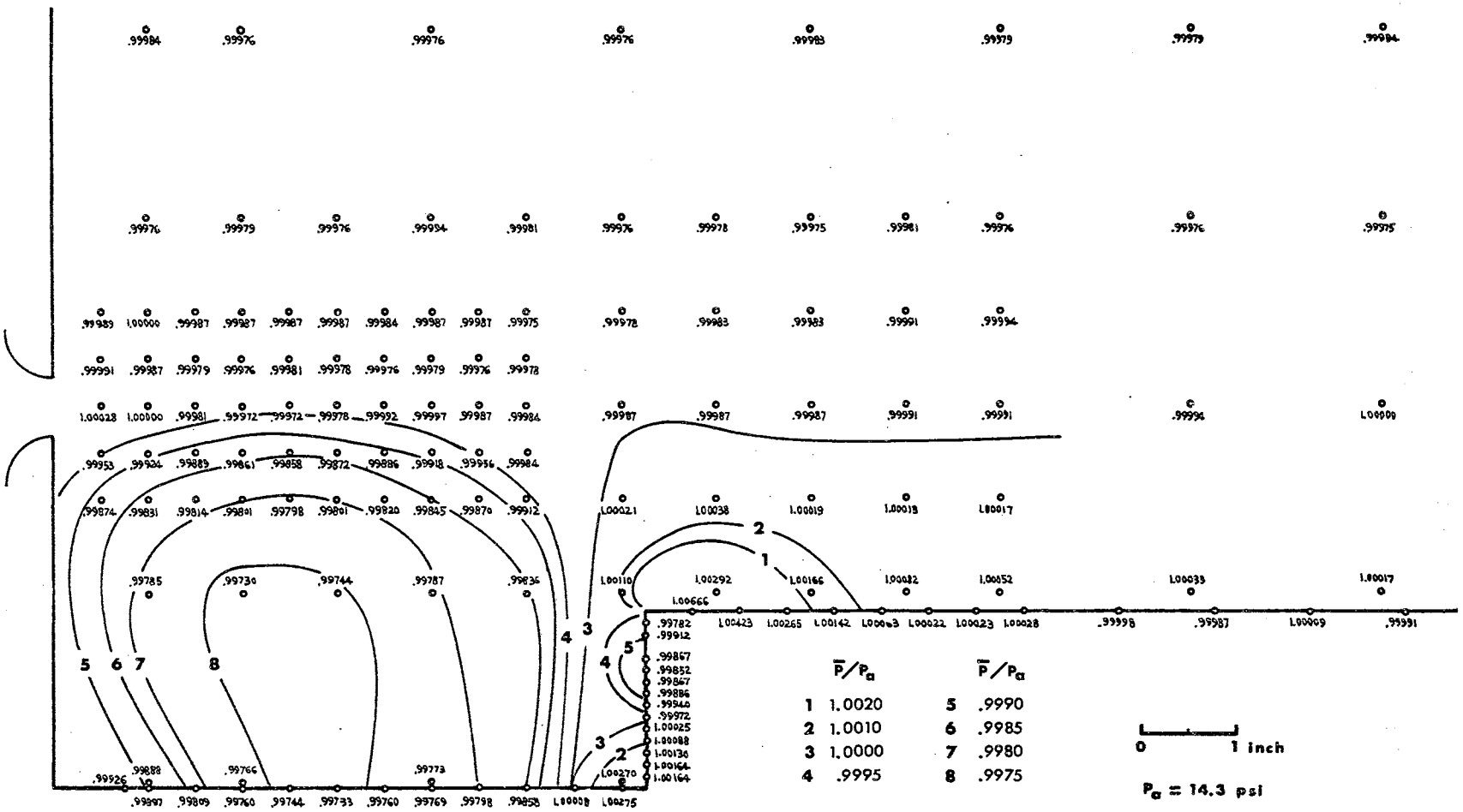

(b)

Figure 31. (Continued)

CHAPTER VII

COMPARISON OF MEASURED AND COMPUTED RESULTS

The measured velocity profiles plotted in Fig. 30 (a) and the computed velocity profiles plotted in Figs. 10 and 15 are all for the same geometry and flow conditions (nozzle exit velocity of 200 fps). Comparison of the measured and computed velocity profiles shows that the rate of jet centerline velocity decay was excessive for the computed profiles. At 11 nozzle widths downstream, the x-component centerline velocity was experimentally 78% of the nozzle exit velocity, whereas the computed velocity showed only about 34%. Prediction of the reverse flow in the cavity was not successful; experiment showed a fairly strong recirculation of fluid in the cavity. The computed velocity profiles were almost unaffected by the cavity.

For low jet velocities the pressure distribution in the flow field was practically atmospheric as can be seen in the constant pressure lines plotted in Fig. 31 (a). The accumulated truncation and round-off error of the computer solution might have exceeded the actual change of the pressure in the field under consideration.

The velocity profiles computed for the supersonic flow jet case (Fig. 19) show a similarity to the measured profiles with the 200 fps jet (Fig. 30 (a)). The jet centerline velocity at 11 nozzle widths downstream from the nozzle for this case is about 66%, which

is closer to reality. The recirculation in the cavity is also stronger for this computed case. The computed pressure distributions associated with the supersonic flow jet and the measured pressure distributions associated with the low speed jet of 200 fps are also similar, as shown in Figs. 20 and 31 (a). These results suggest the use of a higher value than the actual velocity for computation and then a suitable reduction of the computed results for the actual case being considered.

An order of magnitude analysis is carried out below to explain why the supersonic flow computed results compared better with actual measurements than did those for the subsonic case. The governing equations, equations (3-15) and the general difference equation, equation (3-26) are rewritten here for convenience:

$$f = \begin{bmatrix} \bar{\rho} \\ \bar{\rho}\,\bar{u} \\ \bar{\rho}\,\bar{v} \\ \bar{e} \end{bmatrix}$$

$$F^x = \begin{bmatrix} \bar{\rho}\,\bar{u} \\ \bar{\rho}\,\bar{u}^2 + \bar{p} - 2\bar{\rho}\,\bar{\epsilon}\,\dfrac{\partial \bar{u}}{\partial x} \\ \bar{\rho}\,\bar{u}\,\bar{v} - \bar{\rho}\,\bar{\epsilon}\left(\dfrac{\partial \bar{u}}{\partial y} + \dfrac{\partial \bar{v}}{\partial x}\right) \\ (\bar{e} + \bar{p})\bar{u} - 2\bar{\rho}\,\bar{u}\,\bar{\epsilon}\,\dfrac{\partial \bar{u}}{\partial x} - \bar{\rho}\,\bar{v}\,\bar{\epsilon}\left(\dfrac{\partial \bar{u}}{\partial y} + \dfrac{\partial \bar{v}}{\partial x}\right) \end{bmatrix}, \qquad (3\text{-}15)$$

$$F^y = \begin{bmatrix} \bar{\rho}\,\bar{v} \\ \bar{\rho}\,\bar{v}\,\bar{u} - \bar{\rho}\,\bar{\epsilon}\left(\dfrac{\partial \bar{u}}{\partial y} + \dfrac{\partial \bar{v}}{\partial x}\right) \\ \bar{\rho}\,\bar{v}^2 + \bar{p} - 2\bar{\rho}\,\bar{\epsilon}\,\dfrac{\partial \bar{v}}{\partial y} \\ (\bar{e} + \bar{p})\bar{v} - 2\bar{\rho}\,\bar{v}\,\dfrac{\partial \bar{v}}{\partial y} - \bar{\rho}\,\bar{u}\,\bar{\epsilon}\left(\dfrac{\partial \bar{u}}{\partial y} + \dfrac{\partial \bar{v}}{\partial x}\right) \end{bmatrix},$$

and

$$f^{n+1}_{m,\ell} = f^{n}_{m,\ell} - \frac{\tau}{2h_1}\left[F^{x}_{m+1,\ell} - F^{x}_{m-1,\ell}\right]^{n}$$

$$- \frac{\tau}{2h_2}\left[F^{y}_{m,\ell+1} - F^{y}_{m,\ell-1}\right]^{n} \qquad (3\text{-}26)$$

$$+ \frac{1}{2}\omega\sigma_o\left[(f_{m+1,\ell} - 2f_{m,\ell} + f_{m-1,\ell})\sin^2\chi\right.$$

$$\left. + (f_{m,\ell+1} - 2f_{m,\ell} + f_{m,\ell-1})\cos^2\chi\right]^{n} .$$

Here, all qualities will be regarded as dimensionless and a square mesh will be taken for convenience. The time increment τ can be expressed in following form:

$$\tau = \frac{\sigma_o\,(h_1)(h_2)}{(w + c)(h_1^2 + h_2^2)^{1/2}} \quad . \qquad (7\text{-}1)$$

For a square mesh the dimensionless h_1 and h_2 are identical and equal to 1; equation (7-1) becomes

$$\tau = \frac{\sigma_o}{\sqrt{2}\,(w + c)} \quad . \qquad (7\text{-}2)$$

If equation (7-2) is substituted in equation (3-26),

$$f^{n+1}_{m,\ell} = f^{n}_{m,\ell} - \frac{\sigma_o}{2\sqrt{2}}\left\{\frac{1}{(w + c)}\left[(F^{x}_{m+1,\ell} - F^{x}_{m-1,\ell}) + (F^{y}_{m,\ell+1} - F^{y}_{m,\ell-1})\right]\right.$$

$$+ \omega\left[(f_{m+1,\ell} - 2f_{m,\ell} + f_{m-1,\ell})\right. \qquad (7\text{-}3)$$

$$\left.\left. + (f_{m,\ell+1} - 2f_{m,\ell} + f_{m,\ell-1})\right]\right\}^{n} \quad .$$

If the dimensionless density and pressure are considered to be order of 1 as used in the computation and the velocity of 200 fps has

a dimensionless value of approximately 0.2, then the specific energy will have a dimensionless value of approximately 2.5. For this low speed jet flow case, the orders of magnitude of the terms in f are always one order higher than those of F^x and F^y in equations (3-15), with the exception of the pressure terms in the momentum equations. If the x-momentum equation is taken as an example, every individual term in equations (7-3) can be written as follows with the order of magnitude indicated directly below every quantity,

$$f^{n+1}_{m,\ell} = \underset{0.2}{(\overline{\rho}\ \overline{u})^{n+1}_{m,\ell}}$$

$$f^{n}_{m,\ell} = \underset{0.2}{(\overline{\rho}\ \overline{u})^{n}_{m,\ell}} \tag{7-4}$$

$$F^x_{m+1,\ell} - F^x_{m-1,\ell} = \underset{0.04 \quad 1 \quad 0.02}{\left[\overline{\rho}\ \overline{u}^2 + \overline{p} - \overline{\rho}\,\frac{\overline{u}_a{}^x}{\sigma^2}\left(\frac{\partial \overline{u}}{\partial x}\right)\right]_{m+1,\ell}}$$

$$- \underset{0.04 \quad 1 \quad 0.02}{\left[\overline{\rho}\ \overline{u}^2 + \overline{p} - \overline{\rho}\,\frac{\overline{u}_a{}^x}{\sigma^2}\left(\frac{\partial \overline{u}}{\partial x}\right)\right]_{m-1,\ell}}$$

$$F^y_{m,\ell+1} - F^y_{m,\ell-1} = \underset{0.04 \qquad 0.02}{\left[\overline{\rho}\ \overline{v}\ \overline{u} - \rho\,\frac{\overline{u}_a{}^x}{2\sigma^2}\left(\frac{\partial \overline{u}}{\partial y} + \frac{\partial \overline{v}}{\partial x}\right)\right]_{m,\ell+1}} \tag{7-5}$$

$$- \underset{0.04 \qquad 0.02}{\left[\overline{\rho}\ \overline{v}\ \overline{u} - \overline{\rho}\,\frac{\overline{u}_a{}^x}{2\sigma^2}\left(\frac{\partial \overline{u}}{\partial y} + \frac{\partial \overline{v}}{\partial x}\right)\right]_{m,\ell-1}}$$

$$f_{m+1,\ell} - 2f_{m,\ell} + f_{m-1,\ell} = \underset{0.2}{(\overline{\rho}\ \overline{u})_{m+1,\ell}} - \underset{0.4}{2(\overline{\rho}\ \overline{u})_{m,\ell}} + \underset{0.2}{(\overline{\rho}\ \overline{u})_{m-1,\ell}}$$

$$f_{m,\ell+1} - 2f_{m,\ell} + f_{m,\ell-1} = \underset{0.2}{(\overline{\rho}\ \overline{u})_{m,\ell+1}} - \underset{0.4}{2(\overline{\rho}\ \overline{u})_{m,\ell}} + \underset{0.2}{(\overline{\rho}\ \overline{u})_{m,\ell-1}} . \tag{7-6}$$

In the above equations, the apparent kinematic viscosity was replaced by equation (3-13), and $\bar{u}_a$ and $\bar{v}$ were considered to have same order of magnitude as the nozzle exit velocity; the value of σ was of order 10 and x was considered to have a value of 50, which is about the maximum value considered in the computation (see Fig. 13).

From equations (7-5), one can see that even a slight change in pressure will have a large effect whereas the turbulent stress terms contribute almost nothing. In the x-momentum equation the terms containing $\bar{\rho}\,\bar{u}$ are of major interest among those found in equations (7-4), (7-5) and (7-6). The quantities containing $\bar{\rho}\,\bar{u}$ in equations (7-6) are 5 times greater than those in equations (7-5). For this low speed jet, the value of $1/(w + c)$ is about 0.7 and even if the value of ω is chosen to be 0.15, the effect of blurring terms will have an effect equal to the momentum terms and the blurring terms outweigh all the turbulent effects.

On the other hand if the order of magnitude of $\bar{u}$ is more than 1, i.e., supersonic, every term in equations (7-4), (7-5) and (7-6) will have same order of magnitude except the turbulent stress terms. For this case, the effect of blurring terms will not surpass that of the true momentum of fluid flow to divert the description of the flow from the original governing equations. This appears to be the reason why the computed results for the supersonic flow case presented in Chapter V described the flow better than the low velocity jet flow case.

CHAPTER VIII

CONCLUSIONS AND RECOMMENDATIONS

As shown by Walker (55), the time dependent, explicit numerical technique showed promise for solving the steady state flow characteristics of a plane, turbulent, supersonic, bounded jet. From the results of Walker and the example shown in Cahpter V, one can see that this numerical method describes the physical flow phenomenon nicely for a supersonic flow case. For a low speed flow case this method was not successful.

The results of this study showed that in a supersonic jet the turbulent shearing stresses are large enough to replace the artificial blurring terms used to stabilize the computation. Walker showed that the ω value needed for a turbulent, supersonic flow jet was about one-tenth of the value required for inviscid flow. This indicated that the shearing stresses alone would be almost sufficient to make the computation stable. It is always desirable to use a small value of blurring parameter, ω, to reduce the effect of the artificial viscosity, but the ω value selected must prevent instability.

In the present study, for subsonic jets, when the ω value selected was held constant and the value of time increment, τ, changed, no differences occurred in the computed results so long as the τ values selected were below a certain limit. For the subsonic case, the order of magnitude of the velocity was one order lower

than that of the density and the energy and the turbulent shearing stresses were always small. Because of this, the stability of computation depended mainly on the artificial viscosity, i.e., a high ω value. With a large ω value, the artificial viscosity term became very significant and this, in most cases, would change the original meaning of the governing equations of the flow and make the accurate description of the physical flow phenomenon practically impossible. This is clearly seen from the high rate of the jet centerline velocity decay.

Several attempts were made to non-dimensionalize the governing equations so that the velocity of the low speed jet would have the same order of magnitude as the other dimensionless flow properties, but it was found that there was only one self-consistent method to non-dimensionalize the governing equations. That is, the reference velocity used to non-dimensionalize the velocity terms in the governing equations has to be the square root of the ratio of the reference pressure and the reference density.

The method of evaluation of the fluid properties at the net points on the field boundary is extremely critical for a low speed jet, because the asymptotic results depend strongly on the boundary values specified. If the representation of the field boundary employed is not proper, computation instability may result. The representation of the net points on the solid boundary is not so critical as those on the field boundary and the reflection technique employed proved to be successful. With slip flow on the solid wall, the computed results yielded a better velocity distribution near the wall than that for non-slip flow.

The imposing of constraints near the nozzle, such as the use of triple-value net points to retard the artificial blurring, or the use of zero velocity net points near the nozzle exit to force the jet separation not to occur too close to the nozzle, was not beneficial. Even the addition of an artificial jet potential core was not effective in lowering the rate of jet centerline velocity decay. Moreover, if a local pressure jump occurred due to the addition of any of such constraint, it caused instability under some unfavorable combinations of computation parameters.

In this study, the limits of application of the time dependent, explicit numerical technique for solving steady state two-dimensional, turbulent, bounded jet problems have been shown. For low velocity jets, the application of this method to describe the physical flow phenomenon is limited due to high artificial viscosity terms required in the computation for stability. Several problem areas have been defined and explored for this type of application.

The following recommendations are made for further study in this field:

1. For the treatment of low velocity jet mixing problems, a different form of blurring term should be devised if the numerical technique discussed in this study is to be employed.
2. It would be desirable to conduct a few sample computations of supersonic jet flow problems for which reliable experimental data are readily available for comparison and determine the lower limit of velocity where this method ceases to yield acceptable results.

3. Further investigation of the representation of the double image point is needed if the reflection technique is to be employed to treat the net points on the convex corner of a solid boundary.

4. Only two-dimensional flow cases have been considered in this study; however, the analysis should be equally applicable to axi-symmetric and three-dimensional supersonic flow problems. Three-dimensional flow cases should be explored because the flow in most fluid amplifiers (fluidic devices) is actually three-dimensional.

5. The study of the mixing of two jets having different thermodynamic properties would also be of great interest.

A SELECTED BIBLIOGRAPHY

1. Abbott, D. E., and S. J. Kline. "Experimental Investigation of Subsonic Turbulent Flow Over Single and Double Backward Facing Steps." J. of Basic Eng., ASME, Series D, Vol. 84 (Sept. 1962), pp. 317-325.

2. Abramovich, G. N. "The Theory of a Free Jet of a Compressible Gas." NACA TM No. 1058.

3. Abramovich, G. N. The Theory of Turbulent Jet, MIT Press, (1963).

4. Albertson, M. L., Y. B. Dai, R. A. Jensen, and Hunter Rouse. "Diffusion of Submerged Jets." Amer. Soc. Civil Engrs. Proceedings, Vol. 74, No. 10 (Dec. 1948), pp. 1571-1596.

5. Barchilon, M., and R. Curtet. "Some Details of the Structure of an Axi-symmetric Confined Jet With Back-Flow." J. of Basic Eng., ASME, Vol. 86, Series D, No. 4 (Dec. 1964), pp. 777-787.

6. Bauer, R. C. "An Analysis of Two-Dimensional Laminar and Turbulent Compressible Mixing." AIAA J., Vol. 4, No. 3 (March 1966), pp. 392-395.

7. Beheim, M. A. "Flow in the Base Region of Axi-symmetric and Two-Dimensional Configurations." NASA TR - R - 77 (1961).

8. Bourque, C., and B. G. Newman. "Reattachment of a Two-Dimensional, Incompressible Jet to an Adjacent Flat Plate." Aero. Quarterly, Vol. XI (Aug. 1960), pp. 201-232.

9. Burstein, S. Z. "Numerical Methods in Multidimensional Shocked Flows." AIAA J., Vol. 2, No. 12 (Dec. 1964), pp. 2111-2117.

10. Channapragada, Rao S. "Compressible Jet Spread Parameter for Mixing Zone Analyses." AIAA J., Vol. 1, No. 9 (Sept. 1963), pp. 2188-2190.

11. Chapman, Dean R. "Laminar Mixing of a Compressible Fluid." NACA TN No. 1800 (Feb. 1949).

12. Chapman, D. R., D. M. Kuehn and H. K. Larson. "Investigation of Separated Flows in Supersonic and Subsonic Streams With Emphasis on the Effect of Transition." NACA TN No. 3869 (1957).

13. Courant, R., E. Issacson and M. Rees. "On the Solution of Nonlinear Hyperbolic Differential Equations by Finite Differences." Comm. Pure and Applied Math., Vol. V, (1952), pp. 243-255.

14. Charwat, A. F., J. N. Roos, F. C. Dewey, Jr. and J. A. Hits. "An Investigation of Separated Flows - Part I. The Pressure Field." J. Aerospace Sci., Vol. 28, No. 6 (June 1961), pp. 457-470.

15. Charwat, A. F., F. C. Dewey, Jr., J. N. Roos, J. A. Hits. "An Investigation of Separated Flows - Part II. Flow in the Cavity and Heat Transfer." J. Aerospace Sci., Vol. 28, No. 7 (July 1961), pp. 513-527.

16. Crane, L. J. and D. C. Pack. "The Laminar and Turbulent Mixing of Jets of Compressible Fluid: Part I. Flow Far from the Orifice." J. Fluid Mechanics, Vol. 2, Part 5, (July 1957), pp. 449-455.

17. Crane, L. J. "The Laminar and Turbulent Mixing of Jets of Compressible Fluid: Part II. The Mixing of Two Semi-Infinite Streams." J. Fluid Mechanics, Vol. 3, Part 1, (Oct. 1957), pp. 81-92.

18. Forthmann, E. "Turbulent Jet Expansion." NACA TM No. 789, (1935).

19. Foss, J. F. and J. B. Jones. "A Study of Incompressible Turbulent Bounded Jets." Purdue Research Foundation Project No. 3728, Prepared for Harry Diamond Laboratories, Washington, D.C., (Oct. 16, 1964).

20. Fox, Jay. "Flow Regions in Tranverse Rectangular Cavities." Proceedings of the 1965 Heat Transfer and Fluid Mechanic Institute, (June 1965), pp. 230-247.

21. Fox, Jay. "A Criterion for the Transition Between Flow Regions in Turbulent Cavity Flow." AIAA J., Vol. 4, No. 2 (Feb. 1966), pp. 364-365.

22. Frank, R. M. and R. B. Lazarus. "Mixed Eulerian-Lagrangian Method." Methods in Computational Physics, Vol. 3, Fundamental Methods in Hydrodynamics, Academic Press, New York, (1964), pp. 46-67.

23. Fromm, Jacob. "The Time Dependent Flow of an Incompressible Viscous Flow." Methods in Computational Physics, Vol. 3. Fundamental Methods in Hydrodynamics, Academic Press, New York, (1964), pp. 345-382.

24. Ginevskii, A. S. "Turbulent Wake and Jet in a Flow in the Presence of a Longitudinal Pressure Gradient." TIL/T.5261 IZV. AKAD. NAUK, O.T.N., MEKH I MASH., (2), 31-36, (1959), USSR. Translated and Issued September 1963 by Technical Information and Library Services, Ministry of Aviation.

25. Grant, H. P. and R. E. Kronauer. "Fundamentals of Hot Wire Anemometry." Symposium on Measurement in Unsteady Flow, ASME, (May 21-23, 1962), pp. 44-53.

26. Harlow, Francis H. "The Particle-in-Cell Computing Method for Fluid Dynamics." Methods in Computational Physics, Vol. 3, Fundamental Methods in Hydrodynamics, Academic Press, New York, (1964), pp. 319-343.

27. Hinze, J. P. Turbulence. McGraw-Hill, New York, (1959).

28. Kawaguti, Mitutosi. "Numerical Solutions of the Navier-Stokes Equations for the Flow in a Channel with a Step." MRC Technical Summery Report #574, Contract No. DA-11-022-ORD-2059, The University of Wisconsin (May 1965).

29. Korst, H. H., R. H. Page and M. E. Childs. "Compressible Two-Dimensional Jet Mixing at Constant Pressure." ME Technical Note 392-1, University of Illinois (April 1954).

30. Lax, P. D. "Weak Solutions of Nonlinear Hyperbolic Equations and Their Numerical Computation." Comm. Pure and Appl. Math., Vol. VII (1954), pp. 159-193.

31. Liepmann, H. W. and J. Laufer. "Investigation of Free Turbulent Mixing." NACA TN 1257, (1947).

32. Maull, D. J. and L. F. East. "Three-Dimensional Flow in Cavities." J. Fluid Mech., Vol. 116 (1963), pp. 620-632.

33. Maydew, R. C. and J. F. Reed. "Turbulent Mixing of Compressible Free Jets." AIAA J., Vol. 1, No. 6 (June 1963), pp. 1443-1444.

34. Miller, D. R. and E. W. Comings. "Static Pressure Distribution in the Free Turbulent Jet." J. Fluid Mech., Vol. 3 (1957-58), pp. 1-16.

35. Mueller, T. J. and R. E. Olson. "Spreading Rates of Compressible Two-Dimensional Reattaching Jet." Proceedings of the Fluid Amplification Symposium, Vol. 1 (May 1964), pp. 63-79.

36. Noh, W. F. "CEL: A Time-Dependent Two-Space-Dimensional Coupled Eulerian-Lagrange Code." Methods in Computational Physics, Vol. 3. Fundamental Methods in Hydrodynamics, Academic Press, New York, (1964), pp. 117-179.

37. Olson, R. E. and D. P. Miller. Fluid Amplification. 6. Aerodynamic Studies of Free and Attached Jets. A-1771-24, Research Laboratories, United Aircraft Corp., prepared for Harry Diamond Laboratories, Washington, D.C. (Oct. 14, 1963).

38. Pai, Shih-I. "Two-Dimensional Jet Mixing of a Compressible Fluid." J. Aero. Sci., Vol. 16, No. 8 (Aug. 1949), pp. 463-469.

39. Pai, Shih-I. Fluid Dynamics of Jets. D. Van Norstrand Co., Inc., New York, (1954).

40. Pai, Shih-I. Viscous Flow Theory II - Turbulent Flow. D. Van Norstrand Co., New York, (1957).

41. Reichardt, H. "On a New Theory of Free Turbulence." Royal Aero. Soci. J., Vol. 47, (1943), pp. 167-176.

42. Reid, K. N. Jr. "Static and Dynamic Interaction of a Fluid Jet and a Receiver-Diffuser." Sc. D. Thesis, Dept. of Mechanical Eng., MIT, (Sept. 1964).

43. Richtmyer, R. D. Difference Methods for Initial-Value Problems. Interscience Publishers, Inc., New York, (1957).

44. Roshko, Anatol. "Some Measurements of Flow in a Rectangular Cutout." NACA TN 3488, (Aug. 1955).

45. Rusanov, V. V. "The Calculation of the Interaction of Non-Stationary Shock Waves and Obstacles." National Research Council of Canada Library, Ottawa, Canada, Tech. Translation by D. A. Sinclair, 1962. Translated from: Zhurnal Vychislitelnoi Fiziki, Akademiya Nauk, SSSR 1, Vol. 1, No. 2 (1961), p. 267.

46. Sawyer, R. A. "The Flow Due to a Two-Dimensional Jet Issuing Parallel to a Flat Plate." J. Fluid Mech., Vol. 9, Part 4 (Dec. 1960), pp. 543-560.

47. Sawyer, R. A. "Two-Dimensional Reattaching Jet Flows Including the Effects of Curvature on Entrainment." J. Fluid Mech., Vol. 17, Part 4 (Dec. 1963), pp. 481-498.

48. Schlichting, H. Boundary Layer Theory, 4th Ed. McGraw-Hill, New York, (1960).

49. Tani, I., M. Iuchi and H. Komoda. "Experimental Investigation of Flow Separation Associated With a Step or Groove." Aeronautical Research Institute Report 364, Univ. of Tokyo, Japan, (1961).

50. Tollmien, Walter. "Calculation of Turbulent Expansion Processes." NACA TM No. 1085, (1945).

51. Townsend, A. A. The Structure of Turbulent Shear Flow. Cambridge University Press, (1956).

52. Tyler, L. D. "Numerical Solutions of the Flow Field Produced by a Plane Shock Wave Emerging Into a Crossflow." Ph.D. Thesis, School of Mechanical Eng., Oklahoma State Univ., (May 1965).

53. Van Driest, E. R. "Turbulent Boundary Layer in Compressible Fluids." J. Aero. Sci., Vol. 18, No. 3 (March 1951), pp. 145-160.

54. Von Neumann, J. and R. D. Richtmyer. "A Method for the Numerical Calculation of Hydrodynamic Shocks." J. Appl. Physics, Vol. 21 (March 1950), pp. 232-237.

55. Walker, W. F. "A Numerical Solution for the Interaction of a Moving Shock Wave With a Turbulent Mixing Region." Ph.D. Thesis, School of Mechanical Eng., Oklahoma State University (May 1966).

56. Zumwalt, G. W. and S. Y. Ruo. "An Analysis of Plane, Incompressible, Turbulent Jets in Adverse Pressure Gradients With Applications to Fluid Amplifiers." Research Report HDL-2 for Harry Diamond Laboratories, School of Mechanical Eng., Oklahoma State University, (July 1964).

57. Zumwalt, G. W. and H. H. Tang. "Transient Base Pressure Study of an Axi-Symmetric Supersonic Missle Flying Head-on Through a Blast Wave." Report SC-TM-65-218, Sandia Corporation, Albuquerque, N. M. (May 1965).

APPENDIX A

DERIVATION OF GOVERNING EQUATIONS FOR TURBULENT FLOW

The governing equations for turbulent flow are derived from the basic equations, equations (3-1), with the aid of equations (3-6) and the rules of averaging, equations (3-5). The general procedure followed in this Appendix is:

1. Express each fluid property appearing in equations (3-1) as the sum of its average value and the fluctuating component.
2. Take the time average of every resulting quantity.
3. Substitute them into equations (3-1) to replace each individual corresponding term.

In addition to the use of u and v for velocity components in x and y directions, respectively, a general form of velocity, u_i or u_j, also will be used to represent either velocity component depending on the direction under consideration.

Continuity and Momentum Equations

The terms appearing in the continuity and the momentum equations are ρ, p, ρu, ρv, ρu^2, ρv^2 and ρuv. These can be written in following forms,

$$\overline{\rho} = \overline{(\overline{\rho} + \rho')} = \overline{\rho} \qquad \text{(A-1)}$$

$$\overline{p} = \overline{(\overline{p} + p')} = \overline{p} \tag{A-2}$$

$$\overline{\rho u_i} = \overline{(\overline{\rho} + \rho') \circ (\overline{u_i} + u_i')} = \overline{\rho}\,\overline{u_i} + \overline{\rho' u_i'} \tag{A-3}$$

$$\overline{\rho u_i u_j} = \overline{(\overline{\rho} + \rho') \circ (\overline{u_i} + u_i') \circ (\overline{u_j} + u_j')}$$

$$= \overline{\rho}\,\overline{u_i}\,\overline{u_j} + \overline{\rho}\,\overline{u_i' u_j'} + \overline{u_i}\,\overline{\rho' u_j'} + \overline{u_j}\,\overline{\rho' u_i'} + \overline{\rho' u_i' u_j'} \,. \tag{A-4}$$

Since the problem of interest here is a low velocity flow and no sudden pressure or density changes are involved, the terms containing density fluction ρ' as noted by Pai (39) can be neglected. Also, in accordance with van Driest (53), the product of three fluctuating components - the triple correlation - may be neglected. After this simplification, equations (A-3) and (A-4), respectively, become

$$\overline{\rho u_i} = \overline{\rho}\,\overline{u_i} \tag{A-5}$$

$$\overline{\rho u_i u_j} = \overline{\rho}\,\overline{u_i}\,\overline{u_j} + \overline{\rho}\,\overline{u_i' u_j'} \,. \tag{A-6}$$

With the above relations, the continuity and the momentum equations for turbulent flow can be written as follows:

Continuity:

$$\frac{\partial}{\partial t}\overline{\rho} + \frac{\partial}{\partial x}(\overline{\rho}\,\overline{u}) + \frac{\partial}{\partial y}(\overline{\rho}\,\overline{v}) = 0$$

x-Momentum:

$$\frac{\partial}{\partial t}(\overline{\rho}\,\overline{u}) + \frac{\partial}{\partial x}\left[\overline{\rho}\,\overline{u}^2 + \overline{p} + \overline{\rho}\overline{(u')^2}\right] + \frac{\partial}{\partial y}\left[\overline{\rho}\,\overline{v}\,\overline{u} + \overline{\rho}\,\overline{u'v'}\right] = 0$$

y-Momentum:

$$\frac{\partial}{\partial t}(\overline{\rho}\,\overline{v}) + \frac{\partial}{\partial x}\left[\overline{\rho}\,\overline{u}\,\overline{v} + \overline{\rho}\,\overline{u'v'}\right] + \frac{\partial}{\partial y}\left[\overline{\rho}\,\overline{v}^2 + \overline{p} + \overline{\rho}\overline{(v')^2}\right] = 0 \,.$$

Energy Equation

Fluid energy per unit volume, is defined as

$$e = \rho C_v T + \frac{\rho}{2}(u^2 + v^2) \quad . \tag{A-7}$$

If the fluid under study is considered to be a perfect gas, then, equation (A-7) can be represented as

$$e = \frac{p}{\gamma - 1} + \frac{\rho}{2}(u^2 + v^2) \quad . \tag{A-8}$$

If the instantaneous values of p, ρ, u and v in equations (3-6) are substituted in the right hand side of equation (A-8) and the time average is taken, the expression for $\bar{e}$ becomes:

$$\bar{e} = \overline{\frac{1}{\gamma - 1}(\bar{p} + p') + \frac{1}{2}(\bar{\rho} + \rho') \cdot [(\bar{u} + u')^2 + (\bar{v} + v')^2]}$$

$$= \frac{\bar{p}}{\gamma - 1} + \frac{1}{2}[\bar{\rho}\,\bar{u}^2 + \bar{\rho}\,\bar{v}^2 + \overline{\rho(u')^2} + \overline{\rho(v')^2} + \overline{\rho'(u')^2}$$

$$+ \overline{\rho'(v')^2} + 2\,\bar{u}\,\overline{\rho' u'} + 2\,\bar{v}\,\overline{\rho' v'}\,]. \tag{A-9}$$

And again, if the terms containing $(\rho' u')$ and $(\rho' v')$ are neglected, this yields

$$\bar{e} = \frac{\bar{p}}{\gamma - 1} + \frac{1}{2}[\bar{\rho}\,\bar{u}^2 + \bar{\rho}\,\bar{v}^2 + \overline{\rho(u')^2} + \overline{\rho(v')^2}\,]. \tag{A-10}$$

The terms appearing in the energy equation of (3-1) are e, eu, ev, pu and pv. They can be written in following forms:

$$\overline{eu_i} = \overline{(\bar{e} + e')\cdot(\bar{u}_i + u_i')} = \bar{e}\,\bar{u}_i + \overline{e' u_i'} \tag{A-11}$$

$$\overline{pu_i} = \overline{(\bar{p} + p')\cdot(\bar{u}_i + u_i')} = \bar{p}\,\bar{u}_i + \overline{p' u_i'} \quad . \tag{A-12}$$

In order to express $\overline{eu_i}$ in terms of the known quantities, $\overline{e' u'}_i$ must

be expanded further. If the fluid energy is written in the form according to the relation in equation (3-6), the fluctuating component of e can be expressed as

$$e' = \bar{e} - e \ .$$

If the relations in equations (3-6) are substituted into the right hand side of equation (A-8) and the result is subtracted from equation (A-9) with the higher order terms neglected, the expression for the fluctuating component of e becomes:

$$e' = \frac{p'}{\gamma - 1} + \bar{\rho}\,\bar{u}\,u' + \bar{\rho}\,\bar{v}\,v' + \bar{u}\,\rho'u' + \bar{v}\,\rho'v' - \bar{u}\,\overline{\rho'u'}$$

$$- \bar{v}\,\overline{\rho'v'} + \frac{1}{2}\left[\bar{\rho}(u')^2 + \bar{\rho}(v')^2 + \rho'\bar{u}^2 + \rho'\bar{v}^2\right.$$

$$\left. -\bar{\rho}\overline{(u')^2} - \bar{\rho}\overline{(v')^2}\right]. \qquad \text{(A-13)}$$

If u and v in equation (A-13) are represented respectively by u_i and u_j, the expression of $\overline{e'u_i'}$ in equation (A-11) can be obtained by multiplying both sides of equation (A-13) by u_i' and taking the average, thus

$$\overline{e'u_i'} = \frac{1}{\gamma - 1}\overline{p'u_i'} + \bar{\rho}\,\bar{u}_i\overline{(u_i')^2} + \bar{\rho}\,\bar{u}_j\,\overline{u_i'u_j'} + \frac{1}{2}\left(\bar{u}_i^2\,\overline{\rho'u_i'} + \bar{u}_j^2\,\overline{\rho'u_j'}\right). \qquad \text{(A-14)}$$

As before, all the terms containing either p' or ρ' in equations (A-12), (A-13) and (A-14) can be neglected and equations (A-11) and (A-12) respectively become

$$\overline{eu_i} = \bar{e}\,\bar{u}_i + \bar{\rho}\,\bar{u}_i\overline{(u_i')^2} + \bar{\rho}\,\bar{u}_j\overline{(u_i'u_j')} \qquad \text{(A-15)}$$

$$\overline{pu_i} = \bar{p}\,\bar{u}_i \ . \qquad \text{(A-16)}$$

With these relations, the energy equation for turbulent flow

can be written as

$$\frac{\partial \overline{e}}{\partial t} + \frac{\partial}{\partial x}\left[(\overline{e} + \overline{p})\overline{u} + \overline{\rho}\,\overline{u(u')^2} + \overline{\rho}\,\overline{v(u'v')}\right]$$

$$+ \frac{\partial}{\partial y}\left[(\overline{e} + \overline{p})\overline{v} + \overline{\rho}\,\overline{v(v')^2} + \overline{\rho}\,\overline{u(u'v')}\right] = 0 \,.$$

In addition to the relations in equations (3-6), van Driest (53) has suggested that (ρu) and (ρv) can also be considered as fluid properties. If this reasoning is used in the derivation of the governing equations for turbulent flow, a slightly different set of the governing equations can be obtained. The difference, however, can be eliminated by a simple assumption which converts the resulting equations to a form identical to those derived earlier, and summarized below.

Summary of the Equations

$$\text{Continuity :} \quad \frac{\partial \overline{\rho}}{\partial t} + \frac{\partial}{\partial x}(\overline{\rho}\,\overline{u}) + \frac{\partial}{\partial y}(\overline{\rho}\,\overline{v}) = 0$$

$$\text{x-Momentum :} \quad \frac{\partial}{\partial t}(\overline{\rho}\,\overline{u}) + \frac{\partial}{\partial x}\left[\overline{\rho}\,\overline{u}^2 + \overline{p} + \overline{\rho(u')^2}\right] + \frac{\partial}{\partial y}\left[\overline{\rho}\,\overline{v}\,\overline{u} + \overline{\rho}\,\overline{u'v'}\right] = 0$$

$$\text{y-Momentum :} \quad \frac{\partial}{\partial t}(\overline{\rho}\,\overline{v}) + \frac{\partial}{\partial x}\left[\overline{\rho}\,\overline{u}\,\overline{v} + \overline{\rho}\,\overline{u'v'}\right] + \frac{\partial}{\partial y}\left[\overline{\rho}\,\overline{v}^2 + \overline{p} + \overline{\rho(v')^2}\right] = 0 \qquad \text{(A-17)}$$

$$\text{Energy :} \quad \frac{\partial \overline{e}}{\partial t} + \frac{\partial}{\partial x}\left[(\overline{e} + \overline{p})\overline{u} + \overline{\rho}\,\overline{u(u')^2} + \overline{\rho}\,\overline{v(u'v')}\right]$$

$$+ \frac{\partial}{\partial y}\left[(\overline{e} + \overline{p})\overline{v} + \overline{\rho}\,\overline{v(v')^2} + \overline{\rho}\,\overline{u(u'v')}\right] = 0$$

APPENDIX B

DERIVATION OF EQUATION $\frac{D\overline{p}}{Dt} = 0$

The continuity and momentum equations for a two-dimensional, inviscid, incompressible flow can be written as

$$\frac{\partial u}{\partial x} + \frac{\partial v}{\partial y} = 0 \tag{B-1}$$

$$\frac{\partial u}{\partial t} + \frac{\partial}{\partial x}(u^2) + \frac{\partial}{\partial y}(uv) + \frac{1}{\rho}\frac{\partial p}{\partial x} = 0 \tag{B-2}$$

$$\frac{\partial v}{\partial t} + \frac{\partial}{\partial x}(uv) + \frac{\partial}{\partial y}(v^2) + \frac{1}{\rho}\frac{\partial p}{\partial y} = 0 \,. \tag{B-3}$$

If equations (B-2) and (B-3) are separately multiplied by u and v and combined, following equation results

$$\left[u\frac{\partial u}{\partial t} + v\frac{\partial v}{\partial t}\right] + u\frac{\partial}{\partial x}(u^2) + v\frac{\partial}{\partial y}(v^2) + u^2\frac{\partial v}{\partial y} + v^2\frac{\partial u}{\partial x}$$

$$+ uv\left(\frac{\partial u}{\partial y} + \frac{\partial v}{\partial x}\right) + \frac{u}{\rho}\frac{\partial p}{\partial x} + \frac{v}{\rho}\frac{\partial p}{\partial y} = 0 \,.$$

The above equation can be combined with equation (B-1) and rewritten in following form:

$$\left[u\frac{\partial u}{\partial t} + v\frac{\partial v}{\partial t}\right] + \frac{1}{2}\left[u\frac{\partial}{\partial x}(u^2 + v^2) + v\frac{\partial}{\partial y}(u^2 + v^2)\right]$$

$$+ \frac{1}{\rho}\left[\frac{\partial}{\partial x}(pu) + \frac{\partial}{\partial y}(pv)\right] = 0 \,. \tag{B-4}$$

Equation (B-4) was derived for an incompressible flow but it may also be regarded as the relation applicable to compressible flow

with small variation of density so that the density can be considered as constant.

If equation (3-2) is substituted into the energy equation of equations (3-1), it follows that

$$\frac{\partial}{\partial t}\left[\frac{p}{\gamma - 1} + \frac{\rho}{2}(u^2 + v^2)\right] + \frac{\partial}{\partial x}\left[\frac{\gamma p u}{\gamma - 1} + \frac{\rho u}{2}(u^2 + v^2)\right] + \frac{\partial}{\partial y}\left[\frac{\gamma p v}{\gamma - 1} + \frac{\rho v}{2}(u^2 + v^2)\right] = 0 . \tag{B-5}$$

Again, if the density is approximated as a constant, the above equation can be rewritten as

$$\rho\left[u\frac{\partial u}{\partial t} + v\frac{\partial v}{\partial t}\right] + \frac{1}{\gamma - 1}\frac{\partial p}{\partial t} + \frac{\gamma}{\gamma - 1}\left[\frac{\partial}{\partial x}(pu) + \frac{\partial}{\partial y}(pv)\right] + \frac{\rho}{2}\frac{\partial}{\partial x}\left[u(u^2 + v^2)\right] + \frac{\rho}{2}\frac{\partial}{\partial y}\left[v(u^2 + v^2)\right] = 0 ,$$

or (B-6)

$$\left[u\frac{\partial u}{\partial t} + v\frac{\partial v}{\partial t}\right] + \frac{1}{\gamma - 1}\frac{1}{\rho}\frac{\partial p}{\partial t} + \frac{\gamma}{\gamma - 1}\frac{1}{\rho}\left[\frac{\partial}{\partial x}(pu) + \frac{\partial}{\partial y}(pv)\right] + \frac{1}{2}\left[u\frac{\partial}{\partial x}(u^2 + v^2) + v\frac{\partial}{\partial y}(u^2 + v^2)\right] = 0 .$$

If equation (B-4) is subtracted from equation (B-6) and every term divided by the common constant, the following results

$$\frac{\partial p}{\partial t} + \frac{\partial}{\partial x}(pu) + \frac{\partial}{\partial y}(pv) = 0 . \tag{B-7}$$

After the relations in equations (3-6) are applied and time averages taken, equation (B-7) becomes:

$$\frac{\partial \bar{p}}{\partial t} + \frac{\partial}{\partial x}(\bar{p}\,\bar{u}) + \frac{\partial}{\partial y}(\bar{p}\,\bar{u}) = 0 . \tag{B-8}$$

Equation (B-8) is only an approximation; it was derived under

the assumption that the density variation of a compressible fluid is so small that it may be regarded as a constant. Since equation (B-8) is already in conservation form, the general difference equation, equation (3-26), can be applied directly.

APPENDIX C

DERIVATION OF EQUATION $\nabla^2 \overline{p} = \overline{Q}$

Since the iteration process for determining pressure is carried out at a fixed time, the time derivative term can be ignored. Then, the basic momentum equations can be written as

$$\frac{\partial}{\partial x}(\rho u^2 + p) + \frac{\partial}{\partial y}(\rho uv) = 0 \qquad (C\text{-}1)$$

$$\frac{\partial}{\partial x}(\rho uv) + \frac{\partial}{\partial y}(\rho v^2 + p) = 0 \,. \qquad (C\text{-}2)$$

Differentiating equations (C-1) and (C-2) by x and y, respectively, and combining them, yields

$$\frac{\partial^2}{\partial x^2} p + \frac{\partial^2}{\partial y^2} p + \frac{\partial^2}{\partial x^2}(\rho u^2) + \frac{\partial^2}{\partial y}(\rho v^2) + 2\frac{\partial^2}{\partial x \partial y}(\rho uv) = 0$$

or (C-3)

$$\frac{\partial^2}{\partial x^2} p + \frac{\partial^2}{\partial y^2} p = -\left[\frac{\partial^2}{\partial x^2}(\rho u^2) + \frac{\partial}{\partial y^2}(\rho v^2) + 2\frac{\partial^2}{\partial x \partial y}(\rho uv)\right] .$$

If the same method applied in Appendix A is used to write equation (C-3) in form applicable to a turbulent flow case, the following results

$$\nabla^2 \overline{p} = \frac{\partial^2}{\partial x^2} \overline{p} + \frac{\partial^2}{\partial y^2} \overline{p} = -\overline{Q} \,, \qquad (C\text{-}4)$$

where

$$\overline{Q} = \frac{\partial^2}{\partial x^2}\left[\overline{\rho}\,\overline{u}^2 + \overline{\rho(u')^2}\right] + \frac{\partial^2}{\partial y^2}\left[\overline{\rho}\,\overline{v}^2 + \overline{\rho(v')^2}\right]$$
$$+ 2\frac{\partial^2}{\partial x \partial y}\left[\overline{\rho}\,\overline{u}\,\overline{v} + \overline{\rho\,u'v'}\right]. \qquad (C\text{-}5)$$

For an incompressible flow case, the density in equation (C-5) is regarded as a constant. If equation (C-5) is to be regarded as a dimensionless equation, the density becomes unity.

If a square mesh is used, equation (C-4) can be written in a difference form as follows:

$$\frac{1}{(\Delta y)^2}\left[\overline{p}_{m+1,\ell} + \overline{p}_{m-1,\ell} + \overline{p}_{m,\ell+1} + \overline{p}_{m,\ell-1} - 4\overline{p}_{m,\ell}\right] = -\overline{Q}$$

or (C-6)

$$\overline{p}_{m,\ell} = \frac{1}{4(\Delta y)^2}\left[\overline{p}_{m+1,\ell} + \overline{p}_{m-1,\ell} + \overline{p}_{m,\ell+1} + \overline{p}_{m,\ell-1} + \overline{Q}\right].$$

Equation (C-6) was used in the iteration process for determining pressure in the examples in Chapters IV and V.

APPENDIX D

PROGRAMMING LOGIC

The general procedure of computation followed the order listed below unless it was directed to another step by a "go to". The computer program was written in FORTRAN IV language and an IBM 7040 computer was used for execution of the program. The size of the field was 48 columns by 39 rows.

① Read: W, H_1, H_2, L, Δx, Δy, γ, R, $\overline{\rho}^*_{max}$, $\overline{\rho}^*_{min}$, (or $\overline{p}^*_{max}$, $\overline{p}^*_{min}$), T_{noz}, $\overline{u}_{noz}$, $\overline{p}^*_{noz}$, σ, σ_o, ω.

② Read: time plane interval for print out, initial time plane number, maximum time plane number, branching indecies for Read or Not Read the initial data from the tape and for Write or Not Write the last set of data on the tape.

③ Read: from tape - all the values as read in ① - if so commanded in ②.

④ Read: from tape - number of the last time plane of the previous computation as the number of the initial time plane of this computation; the next time plane number for print out - if so commanded in ②.

⑤ Print: all the important input data in ① and ② or ③ and ④.

⑥ Calculate:

$$\chi = \tan^{-1} (\Delta y/\Delta x)$$

$$a = \sqrt{32.2\ RT_{noz}}$$

$$\overline{u^*_{noz}} = \overline{u}_{noz}/a$$

$$\Delta x^* = \Delta x/\Delta y$$

$$\Delta y^* = 1.0$$

$$\tau^* = \frac{\sigma_o\,(\Delta x^*)(\Delta y^*)}{\dfrac{\overline{u}_{noz} + \sqrt{32.2\ \gamma\ RT_{noz}}}{a}\cdot\left[(\Delta x^*)^2 + (\Delta y^*)^2\right]^{1/2}}$$

⑦ Define: the flow field in terms of net points by dividing all cavity dimensions by Δy.

⑧ Read: from tape - $\overline{\rho^*}$, $\overline{u^*}$, $\overline{v^*}$, $\overline{p^*}$, identification number of every point in the field of the final results of previous computation - if so commanded and go to ⑩ .

⑨ Define: the identification number of every point in the field according to the nature of the relation of the point to its neighboring points, and the initial conditions.

⑩ Start: general computation - columnwise throughout the field.

ⓐ find the proper value of $\overline{u^*_a}$ and evaluate $\overline{e^*}$ for the column under consideration.

ⓑ compute the fluid properties of the new time plane of every point in the field in the column under consideration.

Continuity ⟶ $\overline{\rho}^*$

x-Momentum ⟶ $\overline{\rho^*}\,\overline{u^*}$ ⟶ $\overline{u}^*$

y-Momentum ⟶ $\overline{\rho}^*\overline{v^*}$ ⟶ $\overline{v}^*$

Energy ⟶ $\overline{e}^*$ ⟶ $\overline{p^*}$

ⓒ if $\overline{\rho^*}$ (or $\overline{p^*}$) is not within the limits imposed, go to ㉒ .

ⓓ if the computation has not covered every column in the field, go to ⓐ .

⑪ Define: new property matrices with the newly computed values.

⑫ Check: if print out is not the time specified in ② or ④ or ⑭, go to ⑮ .

⑬ Print: all the properties, $\overline{\rho}^*$, $\overline{u}^*$, $\overline{v}^*$, $\overline{p}^*$ in the field according to the format specified.

⑭ Define: the next print out time plane number.

⑮ Check: if the current time plane is greater or equal to the the maximum time plane number specified in ②, go to ⑰.

⑯ Define: the number of the new time plane by adding 1, go to ⑩.

⑰ Check: if it is commanded to store final data on tape as specified in ②, go to ⑲.

⑱ Stop

⑲ Write: on tape

ⓐ W, H_1, H_2, L, Δx, Δy, γ, R, $\overline{\rho}^*_{max}$, $\overline{\rho}^*_{min}$, (or $\overline{p}^*_{max}$, $\overline{p}^*_{min}$), T_{noz}, $\overline{u}_{noz}$, $\overline{p}^*_{noz}$, σ, σ_o, ω.

ⓑ number of the final time plane; number of next print out time plane as defined in ⑭.

ⓒ $\overline{\rho}^*$, $\overline{u}^*$, $\overline{v}^*$, $\overline{p}^*$ and identification number of every point in the field.

⑳ Print: message of the completion of the job.

㉑ Stop

㉒ Print: proper message and computed results of the previous time plane.

(23) Stop.

VITA

Song-yeong Ruo

Candidate for the Degree of

Doctor of Philosophy

Thesis: EVALUATION OF THE APPLICABILITY OF AN EXPLICIT NUMERICAL METHOD TO A PLANE, TURBULENT, LOW VELOCITY, PARTIALLY CONFINED JET

Major Field: Mechanical Engineering

Biographical:

Personal Data: Born January 23, 1934, in Toyohara (now Feng-yuan), Formosa, the son of Pan and Miau Ruo.

Education: Graduated from Taiwan Provincial Taichung First Middle School, Taichung City, Formosa, in July, 1952; received the Bachelor of Science degree in Mechanical Engineering from Taiwan Provincial Cheng-Kung University, Tainan City, Formosa, in July, 1957; received the Master of Science degree from the University of Kansas, Lawrence, Kansas, in June, 1961; completed the requirements for the Doctor of Philosophy degree in November, 1966.

Professional Experience: Worked as a summer trainee at Taiwan Aluminum Co., Kaohsiung City (1955) and Tatu Paper Co., Tatu (1956); served in the Chinese Air Force as a Second Lieutenant from August, 1957, to February, 1959; employed by Hsin-Shin Paper Mills, Feng-yuan, as a Mechanical Engineer from March to September, 1959; employed by the Department of Mechanical Engineering at the University of Kansas as a Research Assistant from February, 1960, to May, 1961; worked as a Research Engineer at Electra Manufacturing Co., Independence, Kansas, in the summer of 1961; employed by the School of Mechanical Engineering at the Oklahoma State University as a Graduate Assistant from September, 1961, to August, 1966.

Professional Organizations: The author is a member of the following professional and honorary organizations: American Institute of Aeronautics and Astronautics; Pi Mu Epsilon, Pi Tau Sigma.